Implementation of an Energy Management System for Real-Time Power Flow Control in Behind the Meter Energy Communities Applications

by

Airin Rahman

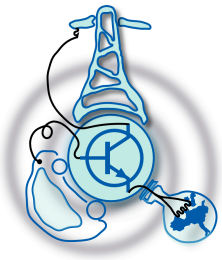

Submitted to the Department of Electrical Engineering, Electronics, Computers and Systems
in partial fulfillment of the requirements for the degree of
Master of Science in Sustainable Transportation and Electrical Power Systems
at the
UNIVERSIDAD DE OVIEDO
September 2021

Author .....

Certified by .....
Pablo Garcia Fernandez
Associate Professor
Thesis Supervisor

Certified by .....
Ramy Georgious Zaher Georgious
Technical director of R&D, ENFASYS
Thesis Supervisor

Implementation of an Energy Management System for Real-Time Power Flow Control in Behind the Meter Energy Communities Applications

by

Airin Rahman

Submitted to the Department of Electrical Engineering, Electronics, Computers and Systems
on August 31, 2021, in partial fulfillment of the
requirements for the degree of
Master of Science in Sustainable Transportation and Electrical Power Systems

Abstract

Energy Management Systems (EMS) can be used for the energy communities (EC) application to reduce energy costing by controlling energy consumption. This thesis work presents the implementation of the proposed EMS algorithm that manages power flow through the AC microgrid (MG) system composed of PV power system, energy storage, load, and utility grid where the MG system operates in the grid-connected mode for EC application. All the relevant theoretical and conceptual backgrounds, as well as the formulas, are presented in the first part of the report. The detailed step-by-step design procedures for the proposed EMS algorithm, PV system, and energy storage system (ESS) are discussed briefly. The proposed EMS algorithm aims to reduce energy costing for the customer by managing the charging/discharging period of the ESS and selling the additional PV power to the utility grid. The proposed algorithm finds the optimal power flow through the system considering PV power generation, load demand, electricity tariff profile, and solar irradiance forecasting as the input constraints. The solar radiance and load demand forecasting are used to avoid charging the ESS from the utility grid when it is possible to charge the battery from next day solar power generation. The complete simulation of the AC MG system has been implemented in MATLAB Simulink® where vector current controller is used to control the power flow based on the proposed EMS algorithm. Also, the Stateflow® model is used for the implementation of the proposed EMS algorithm with real-time data. The effectiveness of the proposed EMS is justified based on the energy cost analysis, where the total energy cost is considering the Levelized cost of energy (LCOE) of the system.

Thesis Supervisor: Pablo Garcia Fernandez
Title: Associate Professor

Thesis Supervisor: Ramy Georgious Zaher Georgious
Title: Technical director of R&D, ENFASYS

Acknowledgments

I would like to express my sincere gratitude and warmest thanks to my academic supervisor Prof. Pablo Garcia for giving me the opportunity to work on this project. I appreciate his advice, guidance and support. His constructive comments and advice helps me learn and work independently.

In addition, I am extremely grateful to my company supervisor Prof. Ramy Georgious Zaher Georgious for his invaluable advice, continuous support and patience during my work. He has supported and guide me from the beginning to the end of the project. I appreciate both of my supervisors support and dedication to finish my work.

Furthermore, I would like to thank Nixen Fernandez, CEO of ENFASYS engineering, for his support and guidance from the beginning of the project in all administrative issue.

Finally, I would like to express my gratitude to my parents, my husband and my friends. Without their tremendous understanding and encouragement throughout the thesis, it would be impossible for me to complete my work.

Last but not the least, I would like to praise Allah the Almighty, the Most Gracious, and the Most Merciful for His blessing given to me during my study and in completing this thesis. May Allah's blessing goes to His final Prophet Muhammad (peace be up on him), his family and his companions.

Contents

List of Figures

List of Tables

Chapter 1

Introduction

1.1 Background

The increasing electricity demand due to a large number of populations, limited conventional resources, concern about environmental issues, and developments of technology have prioritized the use of renewable energy sources. However, the unpredictable nature of renewable sources has come with the concept of a microgrid (MG) system, which is a hybrid combination of distributed generation (DG), grid supply, and energy storage systems (ESS), which can operate in either islanded or in grid-connected mode. Power electronic devices are playing a crucial role to make the MG system smarter and more flexible by managing the weakness and stability issues. To meet the dynamic response and high reference tracking characteristic of those power electronic devices, control methods are vital concerns [1]. When several energy sources are available to feed the load and meet demand requirements, new challenges come for power management, control, and economic operation of the system. Power management and control schemes are systematized into the lower level and upper-level control [2]. Lower level control is responsible for stabilizing voltage and frequency, it is also known as the primary control. Several control schemes have been found which are ensuring the control of voltage and frequency along with the power-sharing in AC distribution networks [3], [4], and DC grids [5], [6]. Numerous types of control approaches have been done to overcome the limitation and improve the reliability of the

MG system. Upper-level control is known as an energy management system (EMS). It is responsible for forecasting renewable energy resources and load demand, also performs scheduling of available power generation and load demand within MG [2]. Grid-connected MG systems are mainly used due to consistent configurations for variable/dynamic loads to be fed without interruption [7]. Grid-connected MG system used for energy community (EC) application. In this work, an EMS is proposed and implemented for real-time power flow control which can be used for EC applications. The development of the EMS with different generation and consumption scenarios, and electricity cost analysis is covered in the project work. In addition, it includes the theoretical and conceptual background of generation systems, microgrids, energy storage, and cost analysis. Also, the energy cost comparison of the grid, grid-connected PV, and hybrid system (AC MG system with PV generation and ESSs) is described for the verification of the proposed algorithm. All the work has been done using MATLAB Simulink® and Stateflow® model in Simulink.

1.2 Objective

The proposed EMS algorithm considers PV power generation, load demand, tariff profile, and solar irradiance forecasting as the input data to decide the system operation mode to maintain the power flow through EC, which will decide the battery charging/discharging period as well as bidirectional grid power flow to sell the additional PV power to the utility grid. This work aims to implement an energy management system (EMS) for EC applications to control the real-time power flow. This EMS is designed for EC applications, where it is a self-consumption installation and can be used among different community owners. The real-time power flow is maintained to decide the battery charging/discharging period along with bidirectional grid power flow so that the additional PV power can sell to the grid. The main objective of the EMS is to reduce the energy costing, not only through controlling battery charging/discharging periods but also by selling additional PV generation to the grid.

1.3 Thesis Structure

Towards the previously mentioned objectives, the thesis work is developed, and the structure is organized as follows:

Chapter1: Introduction

This chapter describes the background and objects of the work which is carried out in this thesis.

Chapter 2: State of Art for Energy Communities, Microgrid, Distributed Generation, Energy Storage and Energy Management System

This chapter presents the state of art for the energy communities, microgrid system, distributed generation, energy storage, and energy management system.

Chapter 3: Development of Energy Management System for Energy Communities Application

This chapter demonstrates the design of system configuration including the design of appropriate PV system and energy storage system as well as the describes the tariff profile data and cost calculation including levelized cost of energy.

Chapter 4: Simulation and Modeling of Microgrid System

This chapter narrates the simulation model of AC microgrid system, the average model inverter, and the design of vector current controller along with the result verification.

Chapter 5: Proposed Algorithm for the Energy Management System

This chapter represents the implementation of the proposed algorithm for the energy management system with flowchart and details description of the operation mode.

Chapter 6: EMS with Stateflow Model This chapter shows the Stateflow model of the proposed EMS and the output result for the justification of the EMS.

Chapter 7: Result and Discussion

This chapter demonstrates the EMS with different scenarios and energy cost comparison to find out the optimal solution

Chapter 8: Conclusion and Future Work

This chapter is about the conclusion and additional future work for the improvement.

Chapter 2

State of Art for Energy Communities, Microgrid, Distributed Generation, Energy Storage and Energy Management System

2.1 Energy Community

2.1.1 Concepts of Energy Community

The energy community (EC) is an international organization, which has been initiated first between the European Union (EU) and several third countries. The aim of establishing an energy community was to extend the EU internal energy market to the territories of third countries. For a clean energy transition, collective and citizen-driven energy actions are being organized by energy communities. EC contributes to increase public acceptance of renewable energy projects and make those projects attract private investments for the clean energy transition. Also, by advancing energy efficiency and lowering consumer's electricity bills, EC is providing direct benefits to

the citizens. EC can provide a flexible electricity system considering demand response and storage.

According to the concept of EC, the EU has introduced citizen energy communities and renewable energy communities. EU has included new rules along with the common rules for the internal electricity market, which is active consumer participation either by generation, consuming, sharing, or selling electricity or by providing flexibility services through demand-response and storage that participation can be individually or through citizen energy community. Energy sharing through system analysis can be categorized based on geographical scope, which has been addressed by the scientific literature, is presented in 2-1.

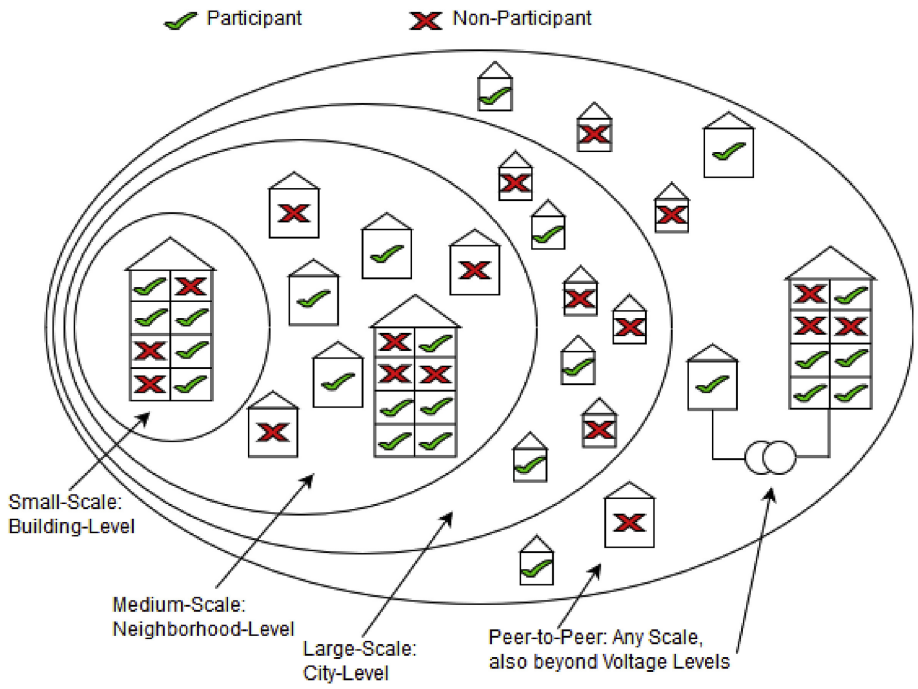

Figure 2-1: Scales of EC implementation

[8]

On the other hand, renewable energy communities aim to strengthen the role of renewable self-consumers to ensure that they can participate in available support schemes on equal footing with large participants. Empowering renewable energy communities to produce, consume, store and sell renewable energy will also help advance energy efficiency in households, support the use of renewable energy and at the same

time contribute to fighting poverty through reduced energy consumption and lower supply tariffs. The legal framework of EC covers legislation in the fields of energy, environment, and competition of the EU legislation.

Legislation scenario of EC is presented in [9]. The legislative and tariffs barriers do not permit that different user can share the point of connection with the public grid. So, the first sign of the situation changing is to consider new approaches toward EC and [9] suggests an innovative solution. Where a power-sharing model has been proposed for energy communities based on the sharing of renewable and other energy services. This suggested model permits the full self-consumption by the users of the local energy generated by renewables.

Major types of EC for the power grid are homogeneous energy community (HEC), mixed energy community (MEC), and self-sufficient energy community (SEC). Detailed of all the types of EC is demonstrated in [10] along with a series of approaches to identify the types.

2.1.2 Microgrid and Energy Communities

Although the concept of MG has existed for more than a decade, application of it was rare because of limited incentives for implementation and multiple barriers [11, 12]. The novel concept of local EC can not only overcome some of these barriers but is also founded on an economic basis trying to maximize the synergy effects between different participants' load profiles and local renewable generation.

The concept of renewable energy communities introduced by the "Revised European Directive" has opened new possibilities for MG, which enhances the value of the energy produced by renewable sources through sharing energy inside an 'energy community' and increasing social welfare. Aggregations consist of different users of multi-apartment and EC, whose power system is based on MG configurations [13,14]. Also, a new concept as a community microgrid is presented in [15,16].

Figure 2-2 represents MG based EC cluster elements with renewable energy.

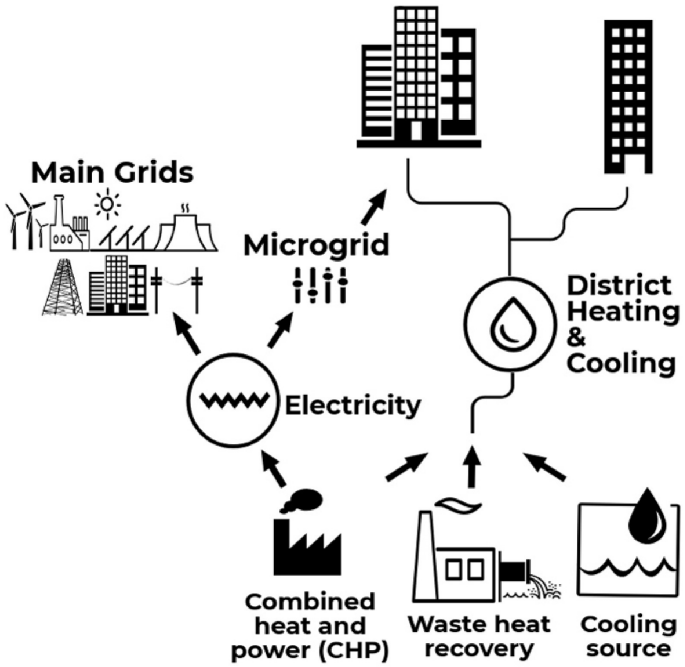

Figure 2-2: MG based EC concept with renewable energy clusters elements [17]

MG based EC, where the MG operates in grid-connected mode with the main utility grid. Where the MG combined all the systems and the EC overcomes the limitation of the MG to offer better flexibility. MG has distributed networks formed by distributed energy resources (DERs), loads, and storage devices, that with new forms of control strategies can make the sources work in a coordinated way [18, 19]. The purpose of the MG system can be described considering different viewpoints. From the technical point of view, MG is the most effective solution to exploit the benefits from the integration of large numbers of small-scale DERs into the distribution electrical systems.

From the end user's viewpoint, MG improves local reliability, reduces emissions, enhances power quality by supporting voltage and reducing voltage dips; also, MG meets both thermal and electricity demand and reduces costs of energy supply. Based on the grid operator's point of view, MG acts as a controlled entity within the power system that can operate as an aggregation of loads and/or generators.

2.2 Microgrid System

2.2.1 Energy Communities for Microgrid

Along with the EMS, aggregation of EC and different apartment is implemented based on the concept of MG. The combination overcome the limitation of the MG system. Figure 2-3 demonstrates EC aggregation based on MG concept.

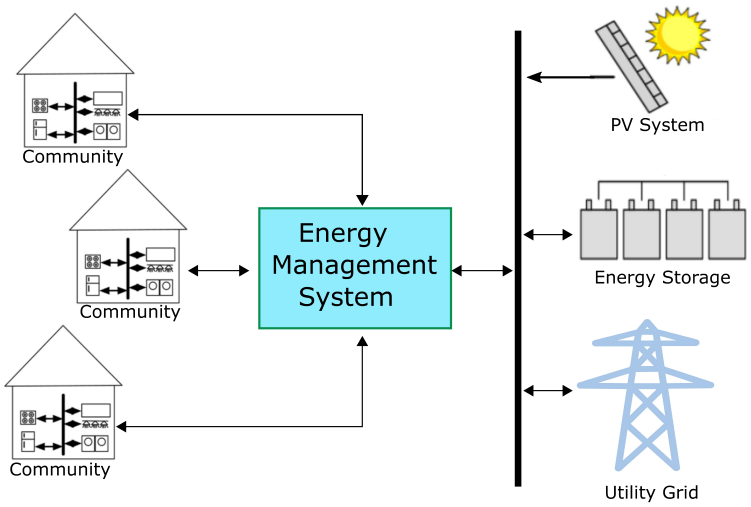

Figure 2-3: Energy communities aggregation

2.2.2 Concepts of Microgrid

MG are localized grids that can operate independently when disconnected from the traditional grid or collaboratively with the grid. As MG has the ability to operate when the main grid is down, it strengthens grid resilience and helps to mitigate grid disturbances. It also works as a grid resource for faster system response and recovery. The concept of MG was first introduced in the technical literature in [18] and [20], where it was a solution to the reliable integration of distributed energy resources(DER), including energy storage system (ESS) and loads. In the literature can be found, a number of microgrid definitions [21] and functional classification schemes [22]. A broadly cited definition which is developed for the U.S. Department of Energy by the Microgrid Ex-change Group reads as follows: "(The microgrid is) a group of intercon-

nected loads and distributed energy resources within clearly defined electrical boundaries that acts as a single controllable entity concerning the grid. A microgrid can connect and disconnect from the grid to enable it to operate in both grid-connected or island mode [23]".

To the utility MG can be thought of as a controlled cell of power system which could be controlled as a single dispatchable load to meet the needs of the transmission system. To the customer MG can be designed to meet their special needs including local reliability enhancement, reduction of feeder losses, support for the local voltage, uninterruptible power supply [18].

MG, which can operate both in grid-connected mode and island mode, is an ideal choice for many applications such as remote areas which are tough to connect to the grid, systems that need efficient and sustainable electricity, and other systems that can use local generations [24]. In the grid-connected mode, the main grid supplies the power deficit, and the additional power generation by MG can be traded with the main grid to provide auxiliary facilities. In the islanded mode of operation, the real and reactive power generated within the microgrid, including the temporary power transfer from/to storage units, should be in balance with the demand of local loads [21].

2.2.3 Structure and Architecture of Microgrid

As mentioned in the literature, there are two main architectures: the American one which is developed by the CERTS [25] and the European one which is described in the 'MICROGRIDS' and 'MORE MICROGRIDS' projects [26].In order to configure a hierarchical scheme for the extension of the MG concept, the Nanogrid (NG) and Picogrid (PG) concepts have been discussed in [22]. The evolution of the MG hierarchical scheme is due to flexibility on the area coverage, size, and the number of distributed generations and loads come up with other small size grids which are applicable in neighborhoods (Microgrid, MG), buildings (Nanogrid, NG) and households (Picogrid, PG) [22]. The microgrid is connected to the grid through the point of common coupling (PCC) utilizing power electronic converters [27–29].

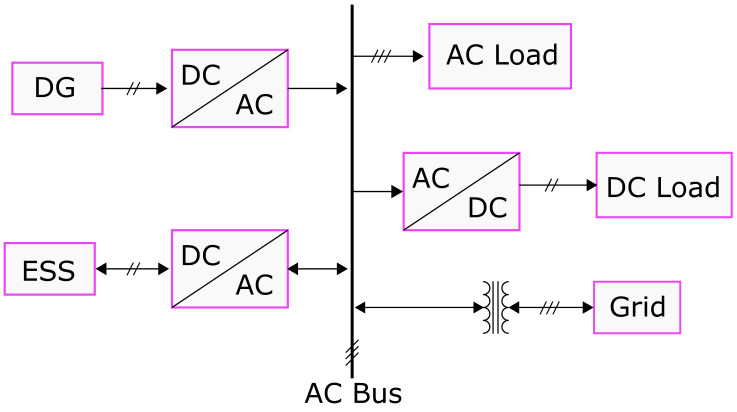

Figure 2-4: AC Microgrid

Based on the type of signal for the interconnection of the MG elements, MG architectures are classified into three types that are AC microgrid, DC microgrid and hybrid AC-DC microgrid [30]. Figure 2-4 shows the schematic diagram of the AC microgrid, where the AC loads or generators are connected directly to the AC bus or through AC/AC converters, and DC units are interfaced to the AC bus through DC/AC converters. In the DC microgrid, the AC units are connected to the DC bus through AC/DC converters, while the units with DC power are connected directly to the DC bus or through DC/DC converter. Figure 2-5 is demonstrating DC microgrid schematic diagram.

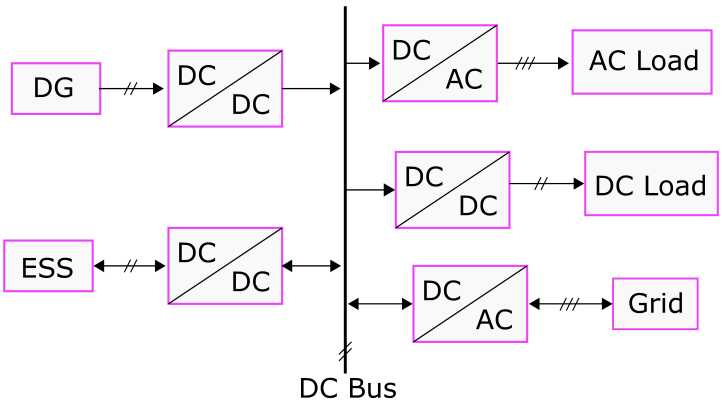

Figure 2-5: DC Microgrid

In a hybrid microgrid, there are two buses for AC and DC units with AC power and DC power, respectively. The power exchange between both AC and DC bus is ensured through bidirectional AC/DC converters. Figure 2-6 represent a schematic diagram of hybrid microgrid.

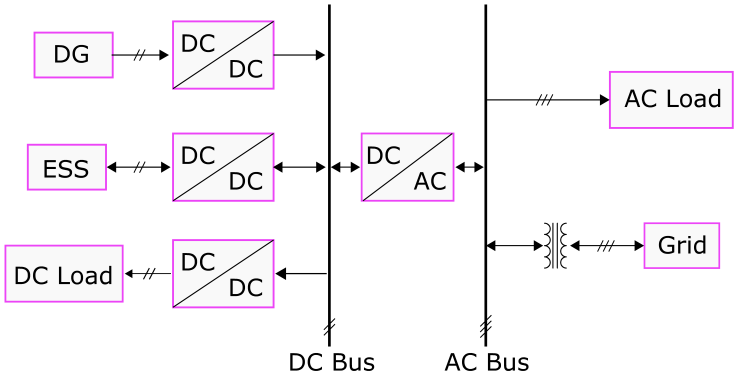

Figure 2-6: Hybrid Microgrid

The concept of AC microgrid with control method is discussed in [31], in [32] the design and control of DC microgrid are stated and in [33] hybrid AC-DC microgrid system which is the joint of AC and DC microgrid connected through an interlink AC/DC bidirectional converter is mentioned. A different hybrid AC-DC microgrid topology is given in [34]and a new alternative topology is presented in [35] which offers the advantage of controllability and flexibility by reducing the effect of distributed generations and microgrid in the utility grid. A detailed comparison of AC microgrid and DC microgrid is presented in [36].

2.2.4 Control features of Microgrid

For reliable, safe, and economical operation, the desirable traits of MG are as following:

- The MG should follow the reference voltage and current values in all of its units to damp the oscillations which are produced through variation of distributed energy resources(DER) output, load disturbances, and fault conditions [37, 38].

- Without any deviations and active power imbalances, all DER units must ensure to regulate and maintain their voltage and frequency setpoint [39].

- In order to cope with load frequency variation and sudden imbalance in power, it is needed to develop proper demand-side management and active participation of the customer. For proper and reliable operation of the MG, critical and non-critical load identification and proper control via load shedding or shifting is crucial [40, 41].

- For risk-free control and management, a fast islanding technique is important to develop in MG [42].

- For cost-effective, reliable operation of MG and to ensure the continuity of service in isolated MG infrastructure, economic dispatch, forecasting of generation for DER, and power prediction for loads are vital in MG control [43].

2.3 Distributed Generation

Distributed generation (DG) refers to a variety of technologies that generate electricity at or near where it will be used. It may serve a single structure, such as a home or business, or it may be part of a microgrid. DG, which is decentralized and has more flexible technologies, has to be connected with the low voltage side feeder in MG, as their rated power is 10 MW or less which is lower compared to the conventional generation plants. It can help support the delivery of clean, reliable power to additional customers and reduce electricity losses along transmission and distribution lines. There is no consistent definition of DG, the relevant issues, and aims about providing a general definition of DG in [44].

Distributed energy resources (DER) system typically use renewable energy sources (RES), including small hydro, biomass, biogas, solar power, wind power, and geothermal power. These resources play an important role in the electric power generation system. A grid-connected energy storage system can also be classified as a DER system. The energy resources which are related to renewable energy sources have in-

termittent behavior due to variation of the weather conditions. Therefore, they have to be interconnected with other dispatchable sources and energy storage to guarantee the continuity and reliability of the power supply within the MG during islanded mode and even when it is connected to the grid to protect power outage in case of failure from the main grid.

Renewable distributed resources require a power electronic interface to interconnect with the main grid, decoupling the primary energy source, and to operate in maximum power point tracking mode (MPPT), if required, to increase the efficiency to its maximum value. A large number of semiconductor equipment, stochastic nature of the RES generation, and bi-directional power flows are the main features of MG with DG. Analysis of power quality indicators and required solutions to reduce the negative impact of distributed generation on power quality in MG are presented in [45].

Where the renewable sources are highly unpredictable or the available renewable energy technology is not matured enough for reliable operation, non-renewable distributed resources are used to generate electricity. The size of non-renewable distributed generators is much lesser than large-scale stand-alone conventional power plants, so the pollutant emissions and fuel costs are lesser compared with conventional ones [46].

Non-renewable distributed generators are used as dispatchable generations and their operation is based on combustion of fossil fuels and electromechanical energy conversion through electric generators.

The most commonly used non-renewable sources are diesel and spark ignition reciprocating internal combustion engines, fuel cells (including solid oxide, molten-carbonate, phosphoric acid, alkaline, and low-temperature proton exchange member), gas turbines combined heat and power (CHP) units, and micro-turbine driven by biogas, propane or natural gas [47]. DG is offering various advantages including reduction of voltage fluctuation, increase reliability, improvement of power quality, reduction of energy cost, and increase of customer satisfaction. The advantages and drawbacks of both renewable and nonrenewable distributed energy resource technologies are explained in [47].

2.4 Energy Storage System

Despite all the benefits associated with DG in power systems, the interconnection of DG with the utility grid leads to some crucial problems such as changing the protection setting, power system stability, and islanding phenomena. Employing most of the RES as DG leads to the main challenges: changeability and uncontrollability of output power.

Indeed, these challenges offer additional fears in DG application in the power system. The use of an energy storage system (ESS) is one of the most appropriate solutions in this area. ESS is playing a vital role to solve the problems related to the intermittent behavior of renewable sources and increase their efficiency and usage. It increases the continuity and reliability of the system and decreases the dependency on dispatchable generations [48].

To overcome the limitations of renewable energy sources, electrical energy storage (EES) is using in MG systems. EES is a process that converts electrical energy from a power network into a form that can be stored and transformed back to electrical energy when needed [49]. Multiple attractive functions of EES to power network operation and load balancing is presented in [50].

2.4.1 Energy Storage System Configuration

Basically, the ESS for MG can be configured in two ways, aggregated and distributed ESS as depicted in [51].In the aggregated ESS, a constant power flows from the DER system to the point of common coupling (PCC), so the total capacity of this ESS is applied to assuage power flow fluctuations [52]. But the cost of energy storage devices increases with their capacity as well as manufacturing and controlling large ESS are difficult. Thus, to attain reliable and effective power regulation, small-scale distributed energy storage can be used.

In distributed energy storage configuration, ESS devices are directly connected to specific distributive sources with numerous interfaces. However, in this configuration controlling power flow is the main challenge faced by the distributed system and also

the storage process suffers losses through power electronic interfaces for distributed resources and ESS [53].

Figure 2-7 demonstrates a typical ESS configuration.

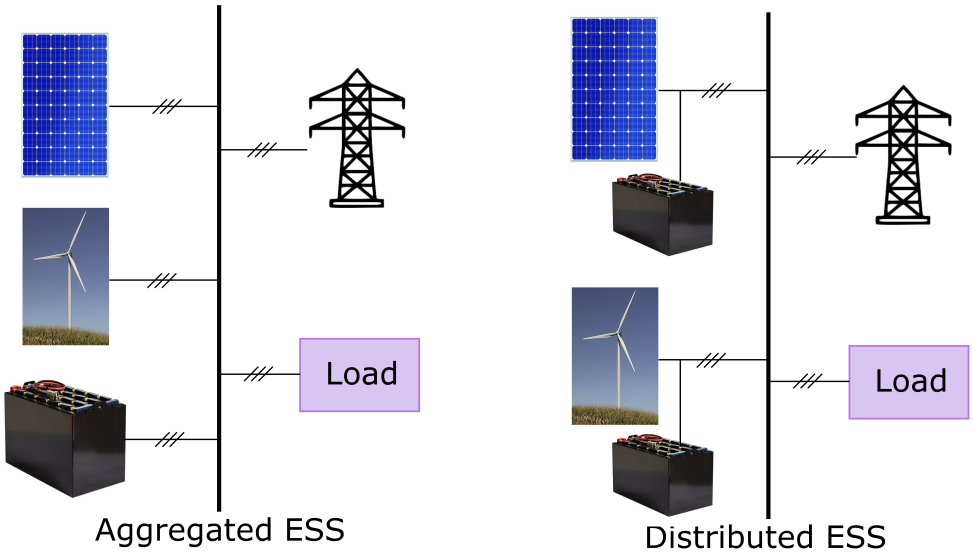

Figure 2-7: Typical ESS configuration

2.4.2 Structures of Energy Storage System

The process of energy-storing is done through transforming electrical energy into another form such as chemical or mechanical energy [54]. The storage systems can be categorized into three parts, which are central storage, power transformation stage, and control stage. The energy is stored in the central storage after conversion. The power transformation stage acts as an interface between the central storage and the power system, where power can transfer bidirectionally.

The level of charge or discharge of the stored energy is determined in the control stage. The determination is done by the use of sensors and other measuring devices [55]. Energy storage devices encounter losses at every step of the storing process, for that reason, they are not the ideal source of energy [54]. The following formula describes

the energy output and energy loss of the stored devices [55].

$$E_{generate} - \Delta E_{loss} = E_{out}\Delta E_{loss} = \Delta E_{ch} + \Delta E_{st} + \Delta E_{disch} \tag{2.1}$$

The total energy storage efficiency can be written as

$$\eta_{st}^{total} = \frac{E_{out}}{E_{generate}} = \eta_{ch} \times \eta_{st} \times \eta_{disch} \tag{2.2}$$

where $\eta_{ch} = \frac{E_{st}}{E_{ch}}$, $\eta_{st} = \frac{E_{st}^*}{E_{st}}$ and $\eta_{disch} = \frac{E_{st}^*}{E_{disch}}$. η_{ch}, η_{st} and η_{disch} are the efficiency of the charge, store and discharge periods, respectively.

Here ΔE_{loss} is the total energy loss and ΔE_{st}, ΔE_{ch}, and ΔE_{disch} are the energy loss during storage, charge and discharge periods, respectively.

The stored energy in the central part is denotes by E_{st} and the existing energy from the same part is represented by E_{st}^*. The generated, output, charging and discharging energy is represented by $E_{generate}$, E_{out}, E_{ch}, and E_{disch}, respectively.

2.4.3 Energy Storage Systems Technologies

The classification of ESS widely depends on the form of converted energy and composition materials. There are mainly six categories which are chemical, electrochemical, electrical, mechanical, thermal and hybrid energy storage.

Mechanical energy storage system, where the energy is stored in the form of kinetic or potential energy [56–58]. The energy is stored in the form of electrostatic or magnetic fields in the electrical energy storage system [57] and [59, 60]. When some chemical substances are subjected to a transformation through a chemical reaction, energy can be stored and recovered, which is known as chemical energy storage system [59–61].

Electrochemical energy storage system is a particular case of chemical energy storage, in which reversible chemical reactions in a combination of cells are used to store electrical energy [57, 62].

Figure 2-8 demonstrates the classification of ESS depending on the physical form in which the energy is stored.

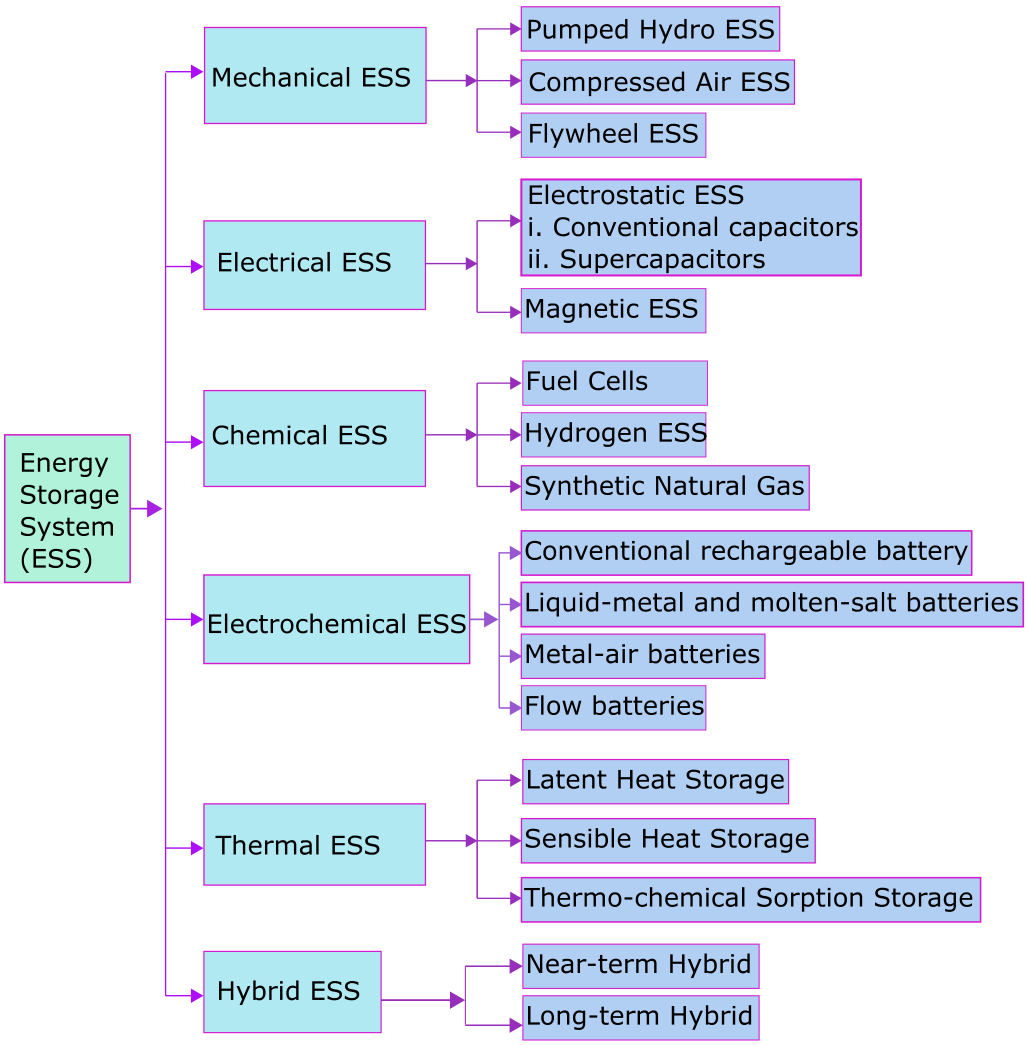

Figure 2-8: Classification of ESS technologies

The most frequently used storage technologies for MG applications are batteries [63], compressed air energy storage [64], flywheel energy storage [65],super capacitor energy storage [66], superconducting magnetic energy storage [67], hydrogen storage [68]and hybrid energy storage [69].

2.5 Energy Management System

For the optimal use of distributed energy resources in intelligent, secure, reliable, and coordinated ways, an energy management system (EMS) is essential for MG. A

microgrid EMS is the control software that operates based on the real-time operating conditions of MG components and the system status to optimally allocate the power output among the DG units, economically serve the load, and automatically enable the system resynchronization response to the operating transition between interconnected and islanded modes. To provide high-quality, reliable, sustainable, and environmentally friendly energy cost-effectively, a sophisticated microgrid EMS has to operate and coordinate a variety of DGs, DERs, and loads [70].

A definition of EMS is in [71], which is provided by the International Electrotechnical Commission in the standard IEC 61970. An MG EMS has the same features related to that definition, consists of modules to perform decision-making strategies. The efficient implementation of EMS decision-making strategies is done through modules of DERs/load forecasting, Human Machine Interfaces(HMI), and supervisory, control, and data acquisition (SCADA) by sending optimal decisions to each generation, storage, and load units [72].

2.5.1 Control Structure of EMS

The supervisory control structure of MG EMS is mainly two types, such as centralized EMS and decentralized EMS. In centralized EMS, all the information including power generation of DERs, cost-function, meteorological data, and energy consumption pattern of each consumer is accumulated by the central controller. After accumulating information, centralized EMS determines the optimum scheduling of MG and sends these decisions to all local controllers. In decentralized EMS architecture, sending and receiving all the information to local controllers are done by MG central controller in real-time. In this architecture, the optimal scheduling is determined by MG central controller. MG EMS strategies have been diversified with the integration of renewable energy resources, ESS, electric vehicles, and demand response from economic dispatch and unit commitment. Scheduling of DERs and loads, minimization of system losses and outages, control of intermittency and volatility of renewable sources, and realization of economical, sustainable, and reliable operation of MG are the other strategies of EMS [71].

2.5.2 Solution Approaches of EMS Strategies

Energy management strategies have been solved by many researchers using various solution approaches to achieve the optimal and efficient operation of MG. Several methods have been used for the critical analysis of MG EMS. Linear programming method used to achieve the best outcome of a mathematical model which requirements are in a linear relationship and nonlinear programming methods, used for optimization problem solving with nonlinear constraints. Different approaches have been proposed based on linear and nonlinear methods in [73–80]. The rule-based approach is presented in [81] for central EMS controls for the energy operation of whole MG, in [82] for a battery state of charge (SOC)-based hierarchical structure with ultra-capacitors for power regulation and smooth operation of MG. Battery SOC rule-based approach is presented in [83] to reduce fluctuations in power transactions with the main grid. Genetic optimization-based EMS is demonstrated in [84] for optimal operation of MG and in [85] is to increase battery life cycle together with the operational cost model of MG. Critical analysis of MG EMS based on the fuzzy logic method is presented in [86–89]. Neural network method-based solution approaches for overall cost minimization of MG and maximum utilization of renewable energy resources and distributed resources, battery lifetime improvement and reduction of carbon emissions are presented in [90] and [91], respectively. Multi-agent system based EMS for microgrid is represented in [92], [93] and [94]. EMS for the cost minimization of battery degradation and energy trading in [95] and for maximizing MG profit by scheduling controllable resources including a risk constrained scenario in [96] are based on stochastic programming method. Robust optimization solution approaches for MG EMS is presented in [97] and [98].

Chapter 3

Development of Energy Management System for Energy Communities Application

3.1 System Configuration

The EMS is used to maintain power flow through a grid-connected MG system based on the available power from the PV generation, utility grid, ESS, and load. The power flow control is managed by considering the tariff profile, solar irradiance forecasting, and load demand. As the EMS is designed for EC application, the MG system operates on grid-connected mode, AC microgrid system has been considered for the development of the EMS. AC MG connects the various energy generation sources and loads in their network using an AC bus system. The following advantages of AC MG emphasize the reason for choosing the AC MG system.

- Capability of integrating with the conventional utility grid and A-based loads.
- No inverter requirement for utility grid and AC loads.
- Cost efficiency in the power protection systems.
- Higher load availability for AC loads.

As the power flow through the ESS is bidirectional, the buck-boost converter is connected between the AC bus of the MG and ESS, so that the voltage can step up during the discharging period to flow the power from ESS to the load and step-down during the charging period as the power is flowing to the ESS. The boost converter is connected between the PV system and AC bus, to boost the voltage level, as the power flow from the PV system is unidirectional.

Figure 3-1 demonstrated the EMS configuration for energy communities application.

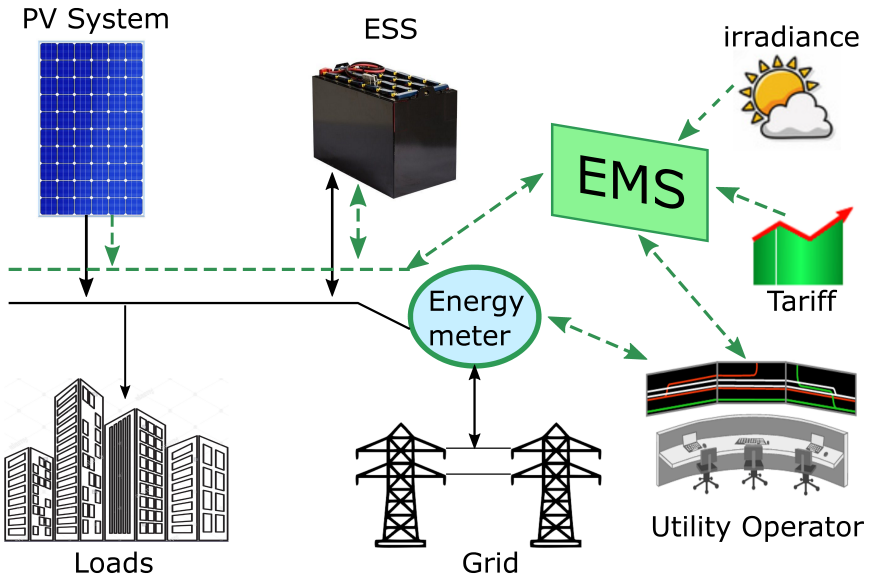

Figure 3-1: Energy management system layout

The following sections are describing all the assumption and consideration has made for the design of the PV and ESS along with the capital cost.

3.2 Design of Photovoltaic System

A grid-connected photovoltaic (PV) system, has been designed to analyze the proposed EMS, which is an electricity generating solar PV power system connected to the utility grid. The installation of a PV system depends on the load demand and the availability of solar radiation on the specific site. So, depending on the load demand

and geographical location, the installation of the PV system has done for 10 kWp. The peak value of each PV module used for the installation is 250 W, so a total 40 PV module is used for the PV system installation. The total number of PV modules is obtained by dividing the PV system maximum power by the PV module maximum power and then taking the round of the nearest integer number. An inverter with rated power 5 kW is used to connect the PV system with the AC bus of the MG. The number of inverters for the PV installation is obtained by dividing the PV system nominal power by the inverter nominal power and then rounding this to the nearest integer number.

Mono-crystalline PV module manufactured by SUN POWER X-SERIES SOLAR PANELS is used to analyze the system. The capital cost of the PV panel including the inverter is 750 €/kWp, so the total capital cost of the PV system is $(750 \times 10) = 7500$ €. The installation of the PV system is 2500 €/kWp, so the required installation cost is 25000 €. Additionally, the operation and maintenance of the PV system are considered as 10 € per kWp.

The maximum power output P_{max} of the PV modules depends on the two most important environmental conditions: global plane-or-array irradiance 'G' and operating cell temperature 'T'. The deviation of the module efficiency $\Delta\eta_{rel}(G,T)$, describe the dependence of output power, at the given conditions G and T relative to the value at the corresponding reference conditions G_{ref} and T_{ref} based on equation (3.1)

$$\Delta\eta_{rel}(G,T) = \frac{P_{max}(G,T)}{P_{max,ref}} \cdot \frac{G_{ref}}{G} - 1 \tag{3.1}$$

where $P_{max,ref}$ is the maximum power output at the reference conditions. The standard conditions (STC) is taken as $G_{ref} = 1000\ W/m^2$, $T_{ref} = 25°C$ [99]. The calculation of PV power can be done considering temperature effect or excluding temperature effect, equation (3.2) and (3.3) shows the relation, respectively.

$$P_{pv} = P_{max,ref} \cdot G \cdot \frac{df}{G_{ref}}(1 + \gamma(T - 25)) \tag{3.2}$$

$$P_{pv} = P_{max,ref} \cdot G \cdot \frac{df}{G_{ref}} \tag{3.3}$$

where P_{pv} is the output power of PV, $P_{max,ref}$ is the PV output power at STC, df is the degradation factor, γ is module temperature coefficient in $\%/\circ C$. The output power of the PV module depends linearly on the operation temperature, so the PV power including temperature effects is considered.

3.3 Design of Energy Storage System

Li-ion battery is used as the ESS of the MG to storage energy from the renewable generation. To design the ESS, eBick180 battery module is used in this work. Table 3.1 represents eBick180 battery module details.

Table 3.1: eBick180 battery cell data

Parameter	Value	Comment
$C_{c_{nom}}$	180	cell rated capacity[Ah]
$V_{c_{nom}}$	3.2	cell rated voltage[V]
$V_{c_{max}}$	3.65	cell charging upper limit voltage[V]
$V_{c_{min}}$	2.5	cell charging lower limit voltage[V]
$I_{c_{chr}}$	1	maximum charging current [1C]
$I_{c_{dschr}}$	1	maximum discharging current [1C]
SoC	[10 90]	recommended SoC limits[%]
R_{C_s}	$0.6e^{-3}$	maximum internal resistance [Ω]
$Tmax_{chr}$	45	maximum temperature charging
$Tmax_{dschr}$	55	maximum temperature discharging

The ESS is designed by using the data from Table 3.1 and multiplying the voltage parameters by the number of series cells ($n_{sc} = 15$), the current capacity parameters by the number of parallel cells ($n_{pc} = 1$) and then calculating the energy parameters and the total internal resistance of the ESS.The maximum, minimum and nominal

voltage, nominal capacity of the battery module can be obtained as:

$$Cb_{nom} = C_{c_{nom}} \cdot n_{pc}$$

$$Vb_{nom} = V_{c_{nom}} \cdot n_{sc}$$

$$Vb_{max} = V_{c_{max}} \cdot n_{sc}$$

$$Vb_{min} = V_{c_{min}} \cdot n_{sc}$$

where $V_{c_{nom}}$ and $V_{b_{nom}}$, $V_{c_{max}}$ and $V_{b_{max}}$, $V_{c_{min}}$ and $V_{v_{min}}$ represents cell and battery nominal, maximum and minimum voltage, respectively. Additionally, $C_{c_{nom}}$ and $C_{b_{nom}}$ stands for cell and battery nominal capacity, respectively. The maximum charging, discharging and nominal current, nominal power and internal resistance of the battery module is calculated as follows:

$$Ib_{nom} = C_{c_{nom}} \cdot n_{pc}$$

$$Ib_{chr} = I_{c_{chr}} \cdot Ib_{nom}$$

$$Ib_{dschr} = I_{c_{dschr}} \cdot Ib_{nom}$$

$$Rb_s = Rc_s \cdot \frac{n_{sc}}{n_{pc}}$$

$$Eb_{nom} = V_{b_{nom}} \cdot Ib_{mon}$$

where Ib_{nom}, Ib_{chr}, and Ib_{dschr} represents battery nominal, maximum charging and discharging current, respectively. Rc_s and Rb_s stands for cell and battery internal resistance, respectively. Eb_{nom} is the battery nominal energy. The following formula is used to calculate the maximum and minimum capacity and energy of the battery:

$$Cb_{max} = Cb_{nom} \cdot \frac{SoC_{max}}{100}$$

$$Cb_{min} = Cb_{nom} \cdot \frac{SoC_{min}}{100}$$

$$Eb_{max} = Eb_{nom} \cdot \frac{SoC_{max}}{100}$$

$$Eb_{min} = Eb_{nom} \cdot \frac{SoC_{min}}{100}$$

where Cb_{max}, and Cb_{min} are maximum and minimum capacity of the battery,respectively and Eb_{max}, and Eb_{min} are the maximum and minimum energy of the battery, respectively. To keep the module voltage of the battery model at 48 V, need to make the energy demand four times the energy capacity of the battery. So, to satisfy the energy demand of the ESS, four battery modules is connected in parallel (n_{pm}) and one module in series (n_{sm}).

The ESS parameters of the system are presented in Table 3.2, where all the parameters are calculated based on the above formulas by replacing n_{sc} and n_{pc} by n_{sm} and n_{pm}.

Table 3.2: Energy storage system parameters

Parameter	Value	Comment
$C_{b_{nom}}$	720	ESS rated capacity[Ah]
$V_{b_{nom}}$	48	ESS rated voltage[V]
$V_{b_{max}}$	54.75	ESS charging upper limit voltage[V]
$V_{b_{min}}$	37.5	ESS charging lower limit voltage[V]
$I_{b_{chr}}$	720	ESS maximum charging current
$I_{b_{dschr}}$	720	ESS maximum discharging current
SoC	[10 90]	recommended ESS SoC limits[%]
R_{b_s}	$0.9e^{-3}$	ESS internal resistance [Ω]
$E_{b_{nom}}$	34.56	ESS nominal energy[kWh]
$E_{b_{max}}$	31.104	ESS maximum energy[kWh]
$E_{b_{min}}$	3.456	ESS minimum energy[kWh]

The capital cost of the battery including the inverter is 500 €/kWh. So, the total capital and installation cost of the ESS with 34.56 kWh of nominal energy is 17280 €. The operation and maintenance cost of the ESS per kWh of energy is 10 €.

3.3.1 ESS Parameters Calculation

The initial SoC_o is take as 50% and the initial battery capacity is calculated as:

$$C_{initial} = \frac{SoC_o}{100} \cdot Cb_{nom}$$

The calculated initial battery capacity is 360 Ah. In addition, the battery voltage during the open circuit is obtained by interpolating the voltage and capacity of the cell and then multiplying by the number of series and parallel cells. The battery rated voltage is the same as the open-circuit voltage value during the initial condition. The battery rated voltage is calculated by equation (3.4).

$$V_b(t) = Vb_{oc}(t) - V_{rs}(t) \tag{3.4}$$

where $Vb_{oc}(t)$ is open circuit voltage and $V_{rs}(t)$ is the voltage drop. Equation (3.5) and (3.6) represent the voltage drop and current $I_b(t)$ of the battery, respectively.

$$V_{rs}(t) = I_b(t-1) \cdot Rb_s \cdot (n_{sm} \cdot n_{pm}) \tag{3.5}$$

$$I_b(t) = \frac{P_b(t)}{V_b(t)} \tag{3.6}$$

The power,SoC and capacity of the ESS system are obtained form equation (3.7), (3.8) and (3.9), respectively.

$$P_b(t) = P_l(t) - P_g(t) - P_{pv}(t) \tag{3.7}$$

$$SoC(t) = \frac{C(t)}{Cb_{nom} \cdot 100} \tag{3.8}$$

$$C(t) = C(t-1) + I_b(t) \cdot \frac{T_s}{3600} \tag{3.9}$$

where $P_b(t)$, $P_l(t)$, $P_g(t)$ and $P_{pv}(t)$ are battery power, load power, grid power and PV power, respectively. $C(t)$ is the capacity of the ESS and T_s is the time step.

3.4 Tariff Profile

The tariff profile is used to decide the proposed EMS. The instantaneous tariff value is used in the EMS. Additionally, the system is considering feed-in-tariff (FiT) and minimum tariff value as the input data to make the decision. FiT is the tariff value to sell energy to the grid, here the FiT value is chosen based on the maximum and minimum tariff values of the day. FiT is a variable from time to time-based on the market price. In the EMS, FiT is considered as a level of the tariff profile where the buying of the electric power from the grid will be done if the instantaneous tariff is lower than FiT, and PV energy will sell if the tariff is equal to or higher than FiT. The real-time tariff profile of Spain is collected from the OMIE website [100], which is the nominated electricity market operator. It manages the day-ahead and intraday wholesale electricity markets.

3.5 Cost Calculation for EC

The energy cost calculation is done to justify the effectiveness of the proposed EMS for the EC application. The costing of the system is done for both power buying from the grid and selling to the grid. Also, the Levelized cost of energy (LCOE) of the system is considered for effective analysis. In all the simulations the cost analysis has been done for three different system combinations, one is the base system case where the load power is coming from the utility grid, another one is the PV only case where the system is considered with PV system only without considering ESS and finally the last one is the hybrid system where the system is considering both PV generation and ESS.

3.5.1 Calculation of the Levelized Cost of Energy

Levelized cost of energy (LCOE) is calculated for the system to get the final cost of energy. LCOE is an economic assessment of the average total cost to build and operate a power-generating asset over its lifetime divided by the total energy output

of the asset over that lifetime. It also can be regarded as the minimum cost at which electricity must be sold to achieve break-even over the lifetime of the project.
The general equation for LCOE [101, 102] is given in equation 3.10.which is the ratio of life cycle cost of the system to the lifetime energy production of the system.

$$LCOE = \frac{\text{Life cycle cost(\$)}}{\text{Life time energy production(kWh)}} \tag{3.10}$$

For the calculation of the LCOE, two methods are commonly used, known as the discounting method and the annuitizing method. The details of these two types of LCOE calculation are presented in [103].
Though, those two methods provide the same Levelized costs, annual energy out for the annuitizing method needed to be constant over the lifetime of the device. But, the annual energy output of renewable technologies would typically vary from day-to-day, because renewable resources depend on the environment. Therefore, the discounting method is more appropriate for calculating the LCOE for renewable sources than the annuitizing method.
The methodology of properly calculating the LCOE for solar PV is presented in [104]. Equation 3.11 is used to calculate the LCOE for a PV system:

$$LCOE = \frac{\sum_{t=0}^{n} \frac{(I_t+O_t+M_t+F_t)}{(1+r)^t}}{\sum_{t=0}^{n} \frac{E_t}{(1+r)^t}} = \frac{\sum_{t=0}^{n} \frac{(I_t+O_t+M_t+F_t)}{(1+r)^t}}{\sum_{t=0}^{n} \frac{S_t(1-d)^t}{(1+r)^t}} \tag{3.11}$$

where I_t is the initial investment, which is the one-off payment and should not be discounted. M_t, O_t, and F_t are the maintenance costs, operation costs, and interest expenditures for time year t, respectively. The electricity generated in a given year E_t is the rated energy output per year St multiplied by the degradation factor (1-d) which decreases the energy with time. n is the lifetime of the system and r is the discount rate.
The Levelized cost of storage (LCOS) is calculated by deducting the cost of charging electricity from the LCOE delivered by the electrical energy storage (EES) which is

presented in equation (3.12) [105].

$$LCOS = LCOE - \frac{\text{Price of charging power}}{\text{Overall efficiency}} \tag{3.12}$$

The formula for the LCOS is proposed by the World Energy Council in equation (3.13), which enables the comparisons between between different types of storage technologies in the terms of average cost per produced and stored kWh.

$$LCOS = \frac{I_o + \sum_{t=1}^{n} \frac{C_{EES_t}}{(1+r)^t}}{\sum_{t=1}^{n} \frac{E_{EES_t}}{(1+r)^t}} \tag{3.13}$$

where I_o is the initial investment cost. C_{EES_t} and E_{EES_t} are the total cost and energy output at year t respectively. The methodology for the calculation of LCOE for a PV and ESS based hybrid system is presented in [106]. LCOE relationship for the hybrid system is presented in (3.14)

$$LCOE_{system} = \frac{\sum_{t=0}^{n} \frac{C_{system_t}}{(1+r)^t}}{\sum_{t=0}^{n} \frac{E_{system_t}}{(1+r)^t}} \tag{3.14}$$

C_{system_t} and E_{system_t} are the total cost and total energy production from the system at time t respectively.

The total cost of the renewable system is the sum of PV electricity generation and storage costs. The total electrical energy produced by the system is the electrical energy output of ESS and the electrical energy directly delivered to the load by PV. The $LCOE_{system}$ considering the cost of PV and ESS, is presented in (3.15).

$$LCOE_{system} = \frac{C_{pvsurplus} + C_{ESS} + C_{pvdirect}}{E_{ESS} + E_{pvdirect}} \tag{3.15}$$

Figure 3-2 presents the energy flow diagram of the PV power flow to the load, grid and ESS of the hybrid system. As the additional PV power generation is using for both battery charging and selling to the utility grid, the power flow shows that $E_{surplus}$ is going to both ESS and grid.

The surplus PV power, which is selling to the grid, is not considering for the LCOE calculation of the system. On the other hand, the surplus PV power, using for battery charging, is utilizing for the LCOE calculation considering round-trip efficiency of the ESS.

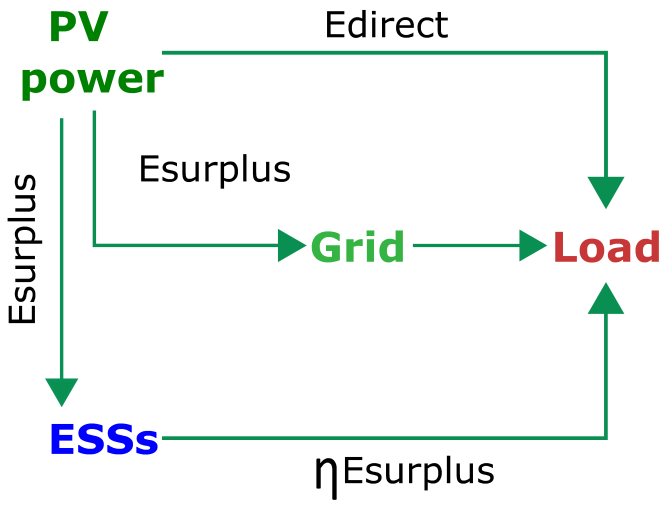

Figure 3-2: Energy flow diagram of the system

In this consideration, the total PV energy produced by the PV system is divided into two parts, known as surplus energy and direct energy. Surplus energy is the extra electricity generated by the PV system and not consumed by the load, which can be stored in the ESS, denoted by $E_{pvsurplus}$. Direct electrical energy, referred to as direct energy $E_{pvdirect}$, is the electrical energy consumed by the load directly. $C_{pvsurplus}$ and $C_{pvdirect}$ are the costs for generating surplus energy and direct energy respectively. The ESS experiences the electrical energy flowing in and flowing out. The energy delivered by the ESS will be reduced due to the round-trip efficiency η. Equation (3.16) to (3.20) are used for the LCOE calculations.

$$C_{ESS} = C_{cap_{ESS}} + \sum_{t=0}^{n} \frac{C_{OM_{ESS}}}{(1+r)^t} \tag{3.16}$$

$$E_{ESS} = \eta \cdot \sum_{t=0}^{n} \frac{E_{surplus_t} \cdot (1 - D_{ESS})^t}{(1+r)^t} \tag{3.17}$$

$$C_{pvsurplus} = (C_{cap_{pv}} + C_{Inst_{pv}} + \sum_{t=0}^{n} \frac{C_{OM_{pv}}}{(1+r)^t}) N_{surplus} \tag{3.18}$$

$$C_{pvdirect} = (C_{cap_{pv}} + C_{Inst_{pv}} + \sum_{t=0}^{n} \frac{C_{OM_{pv}}}{(1+r)^t}) N_{direct} \tag{3.19}$$

$$E_{pvdirect} = \sum_{t=0}^{n} \frac{E_{direct_t}(1-D_{pv})^t}{(1+r)^t} \tag{3.20}$$

E_{direct} is the electricity generated from PV and directly supplied to the load without going through storage and $E_{surplus}$ is the electricity generated from PV and stored to the ESS to avoid wastage.$C_{pvsurplus}$ and $C_{pvdirect}$ are the total lifetime costs of PV electricity generation that produce the surplus and direct consumption of electrical energy for the system respectively. E_{ESS} is the energy output of the ESS and C_{ESS} is the total cost of the ESS.

D_{ESS} and D_{PV} are the annual performance degradation rates for the ESS and the PV array respectively.N_{direct} and $N_{surplus}$ are the fraction of PV array for generating electricity for direct consumption and surplus energy for storage respectively. $C_{cap_{pv}}$, $C_{Inst_{pv}}$, and $C_{OM_{pv}}$ are the capital cost, installation cost, and operation and maintenance cost of the PV system respectively. $C_{cap_{ESS}}$ and $C_{OM_{ESS}}$ are the capital and operation and maintenance cost of the ESS.

3.6 System Parameters with Capital Cost

Table 3.3 represents the summary of the system configuration along with capital cost. Where the capital cost of both PV system and ESS is the cost of PV panel and Li-ion battery along with the inverter respectively.

Table 3.3: System parameters

PV System Parameter	**Value**
PV power	10 [kWp]
Each module power	250 [W]
Capital cost of PV	7500 €
Installation cost of PV	25000 €
ESS Parameter	**Value**
Rated capacity	720 [Ah]
Rated voltage	48 [V]
Capital cost	17280 €

Chapter 4

Simulation and Modeling of Microgrid System

4.1 AC Microgrid System

The simulation of a grid-tied AC MG system has been done before the implementation of the EMS. The aim of the simulation is to understand the concept of power-sharing between load, ESS, and unity grid, also the simulation provides a clear view of power flow control. It demonstrates the working stages of the MG system. The simulation of the AC microgrid system is done in MATLAB Simulink®.

As the AC microgrid system is considered to implement the EMS for the EC application, the simulation of the MG is also implemented for the AC MG system where the power flow controlling is based on AC bus controlling. The design of the AC MG system is done by connecting the distributed generation and energy storage system to the AC bus through the inverter, while the load is directly connected to the AC bus. The grid-tied MG system consists of a PV solar panel, a Li-ion battery as the ESS, local load, and the utility grid. Figure 4-1 shows the design of grid-tied system. The simulation of this grid-tied system is done using PV array block as the PV generation system, where the PV array is used to design 10 kWp like the PV system designed for implementation of the EMS. The PV array block generates PV power considering solar irradiance and temperature. Battery block is used to represent the Li-ion battery

as the energy storage system. In the first stage of the simulation, three-phase pulse width modulation (PWM) based switching model DC-AC inverter is used to connect the PV generation and energy storage system with the AC bus bar. A three-phase ac load with a fixed value and three-phase supply is used as domestic load and the utility grid respectively, which is connected with the AC bus.

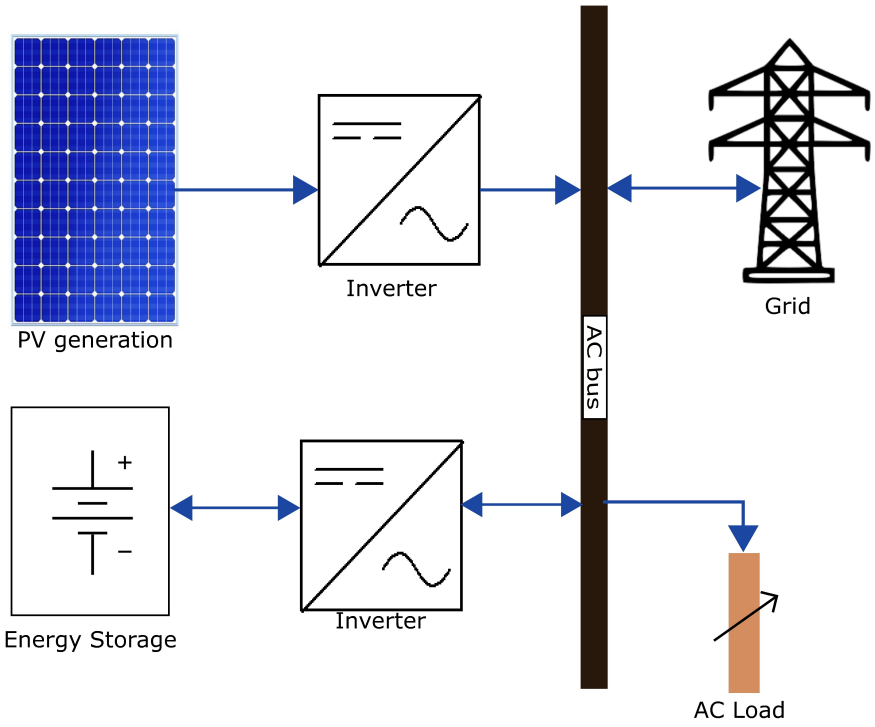

Figure 4-1: Layout of the grid-tied system

A grid-tied inverter is used to convert the DC power to AC, where a sinusoidal pulse width modulation technique is used for the inverter switching. The PWM signals have been generated using a triangular carrier signal with 15 kHz carrier frequency. In the beginning stage, this simulation of the AC microgrid system has been done without considering power flow controlling. The purpose of this simulation was to visualize the grid-tied system, which is going to be considered for the EMS power flow control. This simulation model presents the overall scenario of the AC MG system.

4.2 Average Model Inverter and Current Controller

The objective of using an average model inverter is to reduce the simulation complexity and to get a faster response, which also maintains sufficient dynamic accuracy by keeping the same average V-I terminal relationship on the AC and DC sides. Based on the controller functionality average model is identical to the switching model, while the power stage shows the only key difference. To emulate inverter behavior, three single controlled voltage sources are used in the three-phase average model inverter instead of using a three-phase voltage source inverter component like switching mode. Figure 4-2 shows both the switching model and average model inverter.

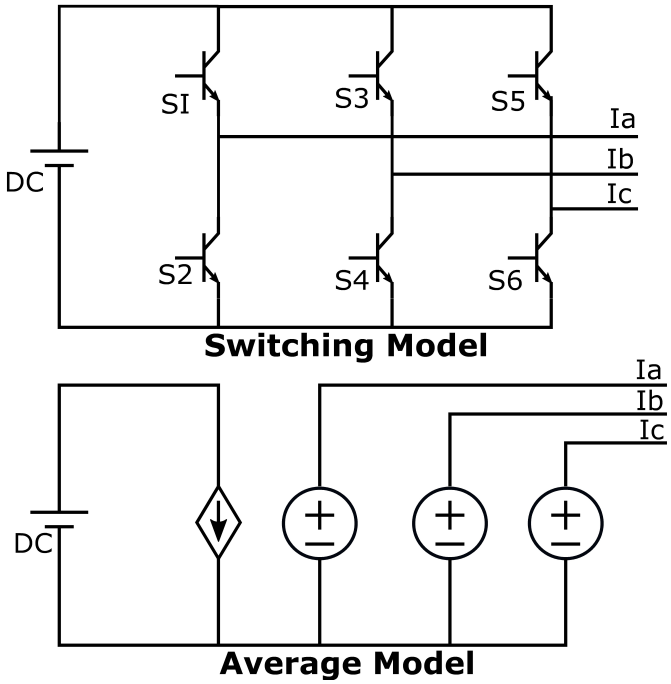

Figure 4-2: Switching model and average model inverter

The average model offers less numerical convergence problem, as the state variable of the model is averaged over the switching period. The topology and concepts of the average model inverter are presented in [107–109].

To make the simulation faster and less complicated, the PV panel and battery block have been replaced by the controlled voltage source. Where in the beginning constant value is used as the input of the controlled voltage source and later real-time data of

PV generation is used to analyze the system to get a real scenario.

At the beginning as the simulation has done without designing the controller, three sinusoidal reference signals with 120° phase shift have been used as the duty ratio to generate the voltage reference signal for the controlled voltage source of the average model. As the average inverter model contain the same average V-I terminal relationship on AC and DC side, the reference voltage and current signals for the controlled sources of the average model inverter are generated using the same duty signal which is generated from the controller.

The generation of the reference signals for controlled current sources and controlled voltage source has done based on equation (4.1) and (4.2) respectively, which balanced the V-I relationship between AC and DC side.

$$I_{ref} = I_{ac} \times dutysignal \tag{4.1}$$

$$V_{ref} = V_{dc} \times dutysignal \tag{4.2}$$

A standard control strategy, vector current controller has been designed for the controlling of the AC microgrid system. The design of a vector current controller is based on the synchronously rotating reference frame, which enables the PI controller to control the active and reactive powers indirectly. Since the synchronous rotating frame transforms the AC values to DC through coordinate transformation, active and reactive power control is performed through d-q axes current controlling. A phase-locked loop (PLL) is used to maintain the synchronization of d-q axes current with the grid voltage. PLL extracted the phase angle and frequency of the grid voltage and provides that as the phase angle for the Park transformation to generate the d-q axes current [110].

Figure 4-3 shows the diagram of a standard current controller. The controller has been designed to regulate the d-q axes current considering both feed-forward and feed-back. Tuning of the PI controller has been done by taking filter inductance as the plant of the system. The generated reference signal from the PI controller is used as the duty of the average model inverter.

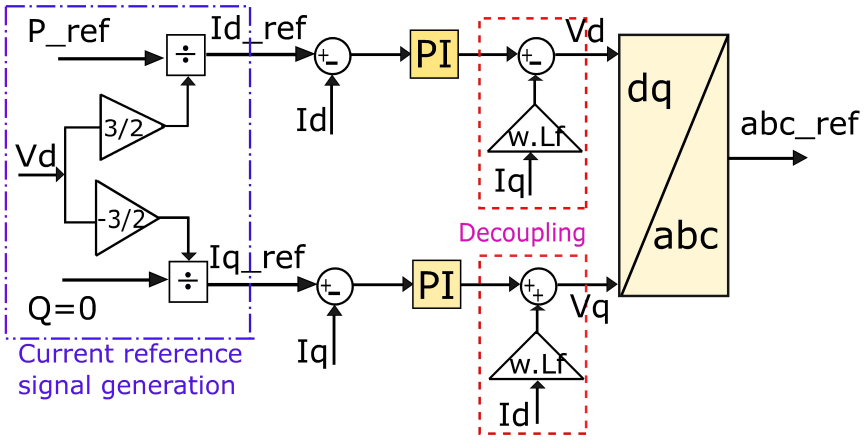

Figure 4-3: Vector current controller

The d-q axes currents reference signals have been generated by taking active and reactive power reference values. Since in the synchronous frame, d axes components are coincident with the instantaneous voltage vector and the q axes component is in quadrature with it [111]. The highlighted 'current reference signal generation' part of Figure 4-3, shows the generation of d-q current reference signals from the active and reactive power. Equations (4.3) and (4.4) define the active and reactive power relation in the d-q frame.

$$P = \frac{3}{2} V_d I_d \tag{4.3}$$

$$Q = \frac{-3}{2} V_d I_q \tag{4.4}$$

Two identical control systems have been designed for both inverters connected with the PV system and ESS.

4.3 Simulation Model and Results

The final simulation of the AC MG system has been done with the average model inverter and vector current controller to generate the duty signal for controlling the power flow through the MG system. Controlled voltage source is used to replace the PV array and battery block in the simulation model.

Table 4.1 shows the system parameters used for the simulation of the AC MG.

Table 4.1: Parameters used for simulation model

System Parameters	**values**
Grid voltage(V_{an})	400 V
Frequency(f)	50 Hz
PV power	$(8-15)$ kW
Load power	$(5-25)$ kW
Battery voltage	48 V
Battery SoC range	$[10-90]\%$
Inverter power	5 kW
Filter inductance(L_f)	7 mH
Filter resistance(R_f)	0.1 Ω
Control Parameters	**values**
Damping ratio(ζ)	0.707
Natural frequency(w_n)	$2\pi 300 rad/s$
K_p,T_i	$18.6, 1.33 \times 10^3$

4.3.1 PV Voltage Calculation

Before performing the simulation of the MG system, another simulation has done using solar cell block to calculate the PV voltage based on the solar irradiance and temperature data, so that the PV array block can be replaced with a controlled voltage source and the calculated PV voltage is used as the input of the controlled voltage source.

In this simulation the solar cell has been designed considering the PV plant capacity as discussed in section 3.2. Taking the solar irradiance and temperature data of the specific location, the simulation has been done to calculate the DC voltage of the PV system with the capacity of 10 kWp.The simulation has done with complete one-year data to get the PV voltage for one year.

Figure 4-4 shows the solar irradiance, temperature, and generated PV voltage for one year. The input is taken per minute to generate per minutes voltage, but the x-axis of the figure is represented in a year for better consideration.

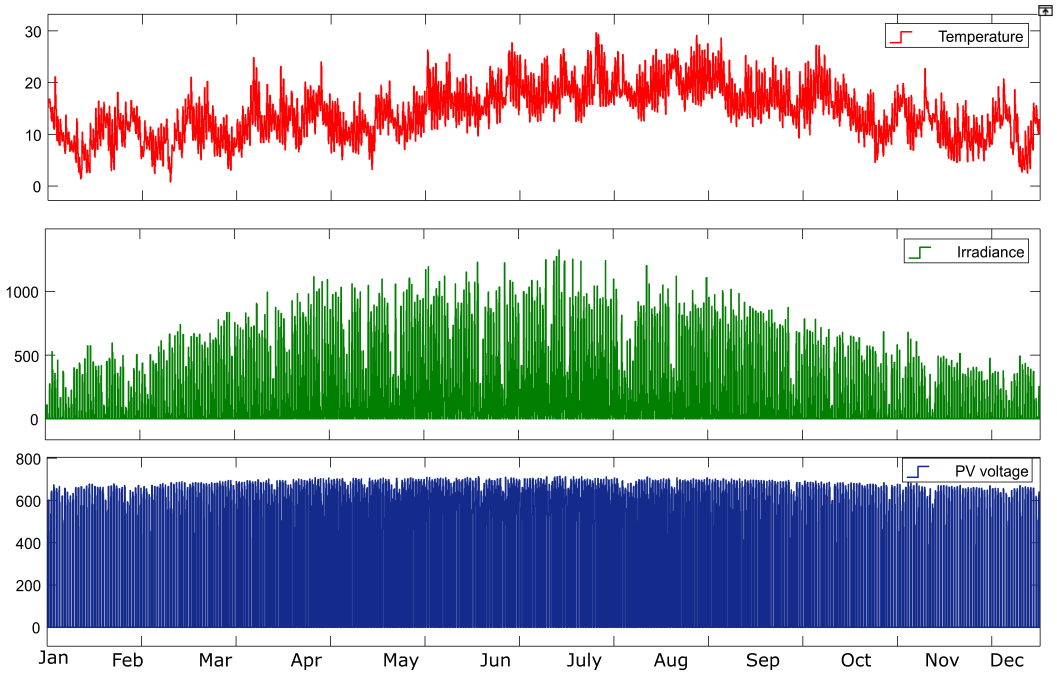

Figure 4-4: DC voltage of the PV system

The generated DC voltage of the PV system is used as the input data of the controlled voltage source that is representing the PV array in the simulation.

4.3.2 Load Current Calculation

Also, the three-phase constant value load is replaced by the three single controlled current sources, where the input of the controlled current source has been generated from the real-time load power data using equation (4.3) and (4.4) and then converting d-q component into abc current values. The subsection of the simulation is generating the three-phase load current to be used as the input of the controlled current source based on the per-minute load power real-time data.

Figure 4-5 shows the load power for the complete year, where the value is in minutes but the x-axis is representation in a year for better understanding.

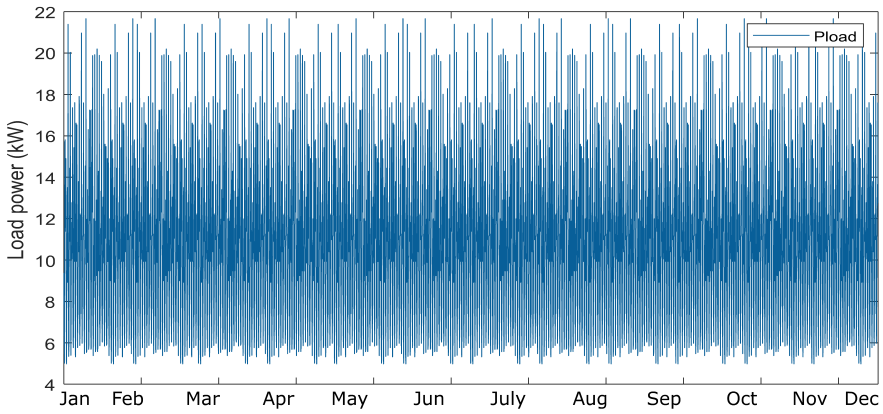

Figure 4-5: Load power of the whole year

4.3.3 Tariff Profile

Real-time tariff profile is used to perform the EMS algorithm. The tariff profile is collected from "OMIE" website. Here in this simulation the tariff profile of year 2020 is used.

Figure 4-6 shows the instantaneous tariff of 2020.

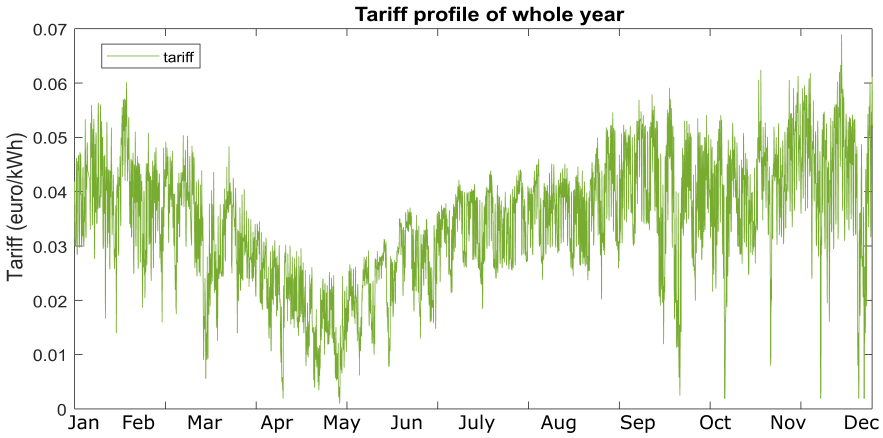

Figure 4-6: Tariff profile of year 2020

4.3.4 Simulation Model Layout and Controller Output

The simulation of the AC MG system is done with the average model inverter to connect the PV system and ESS with the AC bus. Where the PV array and battery

model are replaced by a controlled voltage source and the load is replaced by the controlled current source.

Figure 4-7 shows the simulation model of the AC MG system.

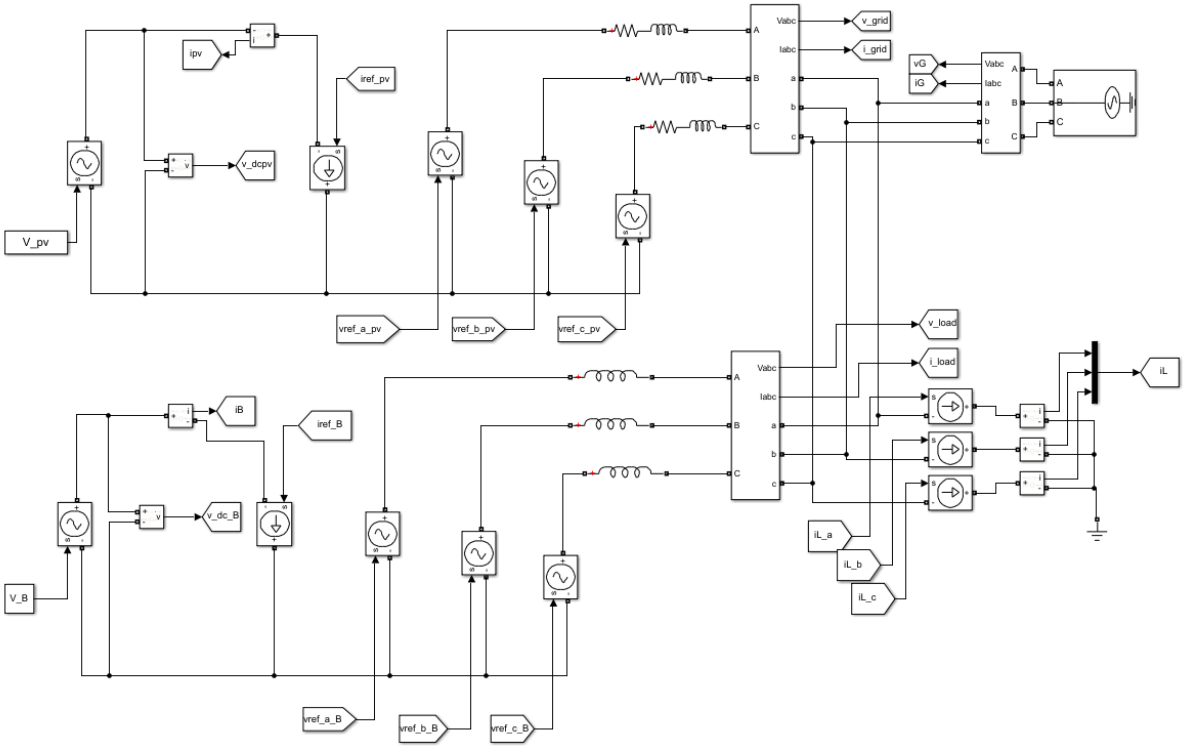

Figure 4-7: Simulation model layout of the AC MG

The reference signal for the average model inverter is generated based on the vector current controller model as demonstrated in Figure 4-3. The control is maintaining the power flow based on the output signal of the EMS algorithm. Where the grid power reference is using for the inverter connected between the PV system and AC bus, while the battery power reference signal generated from the EMS algorithm is using for the inverter used to connect the ESS with the AC bus.

Figure 4-8 represents the power flow through the PV system, load demand, ESS, and grid along with the battery and grid reference power. The battery power reference signal and grid power reference signal are generating from the EMS and Figure 4-8 represents that the battery power and grid power signals are following the reference signal respectively, which indicates that the controller is working properly. The

transient part of the controller is approximately 3 ms.

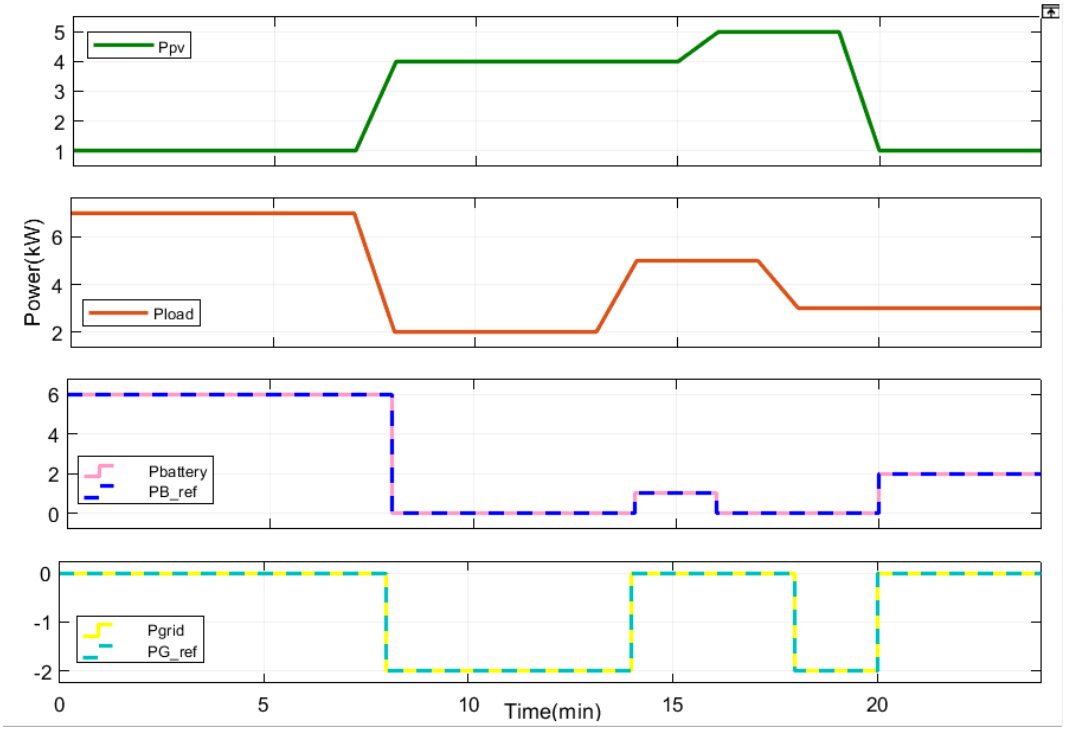

Figure 4-8: Control system operation verification

Chapter 5

Algorithm for Energy Management System

5.1 Proposed EMS Algorithm

The proposed EMS aims to minimize the total cost of energy for the consumer, which is done by managing the power flow through the AC bus of the MG system. The EMS algorithm is proposed taking [112] as a reference. The object of the EMS is to fulfill the load demand with the least energy costing for the consumer. The cost of energy supplied to the load depends on the PV power generation, load demand profile, and the electricity grid price profile, which is known as tariff; these are the variable considered as the input for the EMS. To make the EMS more effective, next day solar irradiance 'G' is also taken as the input of the EMS. Based on the input variable '$tariff'$, the algorithm will select the feed-in-tariff (FiT) variable data. Which varies depending on the all-day tariff profile and uses as the decision-making level for a tariff that indicates either buying or selling grid power will be cost-effective. The aim of the proposed EMS is to find the ESS and grid operation period at each step size which minimizes the total cost of energy supplied to the load. The grid operation period denotes buying power from the grid or selling power to the grid, while the battery operation period reveals the charging, discharging, or idle stage of the battery. The power flow through the ESS is decided considering the state of charge (SoC) of the

battery and maximum battery power. So, the output of the EMS will be the power exchange with the grid, power flow through the battery, and the minimum cumulative cost. Figure 5-1 shows the EMS objectives by revealing the input and output data of the EMS.

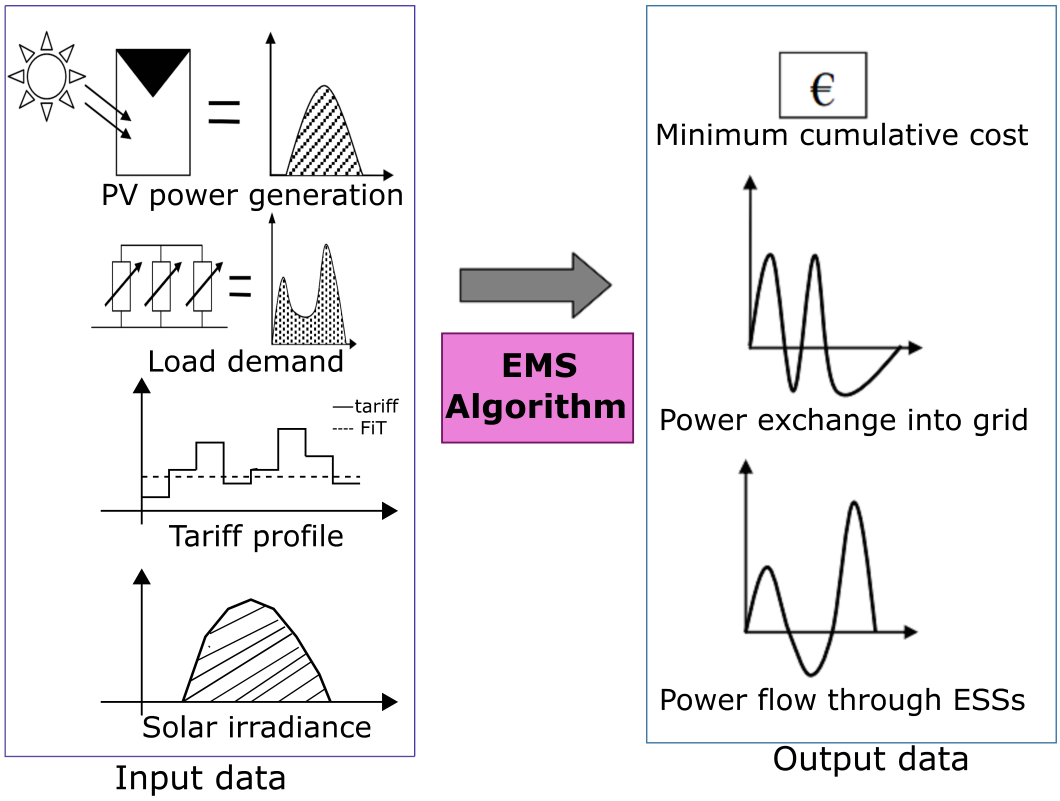

Figure 5-1: Objectives of the proposed algorithm

5.2 Flowchart of the Proposed EMS Algorithm

The EMS operates considering that the power generated by the PV system is used in priority to supply the load demand. When the PV generation is higher than the load demand, the additional PV power generation is used either for battery charging or to sell the power to the grid or both of them. When the PV generation is not sufficient to cover the load demand, the lack of power is provided by either ESS or the grid or both of them. Additionally, the EMS is considering the tariff profile and

next-day solar irradiance 'G' to decide the operation mode, which is minimizing the total costing. The EMS gives the opportunity to purchase electricity from the grid and to sell PV power to the grid. The overall power balancing equation of the MG is given by equation 5.1

$$P_{load} = P_{pv} + P_{grid} + P_{battery} \tag{5.1}$$

where P_{pv} is the PV generation power, P_{grid} is the grid power, $P_{battery}$ is the battery power, and P_{load} is the load demand.

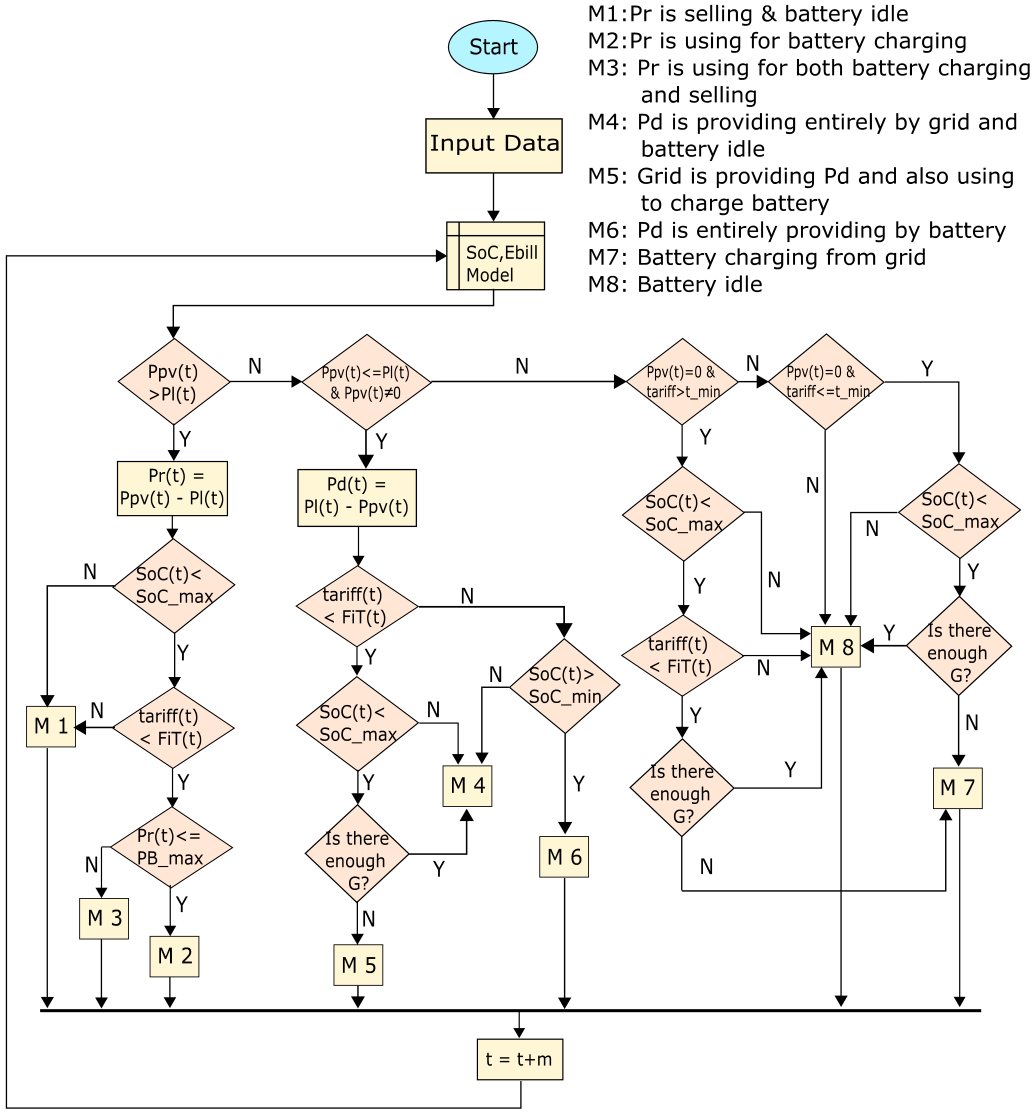

Figure 5-2: Flow chart of proposed EMS

Figure 5-2 shows the flowchart of the proposed algorithm. The input data of the algorithm are based on a discretization of a 24 hours future prediction horizon with a constant step size. In the flowchart, the time variable 't' and the step size variable 'm' are expressed in minutes. The value of the step size can be chosen from one minute to one hour, here in this work the step size is taken as in minutes.
As presented in the flowchart, the algorithm operates at each step size based on the following procedures:

1. Get input profile, $P_{pv}(t)$, $P_l(t)$, tariff(t), and 'G'.
2. Run SoC and E_{bill} model and read SoC and choose FiT value.
3. Execute the condition checking stages to choose the mode of operation.
4. Increment the time variable 't' by the selected step size variable 'm' and start the algorithm from the beginning.

5.3 Description of EMS Algorithm

The proposed EMS algorithm gives several decision procedures at each step size. Depending on the input data and conditions, the system can operate under four cases with eight identical operation modes. The case selection depends on the comparison of PV power generation and tariff profile, while the decision-making for the mode of operation is done based on the battery SoC, FiT, tariff (t), and 'G'. The following sections describe the four cases denoted by *Case A*, *Case B*, *Case C*, and *Case D* of the EMS in details.

5.3.1 Case A, $P_{pv}(t) > P_l(t)$

Case A is considered when the PV generation is higher than the load demand. In this case, all the load demand power is supplied from the PV generation and the remaining power is calculated as in equation (5.2):

$$P_r(t) = P_{pv}(t) - P_l(t) \tag{5.2}$$

where $P_r(t)$ is the remaining power, $P_{pv}(t)$ is the PV generation power, and $P_l(t)$ is the load demand.

If the PV generation is greater than the load demand, the system will enter to the *Case A* and calculate the amount of remaining power based on equation (5.2). In this case, the battery will operate either in charging mode or in idle mode, on the other hand, the grid energy flow will be either on idle mode or on PV power selling mode. After calculating the amount of remaining power, the system will check the battery SoC value and tariff profile to select the mode of operation. The flowchart in Figure 5-2 shows the conditions to enter the operating mode. If the battery SoC is lower than the maximum SoC limit, meaning the battery needs to charge, the system will check the tariff profile to compare the tariff value with FiT. If the tariff is lower than the FiT, the system will enter in battery charging mode or stay in idle mode.

Mode 1 ($M1$) is taken as battery idle mode. The system will enter *Mode* 1 ($M1$) either if SoC is higher than the maximum SoC limit or tariff is greater than FiT value. $M1$ is considered as the battery idle condition, where all the remaining power will feedback to the utility grid to sell the additional PV generation.

Both *Mode* 2 ($M2$) and *Mode* 3 ($M3$) are the battery charging mode, where the selection of these modes depends on the comparison of remaining power with the maximum power range of the battery PB_{max}. If the tariff is lower than the FiT value, the system will compare $P_r(t)$ with PB_{max} to choose the operation mode. If $P_r(t)$ is equal or less than PB_{max}, the system will enter to $M2$. In $M2$ all the remaining power will use to charge the battery and there will be no PV power selling to the grid. If $P_r(t)$ is greater than the maximum battery power, then the system will enter to $M3$ where the remaining power will use for both battery charging and selling to the grid.

5.3.2 Case B, $P_{pv}(t) < P_l(t)$ and $P_{pv}(t) \neq 0$

Case B occurs when the PV generation is less than the load demand but not equal to zero. So, the total load demand is not covered by the PV power and additional power will require to supply the whole load power. The lack of PV generation is denoted as

demanding power and calculated by equation (5.3):

$$P_d(t) = P_l(t) - P_{pv}(t) \tag{5.3}$$

where $P_d(t)$ is the demanding power, $P_{pv}(t)$ is the PV generation power, and $P_l(t)$ is the load demand. This demanding power will either provide by the grid or by the battery. So, the operation mode, in this case, will be either battery discharging or consuming power from the grid for load power or consuming power from the grid for both load and battery charging.

After calculating the demanding power, the system will check the tariff profile and compare the tariff with FiT value. If the tariff is lower than FiT, then the system will consume power from the grid either for only the required load demand or for both the load demand and battery charging. If the tariff is higher than the FiT, the system requires additional load power from battery discharging as long the battery SoC level being higher than its lower range. In this case, the battery charging from the grid power will be done after considering 'G'. The battery will charge only if the next day solar irradiance forecasting suggests that next day solar generation will not be enough to supply the day ahead load demand.

In $Mode$ 4 ($M4$) demanding power $P_d(t)$ will be entirely provided from the grid and the battery will be on the idle case. $Mode$ 5 ($M5$), grid provides $P_d(t)$ to the load and also additional power to charge battery. $Mode$ 6 ($M6$) is the battery discharging period, where the battery will supply the whole $P_d(t)$ to the load and there will be consumed from the grid to avoid high tariff costing.

5.3.3 Case C, $P_{pv} = 0$ and $taiff(t) > minimum\ tariff$

The system enters to $Case\ C$, if there is no PV generation and the tariff of that duration is greater than the minimum tariff level of the day. In this case, the entire load power is consumed from the grid as the PV power is equal to zero. So, the EMS will decide the battery operation period where the battery will be either on charging mode or on the idle mode of operation.

In this case only two modes of operation are considered. $Mode\ 7\ (M7)$ is taken as the battery charging period, the battery will charge from the grid. $Mode\ 8\ (M8)$, where the battery will be idle. In the beginning, the system will check the battery SoC, which indicates the battery needs to charge or not. If the battery needs to charge, then the system will compare the tariff profile with FiT value and after that the next day solar irradiance will consider selecting the mode of operation. The system will enter $M7$ to charge the battery from the grid if the value of G suggests that next, the PV power generation will not be enough to supply the load demand.

5.3.4 Case D, $P_{pv} = 0$ and $tariff(t) <= minimum\ tariff$

$Case\ D$ is considered for the situation when the PV generation is equal to zero and the tariff of that duration is equal to or less than the minimum tariff level of the day. This case also operates on either in $M7$ or in $M8$. Here the system will check the battery SoC to know whether the battery needs to charge or not. If the battery needs to charge, G will consider knowing the next day PV power generation will be more than enough to cover the load demand of that day or not. If the input data G suggests that the PV generation will not be enough to fulfill the load demand, the system will enter to $M7$ to charge the battery from the grid with the lowest tariff value or the system will enter to $M8$ and the battery will stay on idle condition. As there is no PV generation in this case, the total load power will consume from the unity grid in both operating modes.

Chapter 6

EMS with Stateflow Model

6.1 Stateflow Model

Stateflow® is a graphical language, which can use to describe how MATLAB® algorithm and Simulink® models react with the input signals, events, and time-based conditions. It includes state transition diagrams, flow charts, state transition tables, and truth tables. Event-based and interactive graphical design toolbox Stateflow operates based on finite-state machine theory. Stateflow allows graphical programming by visualizing the behavior of the elements to analyze the system performance. Stateflow enables to design and develop supervisory control, task scheduling, fault management, communication protocols, user interface, and hybrid system. Also, it is easy to transform Stateflow to C code, which can implement the proposed EMS convenient for EC applications.

Stateflow is used for dynamically control of the energy management system in Simulink model and it receives or sends all the required inputs of the EMS from or to other Simulink blocks to model the full system in Simulink. For the implementation of the proposed EMS in Stateflow, a chart block is used in the MATLAB/Simulink® where the block takes the input data and performs the EMS algorithm to generate the required output data. The Stateflow model is generated based on the flow chart as discussed in section 5.2 to perform the EMS algorithm. Figure 6-1 shows the basic layout of the EMS using the chart block in the Stateflow model.

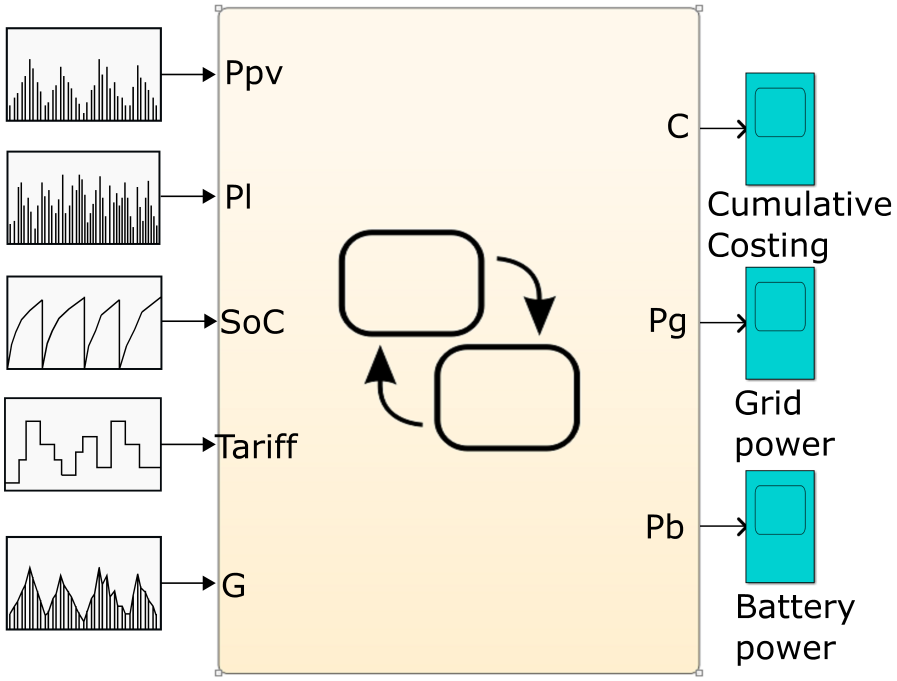

Figure 6-1: EMS with Stateflow model

6.2 Implementation and Verification of EMS Algorithm Stateflow Model

In the Stateflow model, the connective junction is used to perform the proposed algorithm. A connective junction is a graphical object that simplifies Stateflow diagram representations and facilitates the generation of efficient code. Connective junction is one of the best choices to implement and justify a condition-based algorithm.

Figure 6-2 represents the basic layout of the Stateflow model with connective junction. The layout shows how connective junctions (displayed as small circles in yellow color) are used to represent the flow of the algorithm with the if condition. The path between the connective junction is called transitions, which is used to check for the condition of the algorithm and comment the system about the action based on the condition. Where the "Square brackets" used for the condition state of the algorithm

and the "Curly brackets" used to commend the action state need to perform if the condition is satisfied. All the conditions and action states have to be connected to perform the algorithm with the step size.

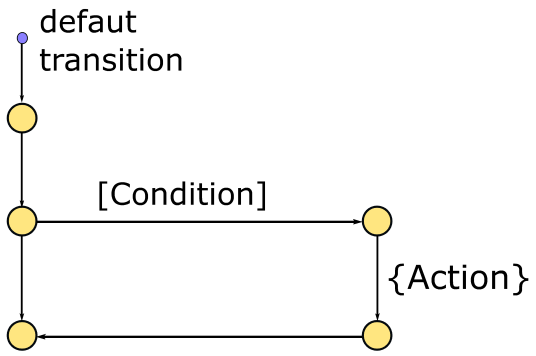

Figure 6-2: Stateflow model using connective junction

6.2.1 Stateflow Model for the Proposed Algorithm

For the implementation of the EMS algorithm, one of the input data is PV generation power and the PV power is calculated from the simulation which is discussed in section 4.3. Load power is the real-time data taken from the system and tariff profile is the real-time data collected from "OMIE". All the input data is taken with a one-minute interval as the step size of the algorithm is chosen in minutes.

The Stateflow model takes all the required input data and performs the algorithm step by step. The first step of the system will compare PV power, load demand, and tariff profile to choose the case of operation. Inside all the operation cases, there will be more conditions to decide the mode of operation. In all the stages, the system will enter any of the operation modes, and based on the action commend it will provide the output regarding grid power, battery power, and costing. After entering the appropriate case, the system will calculate the required value such as $P_r(t)$, $P_d(t)$, and $P_{battery}$, which will use inside the case to perform the action state of the mode of operation. Here $P_r(t)$ is the remaining power calculated based on equation (5.2), $P_d(t)$ is the demanding power calculated from equation (5.3), and $P_{battery}$ is the required

battery power to charge it, which is calculated based on equation (6.1).

$$P_{battery}(t) = PB_{max} - P_b(t) \tag{6.1}$$

where PB_{max} is the maximum power level of the battery, $P_b(t)$ is the instantaneous battery power and $P_{battery}$ is the power required to fully charge the battery. This value of $P_{battery}$ is used for $Case\ C$ and $Case\ D$ to charge battery from the grid. Figure 6-3 shows a part with simple layout of the Stateflow model to demonstrate the implementation of $Case\ A$.

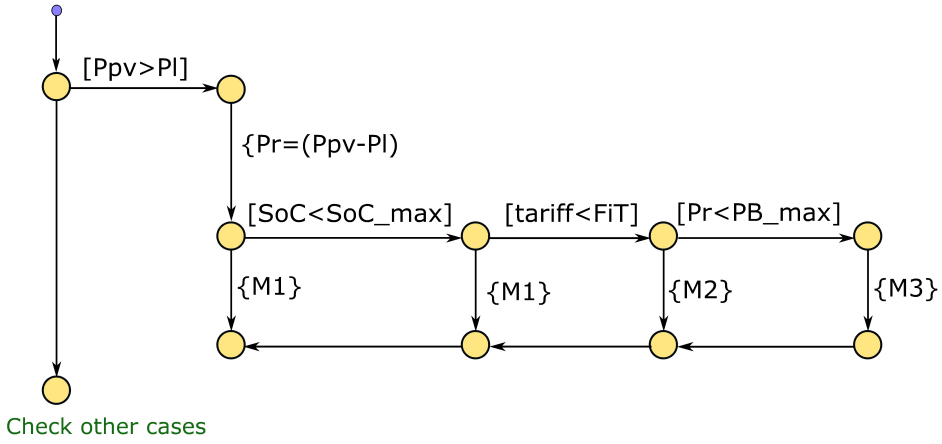

Figure 6-3: Stateflow model using connective junction

The above Stateflow model demonstrated the basic implementation of the proposed algorithm base on the flow chart shown in section 5-2. This demonstration is done for $Case\ A$, where the PV generation is higher than load demand. As shown in the flowchart in Figure 5-2, after entering to the case the system need to perform action state to calculate the remaining power $P_r(t)$ and then it will check other condition. There is three condition state to check and decide the mode of operation. Figure 6-3 shows the condition command and the mode of operation in the active state. All the transition paths between the connective junction have execution order to perform the simulation, which will indicate which transition path will execute. Here all the transition path with condition state are working with execution order 1 and the action states are performing with order 2, so that the system check the

stage of the system first and then take the decision about the operation mode. Thus, if the system satisfies the condition it will move to the forward connective junction, otherwise, it will go backward and perform the action state. All the other cases have been designed considering the same concept, where all the other required calculations are performing inside the action state denoted as mode.

6.2.2 Verification of the Proposed EMS Algorithm

After performing the implementation of the proposed EMS algorithm, the power-sharing between grid and battery is checked to justify that the mode is working shifting properly based on the algorithm. Figure 6-4 shows the power flow through the MG system with the indication of operation mode to justify the implementation of the proposed EMS algorithm.

Some random data of PV generation and load demand has been used to verify the implementation of the proposed algorithm. For the verification, the simulation has been performed by taking data for one day with time intervals in hours. The tariff value used for this simulation is the emulated tariff data for one day. The input data is considered to perform as much mode shifting can occur to verify the algorithm.

Figure 6-4 demonstrates the power flow of the MG system based on the implementation of the proposed EMS algorithm. Where the system is taking PV power and load demand as the input data and providing grid power and battery power as the output data of the system. In the beginning when there is no PV power, as the tariff profile is higher than FiT and also considering next day solar radiance forecasting the system enters to $M8$, which is the battery idle condition. The curve shows that there is no power flow through the battery and the grid is providing the entire load demand, which indicates that the system is operating in $M8$. After that, when the PV generation is less than load demand ($Case\ B$), as the tariff is greater than FiT the system enter to $M6$ where the demanding power P_d is providing from the battery and grid stay in idle condition, the positive battery power flow denotes battery discharging mode.

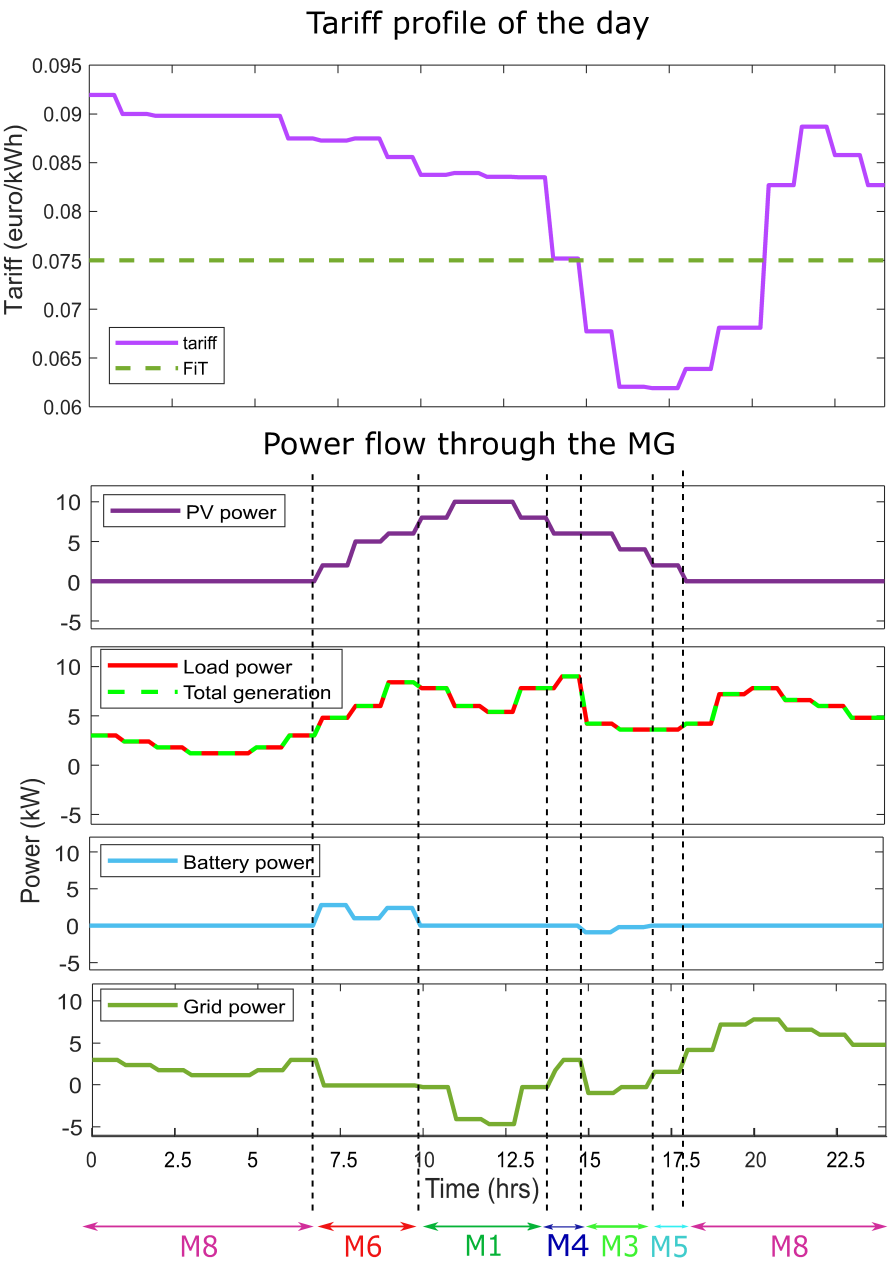

Figure 6-4: Power flow through the MG system to verify the operation of the EMS

Then as the PV generation is greater than load demand (*Case A*), the system checks battery SoC and tariff profile and enters to $M1$. The negative grid power flow indicates the power selling stage, also as there is no battery power flow the system is working on $M1$. In the beginning and end of $M1$, there is a little amount of selling power as the load demand is not much lower than PV generation and in the middle, as

the load demand is less, approximately 4.8 kW PV generation is selling to the utility grid. Then the system enters $M4$ based on the algorithm, where the grid is providing the demanding power P_d to the load and the battery is in idle condition as the tariff of that time period is equal to FiT. After that, the system again enters to $Case\ B$, as the load demand is lower than PV power generation. In that state as the tariff is lower than FiT and $P_{battery}$ is lower than P_r, the system enters to $M3$ where the additional PV generation is using for both battery charging and selling to the grid, though the amount of selling power is lower, the negative power flow through battery and grid indicates the battery charging period and power selling to grid respectively. Then as the load demand goes lower than grid power ($Case\ B$), the system compares the tariff with the FiT value and enters to $M4$ where the grid is providing demanding power to the load to cover the total load demand. Again, when the PV generation is equal to zero, the grid is supplying all the load demand and the battery is in an idle condition which indicates that the system is operating in $M8$. At the beginning of $M8$, the tariff is lower than FiT, as the battery has charged in the previous operation mode and now there is no need to charge, so the system is not operating at $M7$. The mode shifting of the system indicates that the algorithm is executed properly.

6.3 Analysis of the EMS with Real-time Data Input

6.3.1 Power Flow Verification through the MG

After verifying the algorithm with random data, the simulation has been performed for real-time data. In this case, the real-time PV generation, load demand, tariff profile and next day solar irradiance G are used as the input data of the Stateflow model and the simulation has been done for one day considering per minutes time interval. Figure 6-5 shows the value of the next solar irradiance used in this simulation.

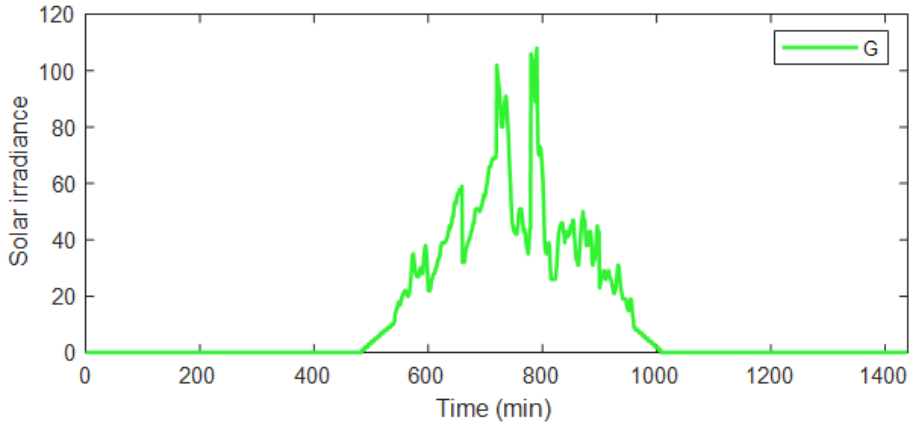

Figure 6-5: Next day solar irradiance profile

Where the PV power generation data is coming from the simulation performed in section 4.3, the load power and tariff profile are the real-time data taking from the system and "OMIE" website respectively. The FiT value is selected considering the maximum and minimum tariff value of the day. Figure 6-6 shows the power flow through the MG system with real-time data.

Figure 6-6 represents the power flow management through the utility grid and battery based on the real PV generation and load demand data of a day with a time interval of 1 minute. At the beginning and end of the day, when there is no PV generation, the EMS check the tariff profile and the next day solar radiation to decide the mode of operation and enter to $M8$. Where the battery remains in idle condition and all the load power is supplied by the grid. When the PV generation is greater than load demand ($Case\ A$), the system operates on $M1$, which is battery idle and PV power selling operating mode. The negative power flow through the grid indicates that the additional PV power is selling to the grid and the amount of PV power is the difference between PV generation and load demand, calculated by using equation (5.2).

Then the system enters to $Case\ B$, where the PV generation is lower than load demand. In this case, the system checks the tariff profile to decide whether the grid or battery will provide the demanding power. First, the system operates in $M6$, where all the demanding power is supplying from the battery, the positive power flow

through the battery indicates discharging period. Then when the tariff goes lower than FiT, the system operates on $M4$. Where the demanding power calculated based on equation (5.3) provides from the grid and battery stays in idle condition.

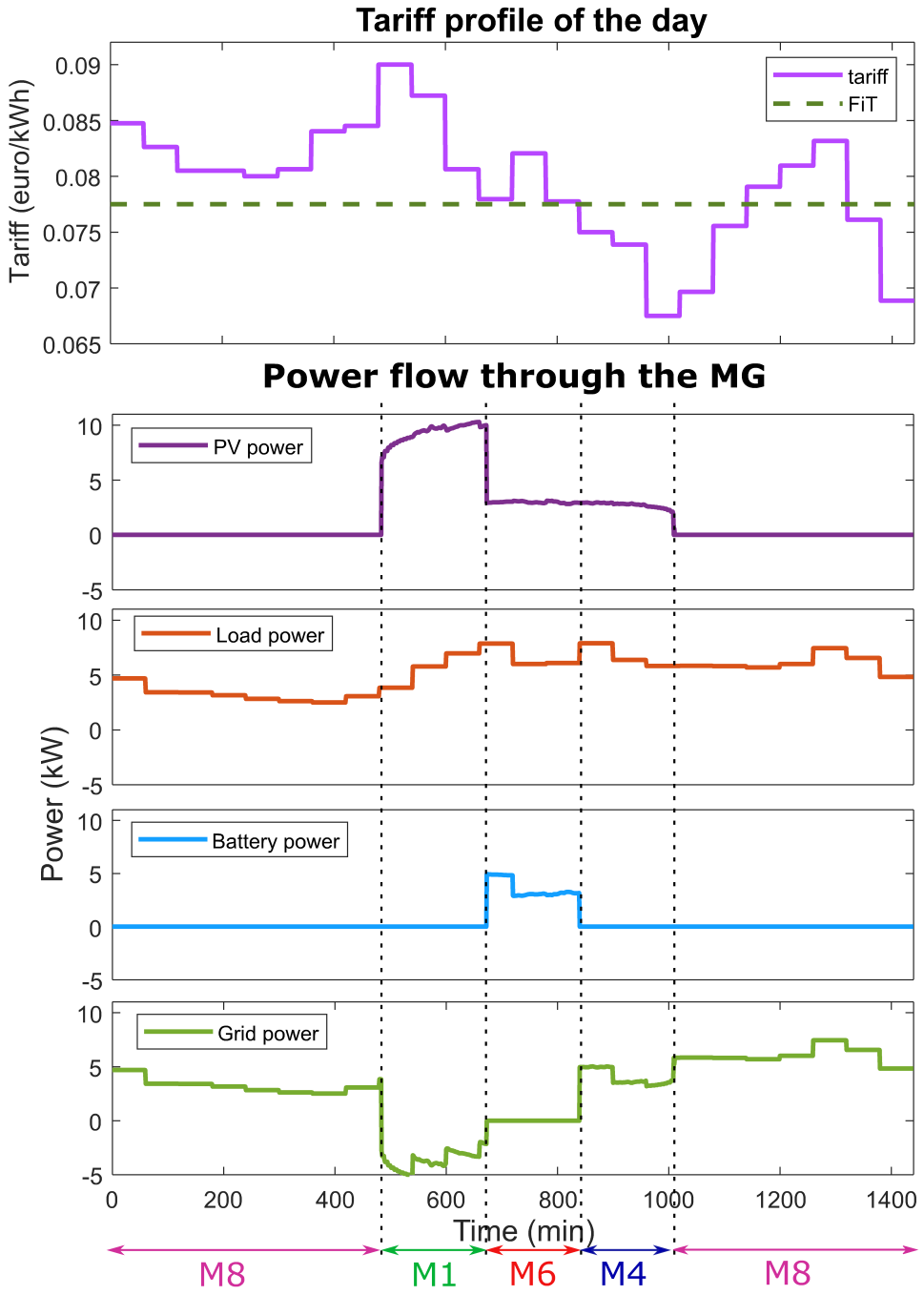

Figure 6-6: Power flow through the MG system with real-time data

Figure 6-7 shows the total power generation and consumption of the MG system, where total generation is the summation of PV power, battery power and power taking from the utility grid and total consumption is the load demand.

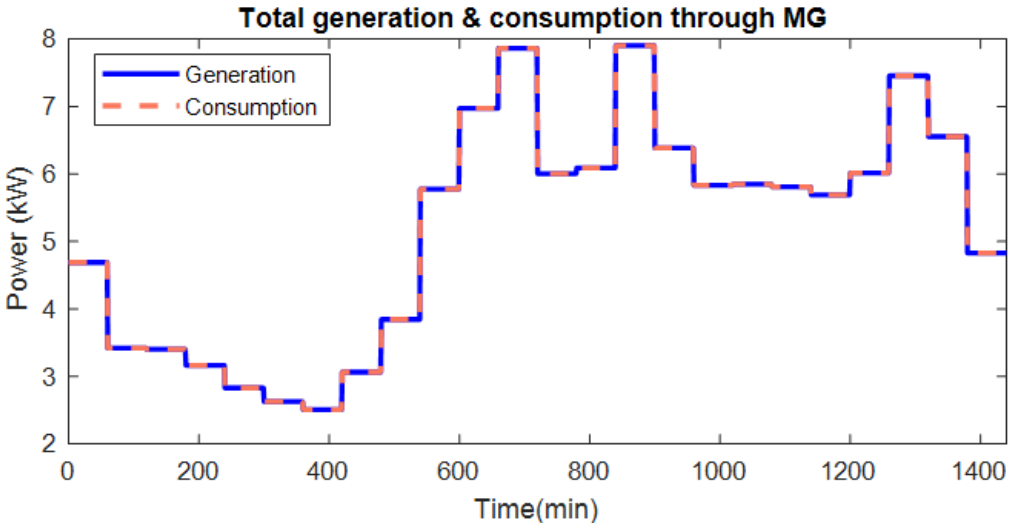

Figure 6-7: Total power generation and consumption of the MG system

6.3.2 Cost calculation of the EC

Since there is both buying and selling power from the grid, so the Stateflow provides costing for both buying power from the grid and selling power to the grid. Then the final costing is calculated by subtracting the selling power cost from the buying power. The calculation of buying and selling power is done inside the active state for the specific operation mode considering the instantaneous tariff profile.

The buying power costing is the cost of grid power which is consuming for load demand and battery charging. While the selling power cost is the cost of PV power that is supplying to the grid, which is calculated based on the tariff value during the PV power selling period.

Figure 6-8 shows the cost of buying power from the grid, selling power to the grid, and finally, the total cumulative cost of the energy need to pay.

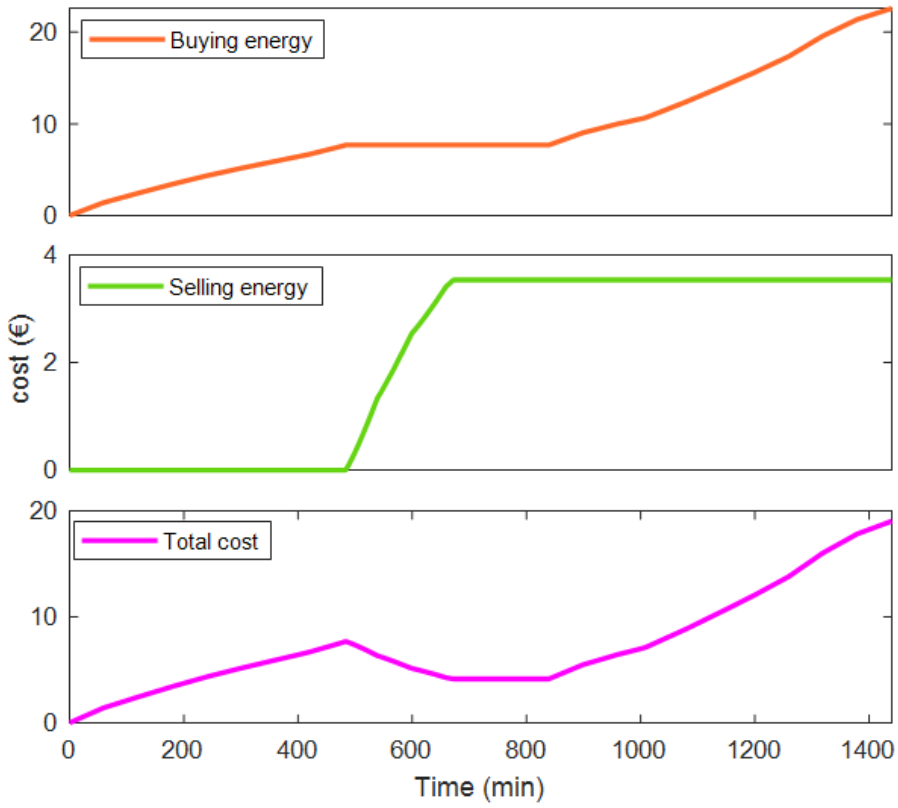

Figure 6-8: Cost of the energy consumption

For better analysis with a different scenario and to find out optimum solution LCOE is also considered for the total cost calculation. The LCOE calculation is done based on the formulas described in section 3.5.1. The formula for LCOE calculation indicates that the only variable which varies with time is the fractional number of PV array used for supplying surplus PV power and direct PV power $N_{surplus}$ and N_{direct} respectively. So, the Stateflow model is performed also to provide output regarding the number of fractional PV arrays for surplus and direct PV power generation.
Table 6.1 shows the parameters considered for the cost analysis of the system to obtain LCOE. Where all the cost assumption is based on section 3.2 and section 3.3 for the PV system and ESSs respectively. The LCOE calculation has been done using MATLAB® function, where the function is an operation based on the instantaneous value of N_{direct} and $N_{surplus}$ and other values are considered as mentioned in the table below.

Table 6.1: Parameters considered for the calculation of the LCOE

Parameters	values
Capital cost of PV panel	750 €/kWp
Installation cost of PV panel	2500 €/kWp
O/M cost of PV system	10 €/kWp
Capital cost of ESSs	500 €/kWh
O/M cost of ESSs	15 €/kWh
Efficiency of ESSs	85%
Life time	20
Degradation rate of PV	0.4%
Degradation rate of ESSs	1%
Discount rate	1%

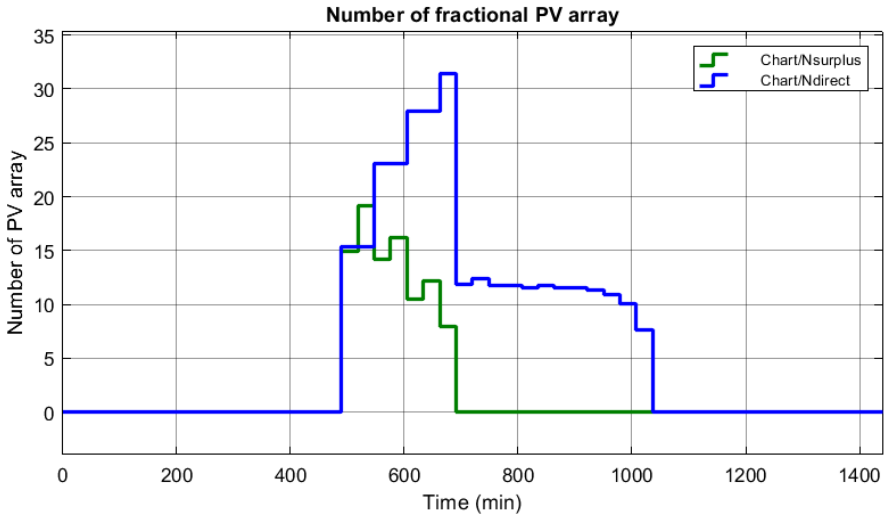

Figure 6-9: Number of fractional PV array for surplus and direct power generation

Figure 6-9 shows the fractional number of surplus and direct PV power generation, which is calculated with the same real-time data input used in the previous section for the verification of the proposed EMS algorithm. Figure 6-9 demonstrates the number of fractional PV array for surplus and direct PV power generation. Direct PV power is the PV generation that is directly going to the load, the blue curve in

the figure indicates the number of fractional PV arrays using for direct power supply. The number of fractional PV array for surplus PV power is indicating by green in the figure, is the PV power which is not using for load demand directly. As in *Case B* after 12 pm of the day with this data input all the PV power is using for load demand, so the value of $N_{surplus}$ is zero at that duration. Also, the graph indicates that the summation of N_{direct} and $N_{surplus}$ is either equal or less than 40. Because the total number of PV arrays used for the system design is 40. The calculation of LCOE of the system is implemented based on equation (3.15) and the implementation is done on MATLAB script taking the continuous value of $N_{surplus}$ and N_{direct}. Figure 6-10 shows the instantaneous and cumulative LCOE.

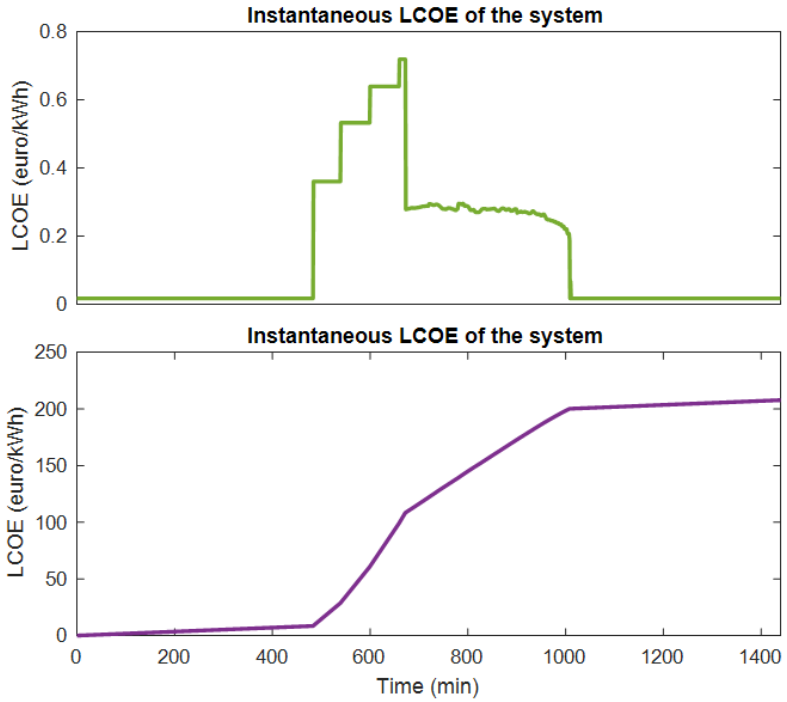

Figure 6-10: LCOE of the system

The equation used for the calculation of the LCOE indicates that the only variable part is the value of $C_{pvsurplus}$, $C_{pvdirect}$ and $E_{pvdirect}$. So the instantaneous LCOE value varies with the value of $N_{surplus}$ and N_{direct}, also there is a small amount of LCOE in case of no PV power generation because of the constant part of the cost and energy of the energy storage. The cumulative LCOE started from zero and increases, the

rate of increase is higher when there is a certain amount of PV generation. Figure 6-11 shows the cumulative total cost considering the LCOE.

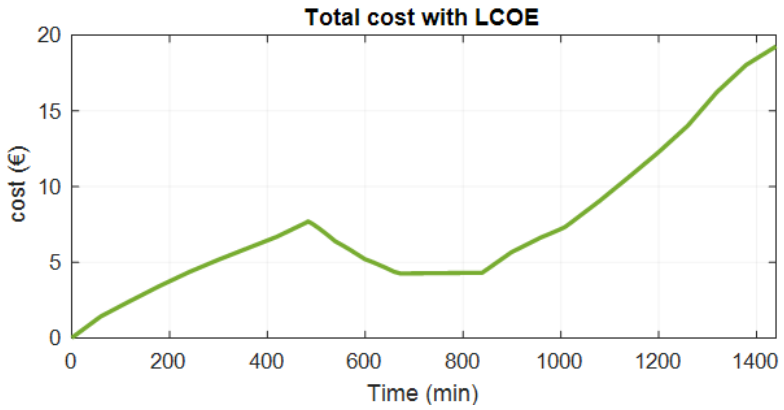

Figure 6-11: Total cost with LCOE

Total cost of the system is calculated by adding the cumulative total cost of the system with the cumulative LCOE of the system. The amount of total cost is 19.14 €. Table 6.2 shows complete one year cost for base system, PV only system and hybrid system.

Table 6.2: Cost comparison considering

System type	**Total cost**
Base system	12880 €
PV system	9282 €
Hybrid system	6955 €

The cost analysis shows that the hybrid system is offering savings of 5925 € at complete one year.

Chapter 7

Result and Discussion

7.1 Analysis of the EMS with Different Input Data

The simulation has been performed taking the input data of another day to observe the behavior of the system and verify the proposed EMS. The value of FiT is selected based on the maximum and minimum level of the tariff value of that day. The solar irradiance of the next day of that day is considered to check the day ahead PV generation will be enough for the load demand or not. The simulation is performed taking the input data of PV power generation, load demand, tariff profile, and next-day solar irradiance.

Figure 7-1 shows the tariff profile with the FiT value of that day and the power flow through the MG system with a specific indication of the operating mode. The power flow through the MG system indicates that the system stays at $M8$ at the beginning of the day when all the load demand is providing from the utility grid and the battery stays on idle condition.

Then when the system enters to *Case A*, where the PV power generation is greater than the load demand, as the tariff profile indicates that the tariff at the duration is either equal or lower than the FiT value, the system will not enter to $M1$. The system will check battery SoC and compare the maximum battery power with the value of remaining power to select the operation mode. In *Case A*, the system operates in $M2$ and $M3$. The operation modes fluctuate between $M2$ and $M3$ based on the value

of PB_{max} and P_r, as described in the flow chart. In $M2$, all the remaining power is used to charge the battery and there is no power flow through the grid, and in $M3$ the remaining power is used for both battery charging and selling PV power to the grid.

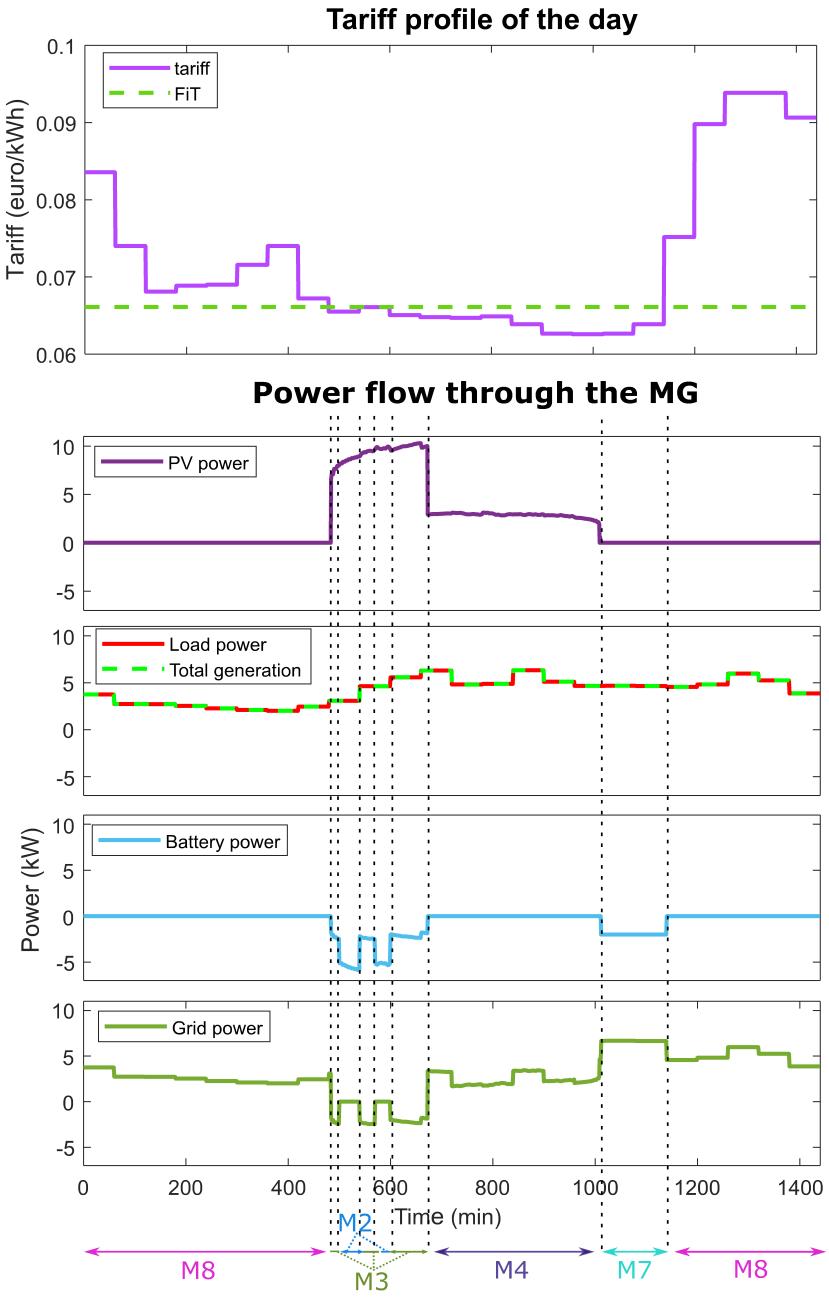

Figure 7-1: Tariff profile and power flow through the MG

After that when the PV power generation goes lower than load demand ($Case\ B$), the system checks the tariff profile to decide that whether the utility grid or battery will supply the demanding power to the load. In this simulation as the tariff profile shows that the tariff value of that time duration is lower than the FiT, the system will enter to $M4$, where all the required demanding power is providing from the grid and the battery stays in idle condition.

Then when the PV generation again goes to zero levels, the system will operate either on $M7$ or $M8$ considering the tariff profile and next-day solar irradiance. In this simulation, the value of G suggests that the next day solar radiation will not be enough to cover all the load demand, so the EMS system will check the tariff profile and use the lower tariff value to charge the battery.

In the time duration roughly between 5 pm to 8 pm, as the tariff is lower than the FiT value the system operates at $M7$ where the battery is charging from the grid, negative power flow through the battery indicates charging periods. Also, the higher grid power flow level indicates that the total load power and battery charging power are coming from the utility grid.

In figure 7-1, the overlapping load power and total generation indicates that the total load demand of the MG system is providing from the total generation of the MG, where the total generation is the summation of PV power, grid power, and battery power with their corresponding sign.

Energy cost calculation has done in this simulation for buying power and selling power, total power is the subtraction of selling power cost from the cost of buying power.

Figure 7-2 shows the cost of energy for buying power, selling power, and the total cost of energy on the day.

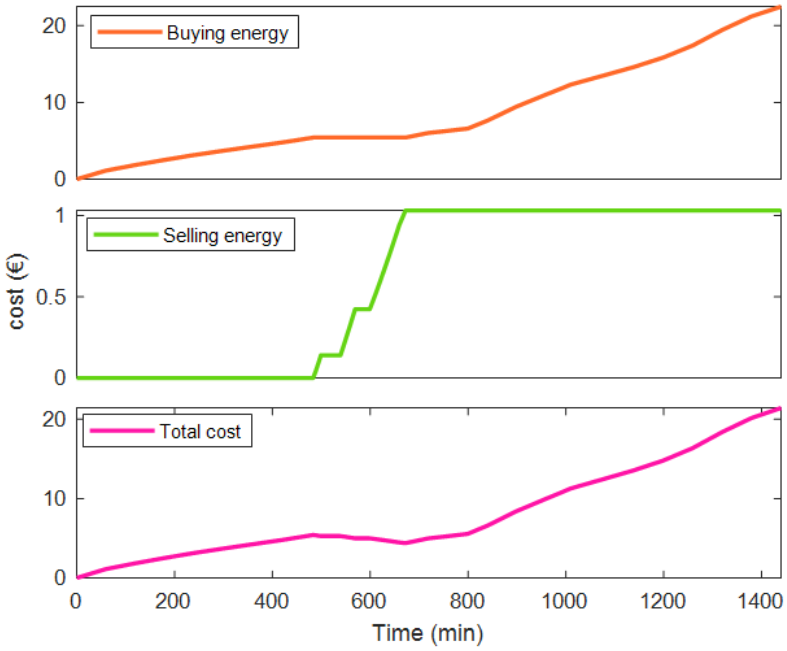

Figure 7-2: Cost of energy

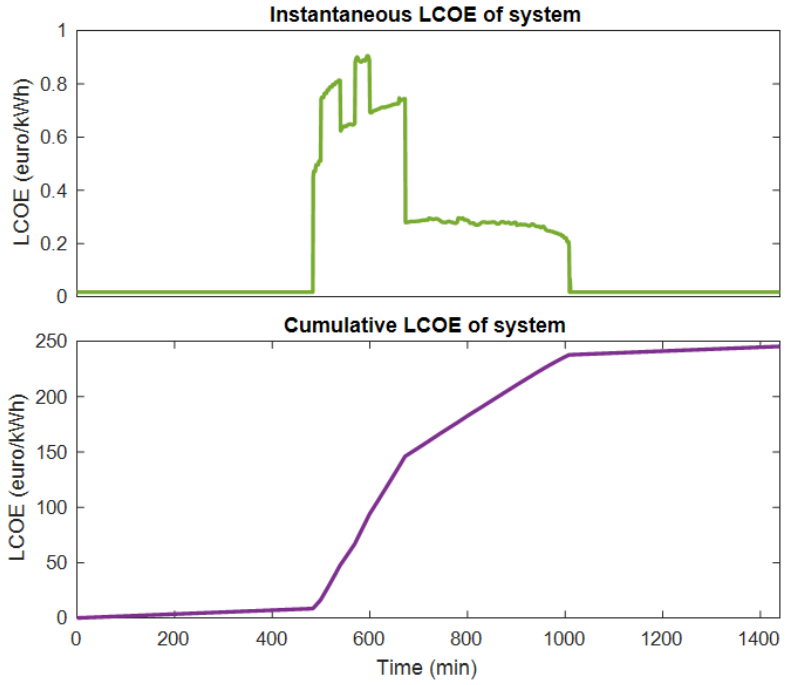

Figure 7-3: LCOE of the system

Figure 7-3 shows the instantaneous and cumulative LCOE of the system with this

combination of operating modes. The LCOE depends on the number of fractional PV array. The higher two level of LCOE value indicates that in this duration there is both the value of N_{direct} and $N_{surplus}$. The value of $N_{surplus}$ is due to the PV generation which is using for battery charging.

The total cost is the summation of total cost of energy and the cumulative LCOE of the system. The total cost for this day is 21.65 €. Table 7.1 shows complete one year cost for base system, PV only system and hybrid system with this combination of input data.

Table 7.1: Cost comparison considering

System type	**Total cost**
Base system	11610 €
PV system	6856 €
Hybrid system	7821 €

The cost analysis shows that the hybrid system is offering savings of 3789 € at complete one year.

7.2 With ± 25% Load Power Variation

To analyze the performance of the system and total cost of the system including LCOE with the EMS, the simulation has been performed at different combinations of input data. In this case, the simulation has been performed by varying the load demand data considering 25% higher and lower load power to analyze and verify the EMS.

7.2.1 Considering 25% Higher Load Demand

The simulation has been performed taking load demand 25% higher than the real load demand of that day to observe the power flow and costing based on the proposed EMS. The real-time value of PV generation and tariff profile of that same day is used

as the input data. In this simulation, the FiT value is selected as 0.0750 €/kWh considering the maximum and minimum tariff value of that day. The value of input data G suggests that the next day solar radiation will not be enough to cover all the load demand.

Figure 7-4 shows the tariff profile of that day, which is considered as one of the input data and power flow through the MG based on the proposed EMS. The operating mode of the system is also indicating below the curve. It indicates that the system operates at $M8$ at the beginning of the when the PV generation is equal to zero as the tariff profile is higher than the FiT level. After that, the system enters into $Case\ A$ and operates at $M1$ where the additional PV generation is selling to the grid as the tariff level is higher than FiT. As the load demand is considered higher, the system stays to $Case\ A$ for less time duration and then enters to $Case\ B$.

During $Case\ B$, the system checks the tariff profile to decide either battery or grid will provide the demanding power. As Figure 7-4 shows that the tariff value is greater than FiT, the system operates at $M6$ where the total demanding power is providing from the battery. The positive battery power flow indicates discharging period and the grid stays at idle condition during that mode of operation. Then as the tariff goes lower than the FiT value, the system enters $M4$ to receive the demanding power from the grid and the battery stays in idle condition.

After that when the PV generation again goes equal to zero, the system operates either on $M7$ or $M8$ based on the tariff value as the input data G indicates next day solar radiation will not be enough for load demand. As long the tariff is lower than the FiT value the system operates at $M7$ where the battery is charging from the grid. When the tariff is higher than the FiT value, the system operates at $M8$ where the battery stays in idle condition and the grid is providing all the load power.

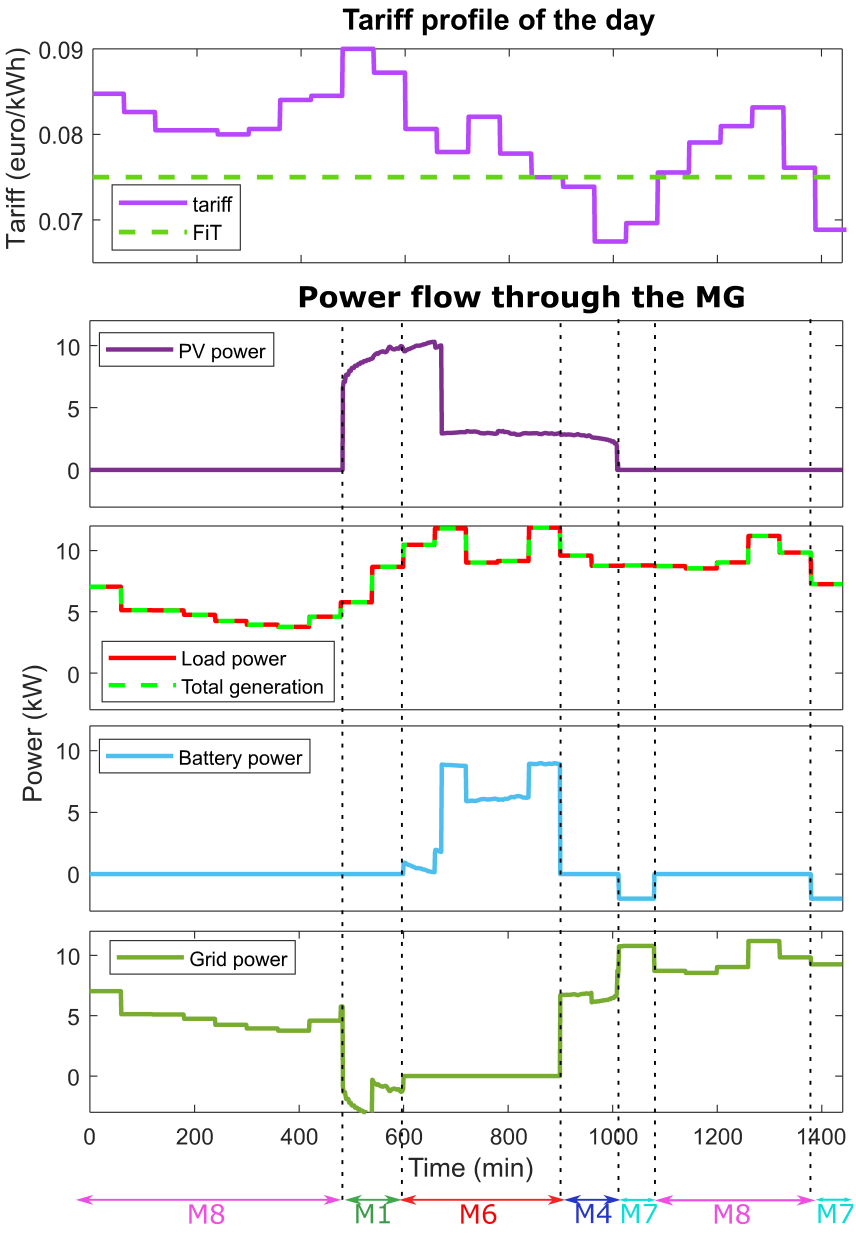

Figure 7-4: Power flow through the MG

Figure 7-5 shows the cost of energy with buying power and selling power cost in a different plot. As the load power is considered 25% higher, so the cost of buying power is higher and the cost of selling power is lower than the real data simulation result as discussed in the previous section. The amount of buying power cost is much higher, so the total cumulative cost of energy of the day is higher. The curve of the total cost of energy indicates that there is not a lot of cost reduction during the period

when the system is operating at $M1$ to sell PV generation to the grid as the amount of selling power is less.

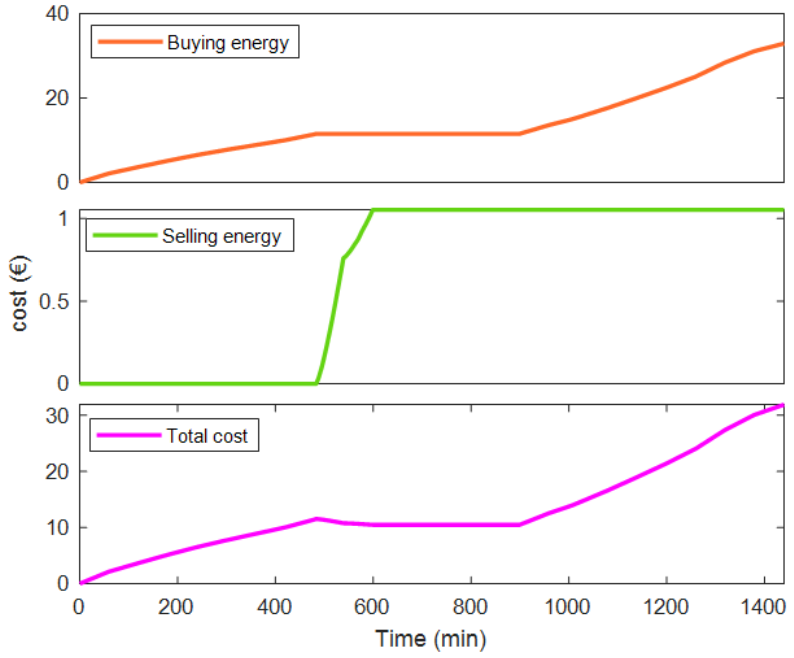

Figure 7-5: Cost of energy

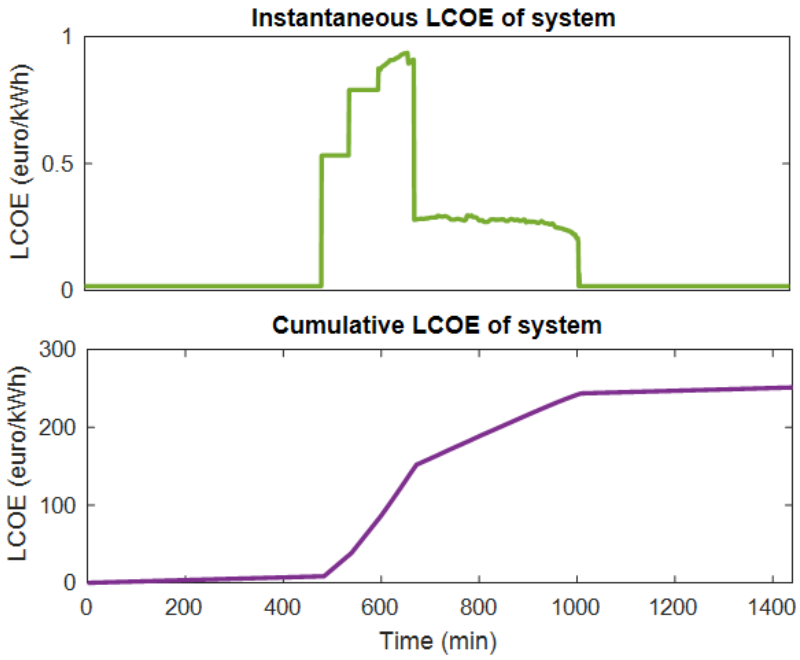

Figure 7-6: LCOE of the system

Also, the instantaneous and cumulative value of LCOE is plotted to analyze the effect of load variation. In this simulation, the highest amount of LCOE calculated is 0.9348 €and the cumulative sum of the LCOE is 250.7 €. Figure 7-6 demonstrates the instantaneous and cumulative LCOE of the system.
The calculated total cost of energy for that day including the LCOE of the system is 31.947 €.
Table 7.2 shows complete one year cost for the base system, PV only system, and hybrid system with this combination of input data.

Table 7.2: Cost comparison considering

System type	**Total cost**
Base system	20090 €
PV system	14520 €
Hybrid system	11650 €

The cost analysis shows that the hybrid system is offering savings of 8440 € at complete one year.

7.2.2 Considering 25% Lower Load Demand

Again the simulation has been performed considering 25% lower load demand than the real data, where all the other input data is kept same as section 7.2.1. As, all the other input data is same, the system operates with the same sequence of mode shifting, only the amount of power flow, duration of operation mode and costing of the system varies.
Figure 7-7 shows the power flow through the MG with mode of operation indication and the tariff profile of that day.

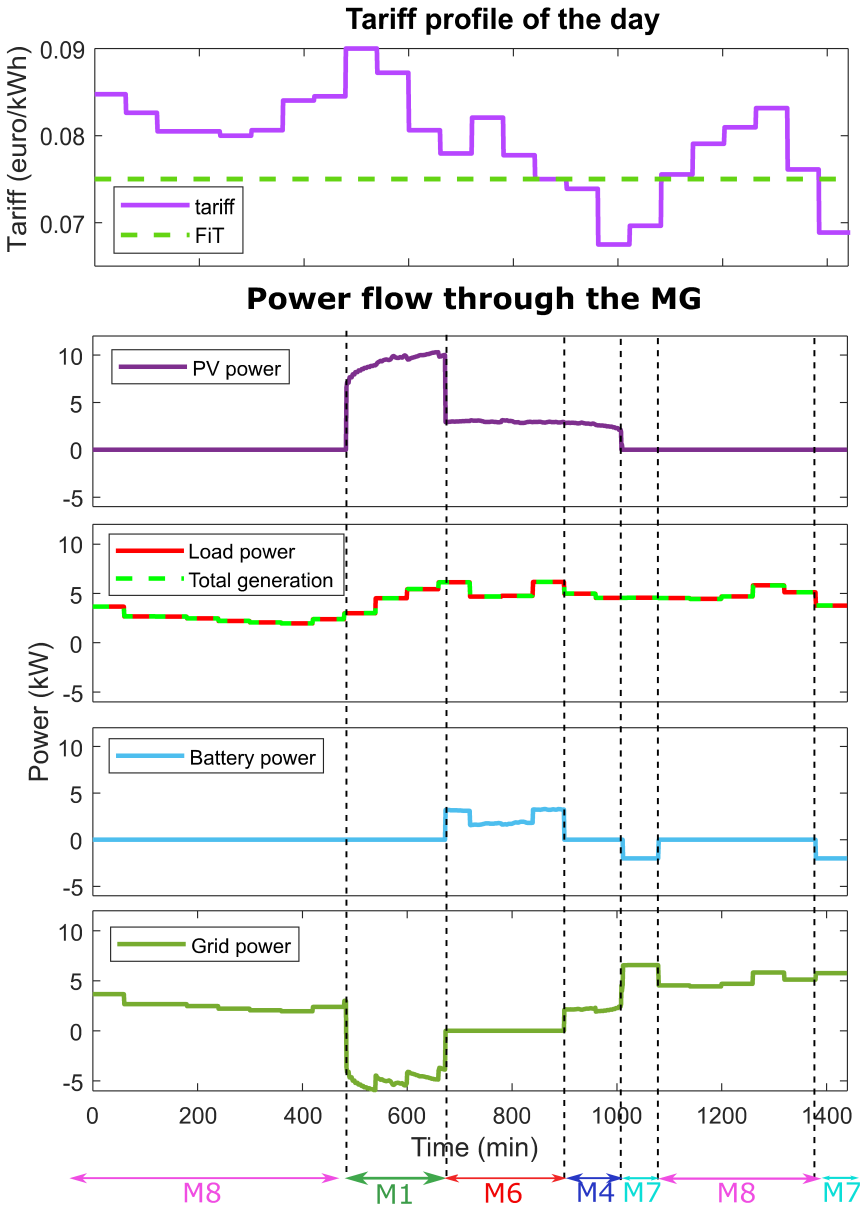

Figure 7-7: Power flow through the MG

In Figure 7-7, although the sequence of mode shifting is same as Figure 7-4 the duration of $M1$ and $M6$ varies. In this simulation, the system stays on $M1$ longer, as the load demand is lower so *Case A* is longer. Here the maximum PV power selling to the grid is 5.91 kW, where it was 3.19 kW for 25% higher load demand case. In $M6$ where the battery is discharging to supply the demanding power, as the load power is 25% lower in this simulation, the maximum amount of battery discharging power

is 3.14 kW in $M6$; while it was 7.8 kW at $M6$ in Figure 7-4.

In $M7$, where the grid supplies all the load demand and also charges the battery, the grid power reaches the maximum level at 6.5 kW. But in the simulation with 25% more load demand, the maximum grid power at $M7$ was 10.77 kW.

Figure 7-8 shows the total cost of energy with buying power cost and selling power cost. As the load demand is considered 25% lower in this simulation, so the cost reduces comparing with the last simulation. In this simulation, the system stays at $M1$ for a longer duration and the amount of selling power is higher, so the cost of selling power is higher and the effect of that is more visible in the total cost curve. The total cost reduces to a certain level during the PV power selling period $M1$. Here the selling power cost is 4744.21 €, while it was only 1053 €for a higher load power combination. Finally, the total cost of energy of the day is 11404.4 €, while it was double (22440 €) in the last simulation.

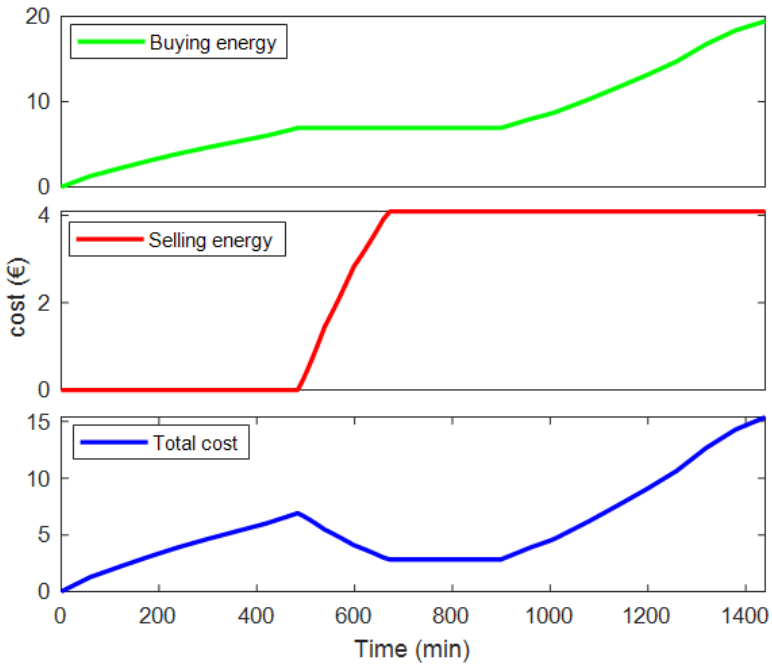

Figure 7-8: Cost of energy

Figure 7-9 shows the instantaneous and cumulative LOCE curve for the simulation with lower load demand. Comparing this curve with Figure 7-6, it is visible that the LCOE decreases with lower load demand. The highest instantaneous LCOE value is

0.564 €, which is lower than the value 0.9348 €at Figure 7-9. The total cumulative LCOE is 186.091 €, while it was 250.7 €for higher load demand simulation.

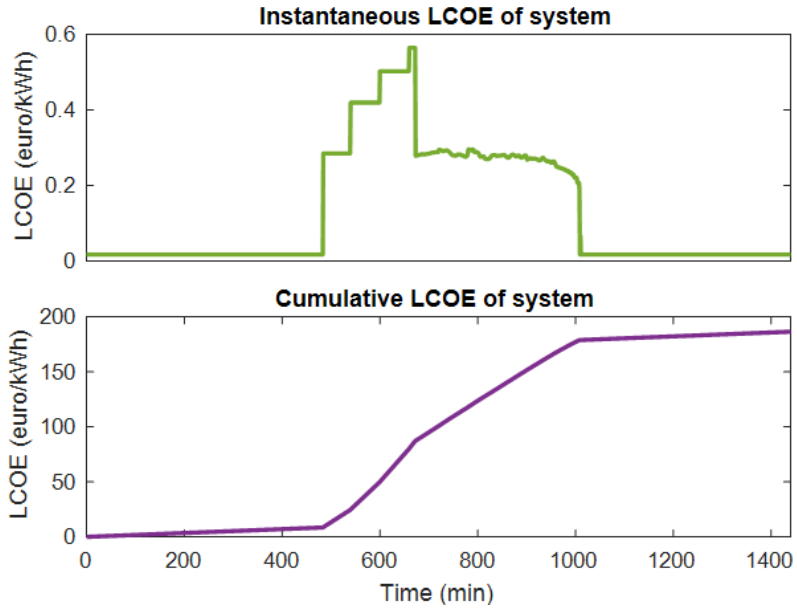

Figure 7-9: LCOE of the system

The total cost of energy including LCOE in this simulation is 15.563 €, which is roughly half of the cost for higher load demand.
Table 7.3 shows complete one year cost for base system, PV only system and hybrid system with this combination of input data.

Table 7.3: Cost comparison considering

System type	Total cost
Base system	12360 €
PV system	8193 €
Hybrid system	5615 €

The cost analysis shows that the hybrid system is offering savings of 6745 € at complete one year.

7.3 Considering the Effect of PV Power Forecasting and PV Power Generation on LCOE

To analyze the effect of PV power generation on LCOE and consider the simulation that the PV forecasting and PV power generation may not be equal, the simulation has been performed simultaneously with real PV data and PV data with error. As the variation PV generation will affect only the calculation of LCOE, the simulation has been performed to analyze the LCOE variation.

The implementation of the EMS with different PV power data is done in the same simulation model by creating a subsystem. In the first stage, the simulation has been performed considering that the PV power generation is lower than the PV power forecasting. So, the simulation model is implemented with two subsystems wherein one subsystem the real-time PV generation value is used as the input data and in the other one, the PV generation forecasting is used. All the other input values are kept the same for both subsystems. As the difference between PV generation and forecasting is not large, in both cases the system operates in the same mode of operation.

Figure 7-10 shows the graph of PV power and LCOE for both real-time PV generation and PV forecasting value. It indicates that the value of instantaneous LCOE goes lower if the PV power generation goes lower than the PV power forecasting. Also, this effect is more visible for *Case B* stage, as in case the LCOE decreases with the same percentage PV power generation goes lower than the PV power forecasting, as in this case all the PV power is supplying load power, so there is only the value of N_{direct} for the calculation of LCOE while the value of $N_{surplus}$ is zero.

In *Case A*, as the additional PV power generation is selling to the grid, so the lower PV power generation is not creating any difference in LCOE calculation because lower PV power generation is not affecting the value of $N_{surplus}$.

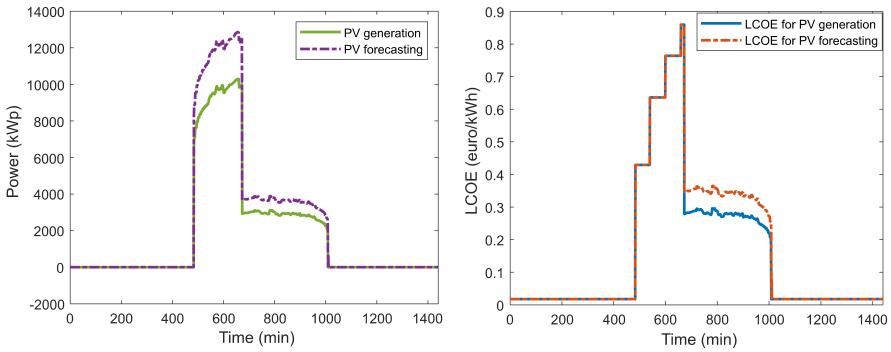

Figure 7-10: Effect of PV power variation on LCOE

Again the simulation is performed considering that the PV power generation is higher than the PV power forecasting to observe the effect of PV power variation on LCOE. Figure 7-11 shows the simulation result with PV power and LCOE to analyze the effect of PV power variation on the LCOE of the system. The graph indicates that the LCOE increases with the higher PV power generation. As the PV power generation is higher than the PV power forecasting, the calculated LCOE goes higher with the same percentage.

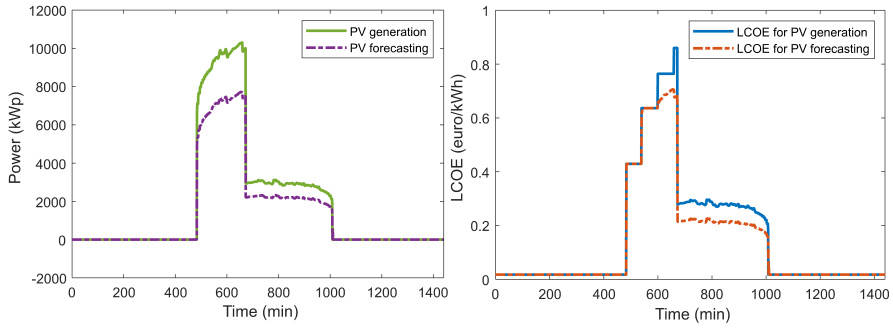

Figure 7-11: Effect of PV power variation on LCOE

7.4 Analysis of LCOE for PV Only and Hybrid system

The analysis of the LCOE is done considering the calculation of the LCOE for the hybrid system and PV only system identically. Here in the hybrid system, the LCOE

is calculated considering both the PV system and ESSs system. While in the PV-only system, the LCOE is calculated for the PV system alone considering that ESSs are not connected. The aim of this simulation is to analyze the LCOE variation. Equation (3.15) is used for the calculation of the LCOE for the hybrid system, while for the calculation of the LCOE for PV only case equation (7.1) is used, where the only difference is that the cost and energy of ESSs is not considering for PV only case.

$$LCOE_{system} = \frac{C_{pvdirect}}{E_{pvdirect}} \tag{7.1}$$

To calculate the LCOE for both hybrid and PV the only system, the simulation is performed with the same input data so that the system operates in the same operating mode. So the same value of N_{direct} and $N_{surplus}$ are used for the calculation of the LCOE based on equation (3.15) and (7.1) for the hybrid system and PV only system respectively.

Figure 7-12 demonstrate the LCOE which is calculated considering both hybrid system and PV only system separately.

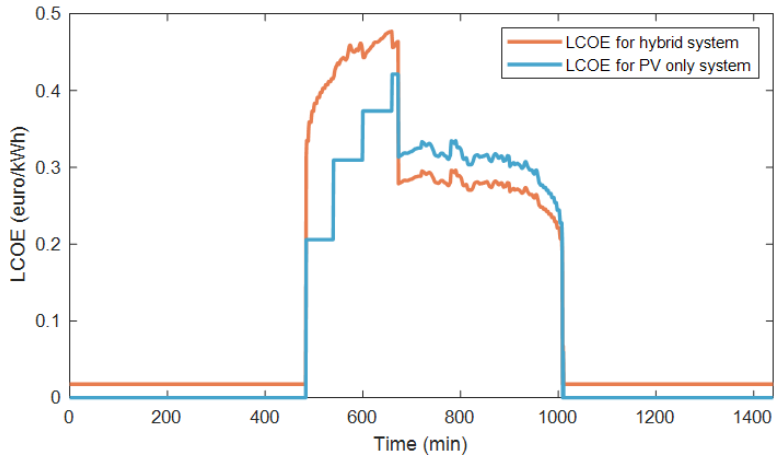

Figure 7-12: Instantaneous LCOE for hybrid system and PV only system

Figure 7-12 shows that in *Case A* when the PV power is greater than load demand, the LCOE for the hybrid system is higher than the LCOE for the PV the only system. As in *Case A*, there is both direct and surplus PV power generation,

so the LCOE for the hybrid system is higher than the PV system. Because in PV only system, only direct PV power generation is considered for the calculation of the LCOE.

In *Case B*, where the PV power is less than load demand, at that duration there will be only PV direct power and no surplus PV generation. So based on equation 3.15 and 7.1, the only difference between the calculation of LCOE for the hybrid system and PV system is the consideration of the cost and energy of the ESSs. As the cost of ESSs is lower than the total energy generation over the whole year, so the formula of the LCOE measurement for PV system denominator has a higher value than the nominator comparing with the formula for the hybrid system. As a result, in that duration, the value of LCOE for the hybrid system goes lower than the LCOE for the PV system.

The cumulative value of LCOE for the hybrid system and PV system has been analyzed to observe the relation between them. Figure 7-13 represents the cumulative LCOE for hybrid system and PV system. As the hybrid system is considering both the PV system and ESSs, whether there is PV generation or not there is an amount of LCOE calculated. So the amount of cumulative LCOE for the hybrid system is greater than the LCOE for the PV system.

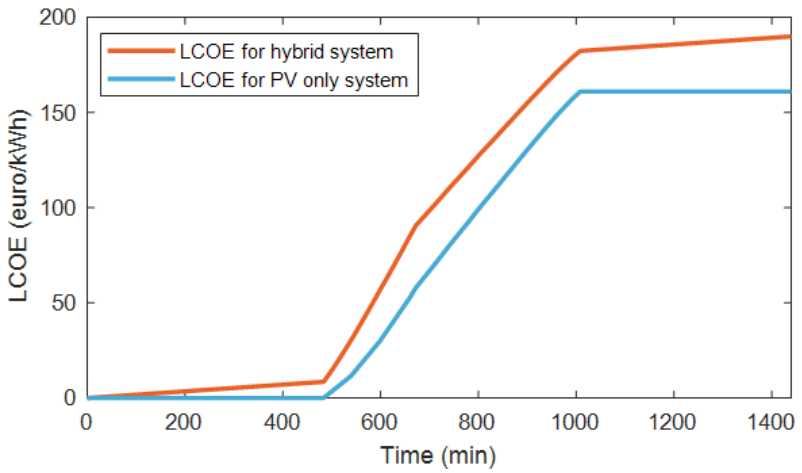

Figure 7-13: Cumulative LCOE for hybrid system and PV only system

The measured LCOE for hybrid system and PV system has also been plotted with

respect to PV power generation. Figure 7-14 represents the LCOE with respect to PV power generation for both hybrid system and PV system. The LCOE for hybrid system is grater than PV system, while the PV generation between 2 to 4 kWp the difference between the LCOE for hybrid system and PV system is comparatively less than other PV power generation range.

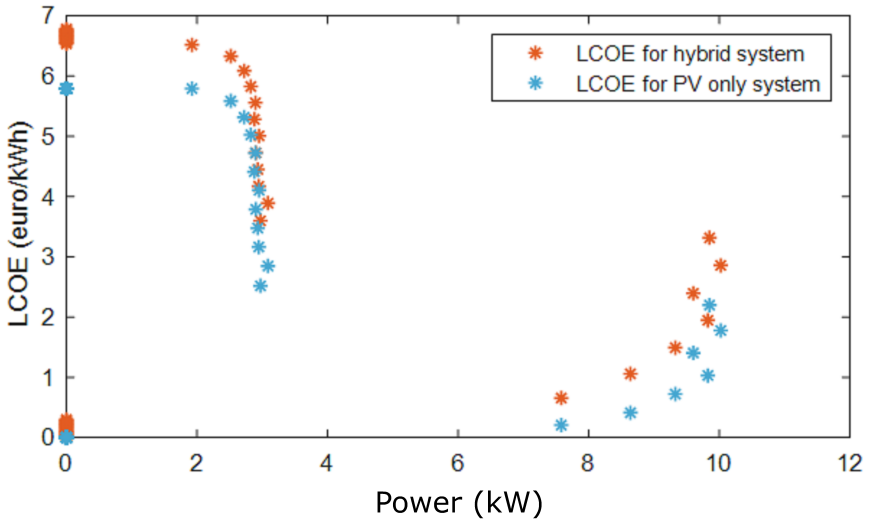

Figure 7-14: LCOE for hybrid system and PV only system with respect to power

7.5 Cost Analysis for One Year

The cost analysis for the whole year has been done separately for the base system, PV system, and hybrid system, where the base system is considered that all the load demand is supplying from the utility grid, the hybrid system is the AC MG including PV generation and ESS, and the PV system is the AC MG which is not connected with the ESS. The cost comparison has been done by varying load demand to find out the optimal solution.

Figure 7-15 shows the cumulative cost comparison result for the base system, PV system, and hybrid system for the complete year considering normal load demand. The curve shows that the cumulative cost of the base system is higher than both PV and hybrid systems, as in the base system the total load demand is supplying

from the utility grid. The PV system is the MG system without ESS and the hybrid system is the AC MG system with PV generation and ESS which is working based on the proposed EMS. The cost analysis indicates that the hybrid system is offering the lowest amount of cost.

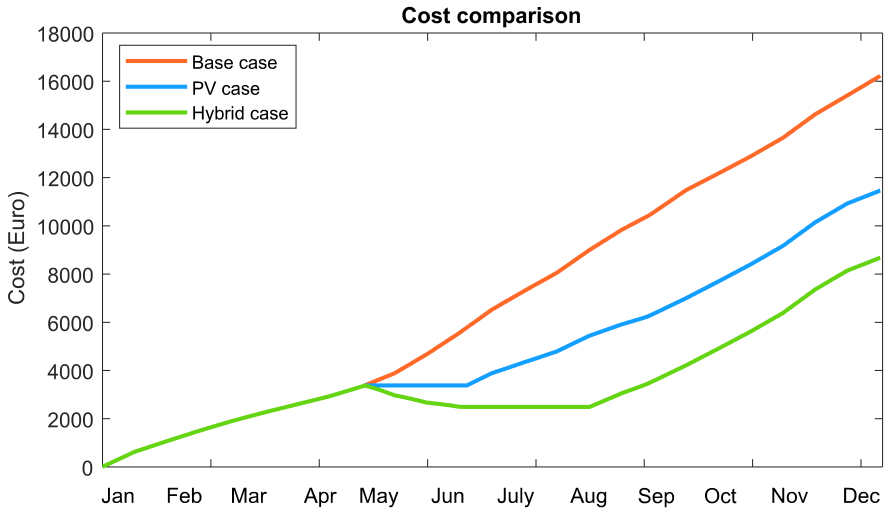

Figure 7-15: Cost comparison considering normal load condition

Table 7.4 shows the final value of cumulative cost for the three different system. Which is justifying that the hybrid system is saving 7544 € electricity costing for the consuming comparing with the base system.

Table 7.4: Cost comparison considering normal load demand

System type	**Cumulative cost**
Base system	16220 €
PV system	11460 €
Hybrid system	8676 €

After that, the cost analysis has been performed considering 25% higher load demand to compare the effectiveness of the proposed EMS algorithm. Figure 7-16 demonstrate the costing for three different systems to compare the saving of electricity costing with EMS. The graph shows that the costing increased for all the systems.

The cost of the hybrid system is offering the lowest amount of cost with this higher load condition.

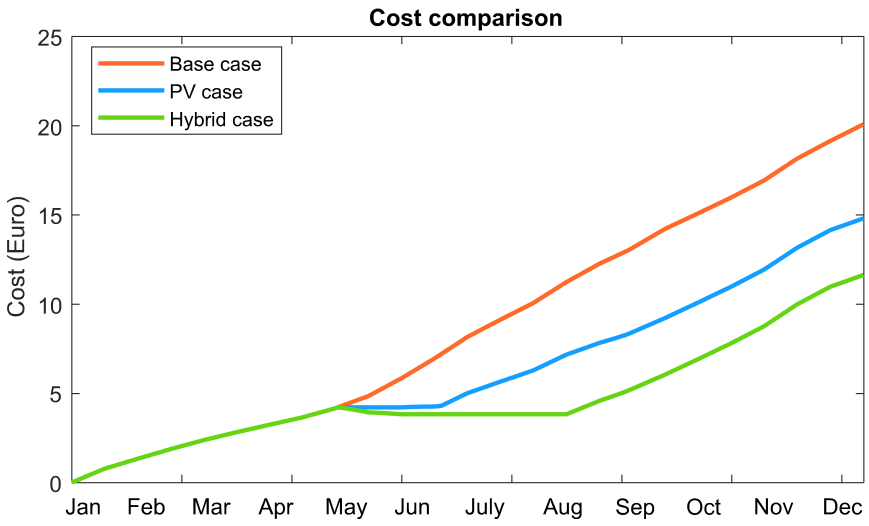

Figure 7-16: Cost comparison considering 25% higher load condition

Table 7.5 shows the final value of cumulative cost for the three different system considering 25% higher load demand. Which is justifying that the hybrid system is saving 8440 € electricity costing for the consuming comparing with the base system. The saving with this combination is higher than the normal load condition. So, the EMS is effective with higher load demand.

Table 7.5: Cost comparison considering 25% higher load demand

System type	Cumulative cost
Base system	20090 €
PV system	14820 €
Hybrid system	11650 €

The simulation has also been performed taking 25% lower load demand to analyze the costing of the base system, PV system, and hybrid system. Figure 7-17 represents the cost analysis for all the three system combination. It shows that the cost is reduced for all combinations as the load demand is considering lower. The curve is

also revealing that the hybrid system cost goes much lower value because based on the proposed algorithm for lower load demand the system will stay longer in *Case A* and sell the additional PV generation.

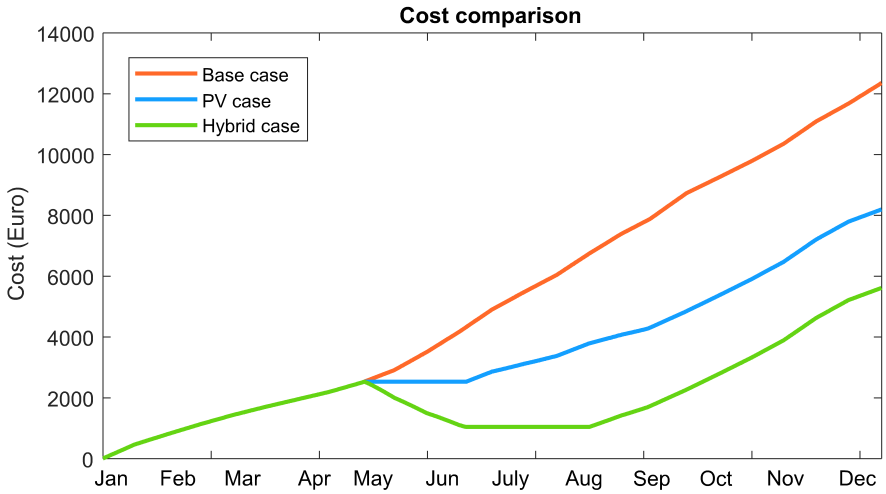

Figure 7-17: Cost comparison considering 25% lower load demand

Table 7.6 shows the final value of cumulative cost for the three different system considering 25% lower load demand. Cost analysis is justifying that the hybrid system is saving 6745 € electricity costing for the consumption comparing with the base system.

Table 7.6: Cost comparison considering 25% lower load demand

System type	**Cumulative cost**
Base system	12360 €
PV system	8193 €
Hybrid system	5615 €

Cost comparison for different system combinations considering various load demands shows that the proposed EMS is offering the highest amount of saving.

7.6 Payback Time Calculation

The payback period is the amount of time the system takes to generate the amount of energy equivalent to the amount that took to produce the system, on the other way it can be said that payback time is the duration the system will take to recover the cost of installation.

The payback time calculation has been done for the hybrid system considering the savings of energy consumption. Based on the data as shown in Table 6.1, the total installation cost of the hybrid system is 49780 €. The calculation of payback time is done by dividing the total installation cost of the hybrid system by the annual savings of the system. The calculation has been done for three different load combinations. Table 7.7 shows the payback time of the hybrid system considering three different load demand data as discussed in section 7.5.

Table 7.7: Payback time

Load demand condition	**Payback time(Years)**
Normal load demand	6
25% higher load demand	5
25% lower load demand	9

7.7 Real-time Implementation

The Stateflow model of the proposed EMS has been implemented and analyzed with real-time data. All the simulation result mentioned in the work has done with real-time data. Besides that, the main advantage of the Stateflow analysis EMS model is that the algorithm can be easily translated to C language and implemented in real-time system analysis.

Figure 7-18 shows a timing diagram for the implementation of the EMS considering that the Stateflow model is implemented using "Raspberry pi".

Where the EMS is operating based on the input data and generating the battery

power and grid power reference signals. The real-time implementation of the EMS is performing on "raspberry Pi" and the hybrid system operation is based on the output signal of it.

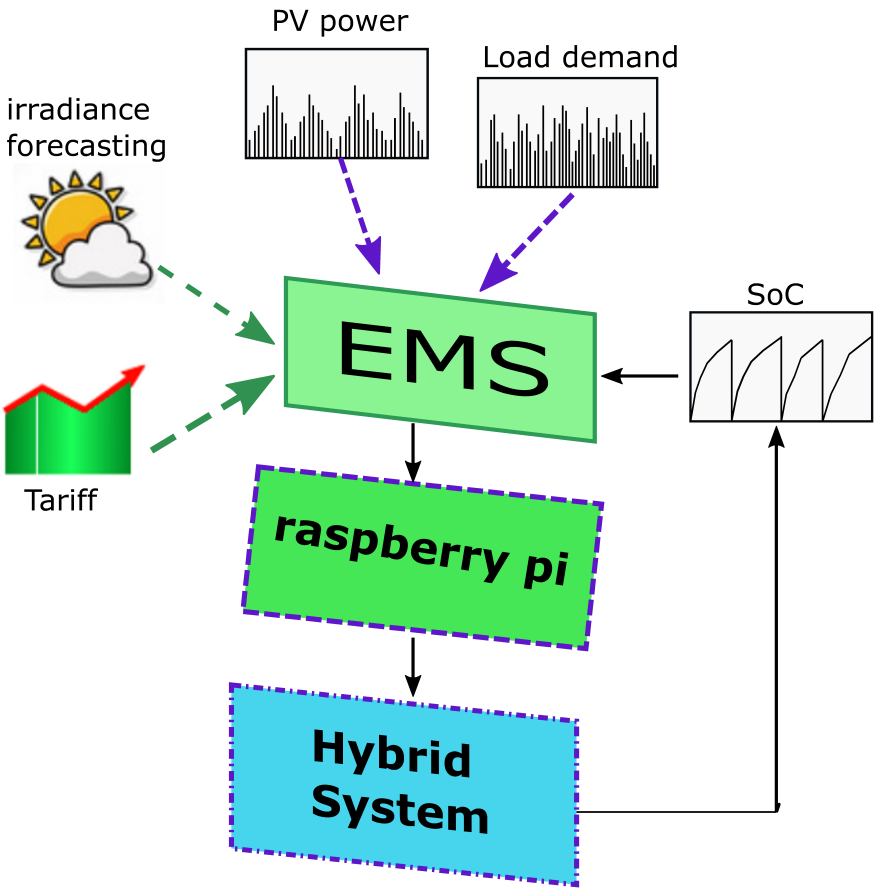

Figure 7-18: Real-time implementation time diagram

After generating the algorithm the next step is implementation, where the Stateflow model is converted to C language. The generated code is used for the integration between software and hardware implementation. For the code generation, the key work is to select the right hardware. Here "Raspberry Pi" is selected for implementing the system.

C code can be generated from Simulink® models that include Stateflow® using Simulink Coder™. In addition to Simulink Coder, Embedded Coder™ can be used to enhance the code generation. When the C code is generated for a target, the

Stateflow parser evaluates the graphical and non-graphical objects and data in each Stateflow machine against the supported chart notation and the action language syntax.

Chapter 8

Conclusion and Future Work

8.1 Conclusion

In this work, the development of EMS for the application of energy communities is demonstrated, where the system is considered PV system as distributed resources and li-ion battery as the energy storage. Besides the PV power generation and load demand input data, the system is considering the tariff profile of the respective day and the next day solar irradiance forecasting to decide the mode of operation.

The basic concept of energy communities, microgrid, distributed generation, energy storage systems, Levelized cost of energy along with all the other relevant terms for the work are discussed at the beginning of the report. The step-by-step design procedures, consideration, mathematical calculations of the system development, and required terms for the work are presented. The concept, consideration, and decision-making of the proposed EMS are discussed in detail with a flowchart and required equation. This work is considering a PV power system with 10 kWp power rating. The temperature and solar radiance data are collected for the specific location. Instantaneous tariff value has been taken from OMIE.

In the first step of the work, the simulation model of the MG system has been implemented for understanding the power management and sharing within the MG. Then the implementation of the proposed EMS has been done and the proposed EMS has been analyzed with several combinations of input data to justify that the algorithm is

working properly. Finally, the cost analysis has been done to verify that the proposed EMS is reducing the cost of electricity. The cost analysis of the system has been done considering LCOE.

The cost analysis has been done for the base case, PV system, and hybrid system. The cost analysis shows that the proposed EMS can reduce 35.93% cost for the PV system and 45.71% cost for the hybrid system comparing with the base system. The implementation of the proposed EMS algorithm has been done using both MATLAB Simulink and Stateflow model in Simulink. The verification of the algorithm has been done with several input combinations for complete one-day real-time data.

8.2 Future Work

The main aim of this thesis is to supply the load with minimum cost for the consumer by selling additional PV generation power, and controlling ESSs charging/discharging periods. Although the LCOE is considered for the costing of the system, the ESSs replacement cost is not included. In addition, the Simulink model to generate PV voltage from the solar irradiance value is introducing some error during the shifting from zero radiance to a certain value of solar irradiance.

The following future work will make the EMS more sophisticated and worthy:

- Consider of battery replacement cost
- Obtain real-time PV generation power, instead of calculating though simulation
- Consider average and instantaneous value of $N_{surplus}$ and N_{direct} for more accurate LCOE
- Implement the Stateflow model in "Raspberry Pi"

Bibliography

[1] Sertac Bayhan and Haitham Abu-Rub. Smart energy management system for distributed generations in ac microgrid. In *2019 IEEE 13th International Conference on Compatibility, Power Electronics and Power Engineering (CPE-POWERENG)*, pages 1–5, 2019.

[2] Syed Furqan Rafique and Zhang Jianhua. Energy management system, generation and demand predictors: a review. *IET Generation, Transmission & Distribution*, 12(3):519–530, jan 2018.

[3] Mir Nahidul Ambia, Ahmed Al-Durra, and S.M. Muyeen. Centralized power control strategy for ac-dc hybrid micro-grid system using multi-converter scheme. In *IECON 2011 - 37th Annual Conference of the IEEE Industrial Electronics Society*, pages 843–848, 2011.

[4] Pablo Arboleya, Cristina Gonzalez-Moran, and Manuel Coto. A hybrid central-distributed control applied to microgrids with droop characteristic based generators. In *2012 15th International Power Electronics and Motion Control Conference (EPE/PEMC)*, pages LS7a.5–1–LS7a.5–8, 2012.

[5] Tomislav Dragičević, Xiaonan Lu, Juan C. Vasquez, and Josep M. Guerrero. Dc microgrids—part i: A review of control strategies and stabilization techniques. *IEEE Transactions on Power Electronics*, 31(7):4876–4891, 2016.

[6] Dong Chen and Lie Xu. Autonomous dc voltage control of a dc microgrid with multiple slack terminals. *IEEE Transactions on Power Systems*, 27(4):1897–1905, 2012.

[7] Usman Bashir Tayab, Mohd Azrik Bin Roslan, Leong Jenn Hwai, and Muhammad Kashif. A review of droop control techniques for microgrid. *Renewable and Sustainable Energy Reviews*, 76:717–727, sep 2017.

[8] Bernadette Fina, Hans Auer, and Werner Friedl. Profitability of pv sharing in energy communities: Use cases for different settlement patterns. *Energy*, 189:116148, 2019.

[9] Luigi Martirano, Sara Rotondo, Mostafa Kermani, Ferdinando Massarella, and Roberto Gravina. Power sharing model for energy communities of buildings. *IEEE Transactions on Industry Applications*, 57(1):170–178, 2021.

[10] Yuan Hong, Sanjay Goel, Haibing Lu, and Shengbin Wang. Discovering energy communities for microgrids on the power grid. In *2017 IEEE International Conference on Smart Grid Communications (SmartGridComm)*, pages 64–70, 2017.

[11] Daniel Akinyele, Juri Belikov, and Yoash Levron. Challenges of microgrids in remote communities: A steep model application. *Energies*, 11(2), 2018.

[12] Amjad Ali, Wuhua Li, Rashid Hussain, Xiangning He, Barry W. Williams, and Abdul Hameed Memon. Overview of current microgrid policies, incentives and barriers in the european union, united states and china. *Sustainability*, 9(7), 2017.

[13] Ting Zhu, Zhichuan Huang, Ankur Sharma, Jikui Su, David Irwin, Aditya Mishra, Daniel Menasche, and Prashant Shenoy. Sharing renewable energy in smart microgrids. In *2013 ACM/IEEE International Conference on Cyber-Physical Systems (ICCPS)*, pages 219–228, 2013.

[14] Guglielmina Mutani, Valeria Todeschi, Angelo Tartaglia, and Giovanni Nuvoli. Energy communities in piedmont region (it). the case study in pinerolo territory. In *2018 IEEE International Telecommunications Energy Conference (INTELEC)*, pages 1–8, 2018.

[15] Laurine Duchesne, Bertrand Cotnélusse, and Iacopo Savelli. Sensitivity analysis of a local market model for community microgrids. In *2019 IEEE Milan PowerTech*, pages 1–6, 2019.

[16] Atanda K. Raji and Doudou N. Luta. Modeling and optimization of a community microgrid components. *Energy Procedia*, 156:406–411, 2019. 5th International Conference on Power and Energy Systems Engineering (CPESE 2018).

[17] J. Lowitzsch, C.E. Hoicka, and F.J. van Tulder. Renewable energy communities under the 2019 european clean energy package – governance model for the energy clusters of the future? *Renewable and Sustainable Energy Reviews*, 122:109489, 2020.

[18] R. Lasseter. Microgrids. In *2002 IEEE Power Engineering Society Winter Meeting. Conference Proceedings*, volume 1, pages 305–308 vol.1, 2002.

[19] Nikos Hatziargyriou, Hiroshi Asano, Reza Iravani, and Chris Marnay. Microgrids. *IEEE Power and Energy Magazine*, 5(4):78–94, jul 2007.

[20] B. Lasseter. Microgrids [distributed power generation]. In *2001 IEEE Power Engineering Society Winter Meeting. Conference Proceedings (Cat. No.01CH37194)*, volume 1, pages 146–149 vol.1, 2001.

[21] Daniel E. Olivares, Ali Mehrizi-Sani, Amir H. Etemadi, Claudio A. Cañizares, Reza Iravani, Mehrdad Kazerani, Amir H. Hajimiragha, Oriol Gomis-Bellmunt,

Maryam Saeedifard, Rodrigo Palma-Behnke, Guillermo A. Jiménez-Estévez, and Nikos D. Hatziargyriou. Trends in microgrid control. *IEEE Transactions on Smart Grid*, 5(4):1905–1919, 2014.

[22] F. Martin-Martínez, A. Sánchez-Miralles, and M. Rivier. A literature review of microgrids: A functional layer based classification. *Renewable and Sustainable Energy Reviews*, 62:1133–1153, 2016.

[23] Dan T. Ton and Merrill A. Smith. The u.s. department of energy's microgrid initiative. *The Electricity Journal*, 25(8):84–94, 2012.

[24] Athanasios Vasilakis, Igyso Zafeiratou, Dimitris T. Lagos, and Nikos D. Hatziargyriou. The evolution of research in microgrids control. *IEEE Open Access Journal of Power and Energy*, 7:331–343, 2020.

[25] Madureira AG. Coordinated and optimized voltage management of distribution networks with multi-microgrids. *Universidade do Porto, Facultade de Engenharia*, 2010.

[26] Huang Jiayi, Jiang Chuanwen, and Xu Rong. A review on distributed energy resources and microgrid. *Renewable and Sustainable Energy Reviews*, 12(9):2472–2483, 2008.

[27] Alexis Kwasinski and Philip T. Krein. A microgrid-based telecom power system using modular multiple-input dc-dc converters. In *INTELEC 05 - Twenty-Seventh International Telecommunications Conference*, pages 515–520, 2005.

[28] Tomislav Dragičević, Xiaonan Lu, Juan C. Vasquez, and Josep M. Guerrero. Dc microgrids—part i: A review of control strategies and stabilization techniques. *IEEE Transactions on Power Electronics*, 31(7):4876–4891, 2016.

[29] Tomislav Dragičević, Xiaonan Lu, Juan C. Vasquez, and Josep M. Guerrero. Dc microgrids—part ii: A review of power architectures, applications, and standardization issues. *IEEE Transactions on Power Electronics*, 31(5):3528–3549, 2016.

[30] K.A.Jadav H.M.Karkar and IN Trivedi. A review of microgrid architectures and control strategy. *In: Journal of The Institution of Engineers (India)*, 98(6):591–598, 2017.

[31] Sajjad M. Kaviri, Majid Pahlevani, Praveen Jain, and Alireza Bakhshai. A review of ac microgrid control methods. In *2017 IEEE 8th International Symposium on Power Electronics for Distributed Generation Systems (PEDG)*, pages 1–8, 2017.

[32] Adel El-Shahat and Sharaf Sumaiya. Dc-microgrid system design, control, and analysis. *Electronics*, 8(2), 2019.

[33] Xiong Liu, Peng Wang, and Poh Chiang Loh. A hybrid ac/dc microgrid and its coordination control. *IEEE Transactions on Smart Grid*, 2(2):278–286, 2011.

[34] E. Unamuno and J. Barrena. Hybrid ac/dc microgrids—part i: Review and classification of topologies. *Renewable Sustainable Energy Reviews*, 52:1251–1259, 2015.

[35] Ajay Gupta, Suryanarayana Doolla, and Kishore Chatterjee. Hybrid ac–dc microgrid: Systematic evaluation of control strategies. *IEEE Transactions on Smart Grid*, 9(4):3830–3843, 2018.

[36] Jackson John Justo, Francis Mwasilu, Ju Lee, and Jin-Woo Jung. Ac-microgrids versus dc-microgrids with distributed energy resources: A review. *Renewable and Sustainable Energy Reviews*, 24:387–405, 2013.

[37] Andrew F. Burke. Batteries and ultracapacitors for electric, hybrid, and fuel cell vehicles. *Proceedings of the IEEE*, 95(4):806–820, 2007.

[38] Xiangjun Li, Dong Hui, and Xiaokang Lai. Battery energy storage station (bess)-based smoothing control of photovoltaic (pv) and wind power generation fluctuations. *IEEE Transactions on Sustainable Energy*, 4(2):464–473, 2013.

[39] M. Ilic-Spong, J. Christensen, and K.L. Eichorn. Secondary voltage control using pilot point information. *IEEE Transactions on Power Systems*, 3(2):660–668, 1988.

[40] Yao Wang, Xin Ai, Zhongfu Tan, Lei Yan, and Shuting Liu. Interactive dispatch modes and bidding strategy of multiple virtual power plants based on demand response and game theory. *IEEE Transactions on Smart Grid*, 7(1):510–519, 2016.

[41] Johanna L. Mathieu, Phillip N. Price, Sila Kiliccote, and Mary Ann Piette. Quantifying changes in building electricity use, with application to demand response. *IEEE Transactions on Smart Grid*, 2(3):507–518, 2011.

[42] Quanyuan Jiang, Meidong Xue, and Guangchao Geng. Energy management of microgrid in grid-connected and stand-alone modes. *IEEE Transactions on Power Systems*, 28(3):3380–3389, 2013.

[43] F. Katiraei, M.R. Iravani, and P.W. Lehn. Micro-grid autonomous operation during and subsequent to islanding process. *IEEE Transactions on Power Delivery*, 20(1):248–257, 2005.

[44] Thomas Ackermann, Göran Andersson, and Lennart Söder. Distributed generation: a definition. *Electric Power Systems Research*, 57(3):195–204, 2001.

[45] Andrey V. Shalukho, Ivan A. Lipuzhin, and Alexander A. Voroshilov. Power quality in microgrids with distributed generation. In *2019 International Ural Conference on Electrical Power Engineering (UralCon)*, pages 54–58, 2019.

[46] Temitope Adefarati, Numbi Bubele Papy, Miriam Thopil, and Henerica Tazvinga. *Non-renewable Distributed Generation Technologies: A Review*, pages 69–105. Springer International Publishing, Cham, 2017.

[47] E. Planas, J. Andreu, J. Garate, I. M. D. Alegra, and E. Ibarra. Ac and dc technology in microgrids: A review. *Renewable Sustainable Energy Reviews*, 43:726–749, 2015.

[48] Mathew Aneke and Meihong Wang. Energy storage technologies and real life applications – a state of the art review. *Applied Energy*, 179:350–377, 2016.

[49] Haisheng Chen, Thang Ngoc Cong, Wei Yang, Chunqing Tan, Yongliang Li, and Yulong Ding. Progress in electrical energy storage system: A critical review. *Progress in Natural Science*, 19(3):291–312, 2009.

[50] Xing Luo, Jihong Wang, Mark Dooner, and Jonathan Clarke. Overview of current development in electrical energy storage technologies and the application potential in power system operation. *Applied Energy*, 137:511–536, 2015.

[51] Mohammad Faisal, Mahammad A. Hannan, Pin Jern Ker, Aini Hussain, Muhamad Bin Mansor, and Frede Blaabjerg. Review of energy storage system technologies in microgrid applications: Issues and challenges. *IEEE Access*, 6:35143–35164, 2018.

[52] Wei Li and Geza Joos. Comparison of energy storage system technologies and configurations in a wind farm. In *2007 IEEE Power Electronics Specialists Conference*, pages 1280–1285, 2007.

[53] Xingguo Tan, Qingmin Li, and Hui Wang. Advances and trends of energy storage technology in microgrid. *International Journal of Electrical Power and Energy Systems*, 44(1):179–191, 2013.

[54] O. Palizban and K. Kauhaniemi. Energy storage systems in modern grids—matrix of technologies and applications. *Journal of energy storage*, 6:248–259, 2016.

[55] Mohammad Faisal, Mahammad A. Hannan, Pin Jern Ker, Aini Hussain, Muhamad Bin Mansor, and Frede Blaabjerg. Review of energy storage system technologies in microgrid applications: Issues and challenges. *IEEE Access*, 6:35143–35164, 2018.

[56] P. Medina, A.W. Bizuayehu, J.P.S. Catalão, E.M.G. Rodrigues, and J. Contreras. Electrical energy storage systems: Technologies' state-of-the-art, techno-economic benefits and applications analysis. In *2014 47th Hawaii International Conference on System Sciences*, pages 2295–2304, 2014.

[57] Jamie C. Beardsall, C. Gould, and M. Al-Tai. Energy storage systems: A review of the technology and its application in power systems. *2015 50th International Universities Power Engineering Conference (UPEC)*, pages 1–6, 2015.

[58] Apparao Dekka, Reza Ghaffari, Bala Venkatesh, and Bin Wu. A survey on energy storage technologies in power systems. In *2015 IEEE Electrical Power and Energy Conference (EPEC)*, pages 105–111, 2015.

[59] H. Ibrahim, A. Ilinca, and J. Perron. Energy storage systems—characteristics and comparisons. *Renewable and Sustainable Energy Reviews*, 12(5):1221–1250, 2008.

[60] Steven C. Smith, P.K. Sen, and Benjamin Kroposki. Advancement of energy storage devices and applications in electrical power system. In *2008 IEEE Power and Energy Society General Meeting - Conversion and Delivery of Electrical Energy in the 21st Century*, pages 1–8, 2008.

[61] Sergio Vazquez, Srdjan M. Lukic, Eduardo Galvan, Leopoldo G. Franquelo, and Juan M. Carrasco. Energy storage systems for transport and grid applications. *IEEE Transactions on Industrial Electronics*, 57(12):3881–3895, 2010.

[62] Siraj Sabihuddin, Aristides E. Kiprakis, and Markus Mueller. A numerical and graphical review of energy storage technologies. *Energies*, 8(1):172–216, 2015.

[63] Ibrahim Alsaidan, Amin Khodaei, and Wenzhong Gao. A comprehensive battery energy storage optimal sizing model for microgrid applications. *IEEE Transactions on Power Systems*, 33(4):3968–3980, 2018.

[64] Hussein Ibrahim, Karim Belmokhtar, and Mazen Ghandour. Investigation of usage of compressed air energy storage for power generation system improving - application in a microgrid integrating wind energy. *Energy Procedia*, 73:305–316, 2015. 9th International Renewable Energy Storage Conference, IRES 2015.

[65] A.A. Khodadoost Arani, H. Karami, G.B. Gharehpetian, and M.S.A. Hejazi. Review of flywheel energy storage systems structures and applications in power systems and microgrids. *Renewable and Sustainable Energy Reviews*, 69:9–18, 2017.

[66] Fernando A. Inthamoussou, Jordi Pegueroles-Queralt, and Fernando D. Bianchi. Control of a supercapacitor energy storage system for microgrid applications. *IEEE Transactions on Energy Conversion*, 28(3):690–697, 2013.

[67] T. Nguyen, H. Yoo, and Hak-Man Kim. Applying model predictive control to smes system in microgrids for eddy current losses reduction. *IEEE Transactions on Applied Superconductivity*, 26:1–5, 2016.

[68] Stavros A. Konstantinopoulos, Anestis G. Anastasiadis, Georgios A. Vokas, Georgios P. Kondylis, and Apostolos Polyzakis. Optimal management of hydrogen storage in stochastic smart microgrid operation. *International Journal of Hydrogen Energy*, 43(1):490–499, 2018.

[69] Giovanna Oriti, Alexander L. Julian, Norma Anglani, and Gabriel D. Hernandez. Novel hybrid energy storage control for a single phase energy management system in a remote islanded microgrid. In *2017 IEEE Energy Conversion Congress and Exposition (ECCE)*, pages 1552–1559, 2017.

[70] Wencong Su and Jianhui Wang. Energy management systems in microgrid operations. *The Electricity Journal*, 25(8):45–60, 2012.

[71] Muhammad Fahad Zia, Elhoussin Elbouchikhi, and Mohamed Benbouzid. Microgrids energy management systems: A critical review on methods, solutions, and prospects. *Applied Energy*, 222:1033–1055, 2018.

[72] C. Chen S. Duan T. Cai B. Liu and G. Hu. Smart energy management system for optimal microgrid economic operation. *IET Renew Power Gener*, 5:258–267, 2011.

[73] Norma Anglani, Giovanna Oriti, and Michele Colombini. Optimized energy management system to reduce fuel consumption in remote military microgrids. *IEEE Transactions on Industry Applications*, 53(6):5777–5785, 2017.

[74] Lucı´a Igualada, Cristina Corchero, Miguel Cruz-Zambrano, and F.-Javier Heredia. Optimal energy management for a residential microgrid including a vehicle-to-grid system. *IEEE Transactions on Smart Grid*, 5(4):2163–2172, 2014.

[75] Adriana C. Luna, Lexuan Meng, Nelson L. Diaz, Moisès Graells, Juan Carlos Vasquez, and Josep M. Guerrero. Online energy management systems for microgrids: Experimental validation and assessment framework. *IEEE Transactions on Power Electronics*, 33(3):2201–2215, 2018.

[76] Pedro P. Vergara, Juan Camilo López, Luiz C.P. da Silva, and Marcos J. Rider. Security-constrained optimal energy management system for three-phase residential microgrids. *Electric Power Systems Research*, 146:371–382, 2017.

[77] Daniel Tenfen and Erlon Cristian Finardi. A mixed integer linear programming model for the energy management problem of microgrids. *Electric Power Systems Research*, 122:19–28, 2015.

[78] Gabriele Comodi, Andrea Giantomassi, Marco Severini, Stefano Squartini, Francesco Ferracuti, Alessandro Fonti, Davide Nardi Cesarini, Matteo Morodo, and Fabio Polonara. Multi-apartment residential microgrid with electrical and thermal storage devices: Experimental analysis and simulation of energy management strategies. *Applied Energy*, 137:854–866, 2015.

[79] Mohammad Hossein Amrollahi and Seyyed Mohammad Taghi Bathaee. Techno-economic optimization of hybrid photovoltaic/wind generation together with energy storage system in a stand-alone micro-grid subjected to demand response. *Applied Energy*, 202:66–77, 2017.

[80] Shivashankar Sukumar, Hazlie Mokhlis, Saad Mekhilef, Kanendra Naidu, and Mazaher Karimi. Mix-mode energy management strategy and battery sizing for economic operation of grid-tied microgrid. *Energy*, 118:1322–1333, 2017.

[81] Hristiyan Kanchev, Di Lu, Frederic Colas, Vladimir Lazarov, and Bruno Francois. Energy management and operational planning of a microgrid with a pv-based active generator for smart grid applications. *IEEE Transactions on Industrial Electronics*, 58(10):4583–4592, 2011.

[82] Adel Choudar, Djamel Boukhetala, Said Barkat, and Jean-Michel Brucker. A local energy management of a hybrid pv-storage based distributed generation for microgrids. *Energy Conversion and Management*, 90:21–33, 2015.

[83] Julio Pascual, Javier Barricarte, Pablo Sanchis, and Luis Marroyo. Energy management strategy for a renewable-based residential microgrid with generation and demand forecasting. *Applied Energy*, 158:12–25, 2015.

[84] Moataz Elsied, Amrane Oukaour, Tarek Youssef, Hamid Gualous, and Osama Mohammed. An advanced real time energy management system for microgrids. *Energy*, 114:742–752, 2016.

[85] Santosh Chalise, Jason Sternhagen, Timothy M. Hansen, and Reinaldo Tonkoski. Energy management of remote microgrids considering battery lifetime. *The Electricity Journal*, 29(6):1–10, 2016.

[86] Aymen Chaouachi, Rashad M. Kamel, Ridha Andoulsi, and Ken Nagasaka. Multiobjective intelligent energy management for a microgrid. *IEEE Transactions on Industrial Electronics*, 60(4):1688–1699, 2013.

[87] Yu-Kai Chen, Yung-Chun Wu, Chau-Chung Song, and Yu-Syun Chen. Design and implementation of energy management system with fuzzy control for dc microgrid systems. *IEEE Transactions on Power Electronics*, 28(4):1563–1570, 2013.

[88] Enrico De Santis, Antonello Rizzi, and Alireza Sadeghian. Hierarchical genetic optimization of a fuzzy logic system for energy flows management in microgrids. *Applied Soft Computing*, 60:135–149, 2017.

[89] George Kyriakarakos, Anastasios I. Dounis, Konstantinos G. Arvanitis, and George Papadakis. A fuzzy logic energy management system for polygeneration microgrids. *Renewable Energy*, 41:315–327, 2012.

[90] Wang T. He X. and Deng T. Neural networks for power management optimal strategy in hybrid microgrid. *Neural Comput and Applic*, 31:2635–2647, 2019.

[91] Ganesh Kumar Venayagamoorthy, Ratnesh K. Sharma, Prajwal K. Gautam, and Afshin Ahmadi. Dynamic energy management system for a smart microgrid. *IEEE Transactions on Neural Networks and Learning Systems*, 27(8):1643–1656, 2016.

[92] H. S. V. S. Kumar Nunna and Suryanarayana Doolla. Energy management in microgrids using demand response and distributed storage—a multiagent approach. *IEEE Transactions on Power Delivery*, 28(2):939–947, 2013.

[93] Chun-Xia Dou and Bin Liu. Multi-agent based hierarchical hybrid control for smart microgrid. *IEEE Transactions on Smart Grid*, 4(2):771–778, 2013.

[94] Amjad Anvari-Moghaddam, Ashkan Rahimi-Kian, Maryam S. Mirian, and Josep M. Guerrero. A multi-agent based energy management solution for integrated buildings and microgrid system. *Applied Energy*, 203:41–56, 2017.

[95] Wencong Su, Jianhui Wang, and Jaehyung Roh. Stochastic energy scheduling in microgrids with intermittent renewable energy resources. *IEEE Transactions on Smart Grid*, 5(4):1876–1883, 2014.

[96] Jingshuang Shen, Chuanwen Jiang, Yangyang Liu, and Xu Wang. A microgrid energy management system and risk management under an electricity market environment. *IEEE Access*, 4:2349–2356, 2016.

[97] Yue Xiang, Junyong Liu, and Yilu Liu. Robust energy management of microgrid with uncertain renewable generation and load. *IEEE Transactions on Smart Grid*, 7(2):1034–1043, 2016.

[98] Wuhua Hu, Ping Wang, and Hoay Beng Gooi. Toward optimal energy management of microgrids via robust two-stage optimization. *IEEE Transactions on Smart Grid*, 9(2):1161–1174, 2018.

[99] Kenneth J. Sauer, Thomas Roessler, and Clifford W. Hansen. Modeling the irradiance and temperature dependence of photovoltaic modules in pvsyst. *IEEE Journal of Photovoltaics*, 5(1), 11 2014.

[100] "OMIE", nominated electricity market operator. https://www.omie.es/en/sobre-nosotros. Accessed: 2021-07-30.

[101] Seth B. Darling, Fengqi You, Thomas Veselka, and Alfonso Velosa. Assumptions and the levelized cost of energy for photovoltaics. *Energy Environ. Sci.*, 4:3133–3139, 2011.

[102] Michael Jakob. The fair cost of renewable energy. *Nature Climate Change*, 2(7):488–489, jun 2012.

[103] Grant Allan, Michelle Gilmartin, Peter McGregor, and Kim Swales. Levelised costs of wave and tidal energy in the uk: Cost competitiveness and the importance of "banded" renewables obligation certificates. *Energy Policy*, 39(1):23–39, 2011.

[104] K. Branker, M.J.M. Pathak, and J.M. Pearce. A review of solar photovoltaic levelized cost of electricity. *Renewable and Sustainable Energy Reviews*, 15(9):4470–4482, 2011.

[105] Behnam Zakeri and Sanna Syri. Electrical energy storage systems: A comparative life cycle cost analysis. *Renewable and Sustainable Energy Reviews*, 42:569–596, 2015.

[106] Chun Sing Lai and Malcolm D. McCulloch. Levelized cost of electricity for solar photovoltaic and electrical energy storage. *Applied Energy*, 190:191–203, 2017.

[107] Dong-Yub Hyun, Chang-Soon Lim, Rae-Young Kim, and Dong-Seok Hyun. Averaged modeling and control of a single-phase grid-connected two-stage inverter for battery application. In *IECON 2013 - 39th Annual Conference of the IEEE Industrial Electronics Society*. IEEE, nov 2013.

[108] Zeljko Jankovic, Bora Novakovic, Vijay Bhavaraju, and Adel Nasiri. Average modeling of a three-phase inverter for integration in a microgrid. *IEEE*, sep 2014.

[109] Runxin Wang and Jinjun Liu. Redefining a new-formed average model for three-phase boost rectifiers/voltage source inverters. *IEEE*, feb 2009.

[110] Yonghao Gui, Xiongfei Wang, and Frede Blaabjerg. Vector current control derived from direct power control for grid-connected inverters. *IEEE Transactions on Power Electronics*, 34(9):9224–9235, sep 2019.

[111] Ramy Georgious, Jorge García, Ángel Navarro-Rodríguez, and Pablo García. A study on the control design of nonisolated converter configurations for hybrid energy storage systems. *IEEE Transactions on Industry Applications*, 54(5):4660–4671, 2018.

[112] Y. Riffonneau, S. Bacha, F. Barruel, and A. Delaille. Energy flow management in grid connected pv systems with storage - a deterministic approach. In *2009 IEEE International Conference on Industrial Technology*, pages 1–6, 2009.

Appendix A

Data sheet

Battery module data sheet

48V RANGE

eLion 48285	eLion 48360F	eLion 48430F	eLion 48500F	eLion 48575F	eLion 48645F	eLion 48720F
			48,0 V			
			48,0 V			
			Lithium - LFP			
285 Ah	360 Ah	430 Ah	500 Ah	575 Ah	645 Ah	720 Ah
13,82 kWh	17,28 kWh	20,73 kWh	24,19 kWh	27,64 kWh	31,10 kWh	34,56 kWh
			2H			
			1H			
			6400			
			4500			
			4000			
288 A	360 A	432 A	504 A	576 A	648 A	720 A
576 A	720 A	864 A	1.008 A	1.152 A	1.296 A	1.440 A
			0º // +45º			
			-28 // +45º			
			Status bar incorporated in external display			
			Optional			
			CAN BUS (Optional)			
			Sized as per DIN and BS formats, as well as for machines with proprietary measurementss			

cegasa | 11

Figure A-1: eBick Li-ion battery

SUNPOWER®

MORE ENERGY. FOR LIFE.™

X-SERIES SOLAR PANELS

- **20.3% efficiency**
  Ideal for roofs where space is at a premium or where future expansion might be needed.
- **Maximum performance**
  Designed to deliver the most energy in demanding real world conditions, in partial shade and hot rooftop temperatures.[1, 2, 3]
- **Premium aesthetics**
  SunPower® Signature™ Black X-Series panels blend harmoniously into your roof. The most elegant choice for your home.

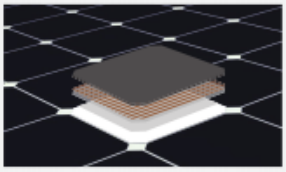

Maxeon® Solar Cells: Fundamentally better.
Engineered for performance, designed for durability.

Engineered for peace of mind
Designed to deliver consistent, trouble-free energy over a very long lifetime.[4,5]

Designed for durability
The SunPower Maxeon Solar Cell is the only cell built on a solid copper foundation. Virtually impervious to the corrosion and cracking that degrade Conventional Panels.[4,5]

Same excellent durability as E-Series panels.
#1 Ranked in Fraunhofer durability test.[10]
100% power maintained in Atlas 25+ comprehensive PVDI Durability test.[11]

UNMATCHED PERFORMANCE, RELIABILITY & AESTHETICS

X20 - 250 PANEL

X20 SERIES

HIGHEST EFFICIENCY[6]

Generate more energy per square foot

X-Series residential panels convert more sunlight to electricity producing 44% more power per panel,[1] and 75% more energy per square foot over 25 years.[3,4]

HIGHEST ENERGY PRODUCTION[7]

Produce more energy per rated watt

High year one performance delivers 8-10% more energy per rated watt.[3] This advantage increases over time, producing 21% more energy over the first 25 years to meet your needs.[4]

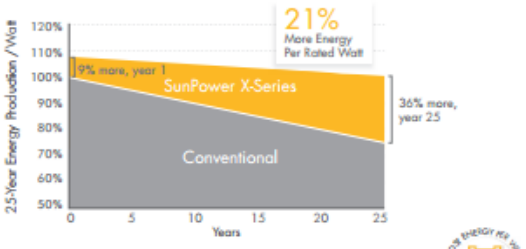

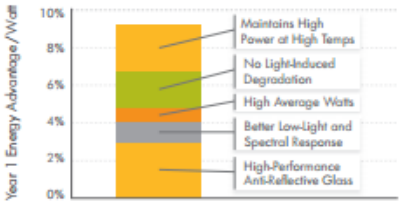

sunpowercorp.com

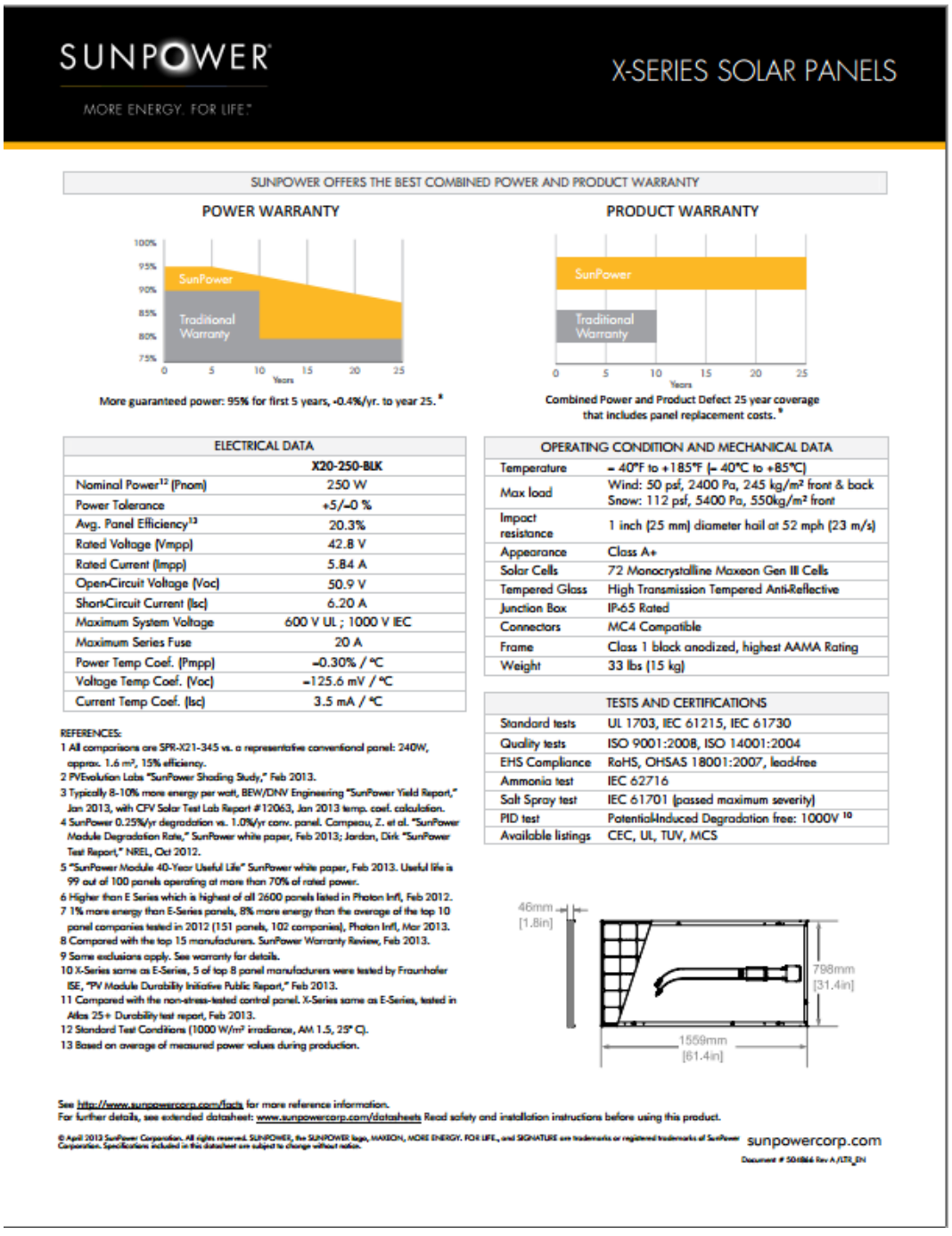

SUNPOWER

MORE ENERGY. FOR LIFE.™

X-SERIES SOLAR PANELS

SUNPOWER OFFERS THE BEST COMBINED POWER AND PRODUCT WARRANTY

POWER WARRANTY

More guaranteed power: 95% for first 5 years, -0.4%/yr. to year 25. *

PRODUCT WARRANTY

Combined Power and Product Defect 25 year coverage that includes panel replacement costs. *

ELECTRICAL DATA	X20-250-BLK
Nominal Power[12] (Pnom)	250 W
Power Tolerance	+5/–0 %
Avg. Panel Efficiency[13]	20.3%
Rated Voltage (Vmpp)	42.8 V
Rated Current (Impp)	5.84 A
Open-Circuit Voltage (Voc)	50.9 V
Short-Circuit Current (Isc)	6.20 A
Maximum System Voltage	600 V UL ; 1000 V IEC
Maximum Series Fuse	20 A
Power Temp Coef. (Pmpp)	–0.30% / °C
Voltage Temp Coef. (Voc)	–125.6 mV / °C
Current Temp Coef. (Isc)	3.5 mA / °C

OPERATING CONDITION AND MECHANICAL DATA	
Temperature	– 40°F to +185°F (– 40°C to +85°C)
Max load	Wind: 50 psf, 2400 Pa, 245 kg/m² front & back Snow: 112 psf, 5400 Pa, 550kg/m² front
Impact resistance	1 inch (25 mm) diameter hail at 52 mph (23 m/s)
Appearance	Class A+
Solar Cells	72 Monocrystalline Maxeon Gen III Cells
Tempered Glass	High Transmission Tempered Anti-Reflective
Junction Box	IP-65 Rated
Connectors	MC4 Compatible
Frame	Class 1 black anodized, highest AAMA Rating
Weight	33 lbs (15 kg)

TESTS AND CERTIFICATIONS	
Standard tests	UL 1703, IEC 61215, IEC 61730
Quality tests	ISO 9001:2008, ISO 14001:2004
EHS Compliance	RoHS, OHSAS 18001:2007, lead-free
Ammonia test	IEC 62716
Salt Spray test	IEC 61701 (passed maximum severity)
PID test	Potential-Induced Degradation free: 1000V [10]
Available listings	CEC, UL, TUV, MCS

REFERENCES:

1 All comparisons are SPR-X21-345 vs. a representative conventional panel: 240W, approx. 1.6 m², 15% efficiency.
2 PVEvolution Labs "SunPower Shading Study," Feb 2013.
3 Typically 8-10% more energy per watt, BEW/DNV Engineering "SunPower Yield Report," Jan 2013, with CFV Solar Test Lab Report #12063, Jan 2013 temp. coef. calculation.
4 SunPower 0.25%/yr degradation vs. 1.0%/yr conv. panel. Compeau, Z. et al. "SunPower Module Degradation Rate," SunPower white paper, Feb 2013; Jordan, Dirk "SunPower Test Report," NREL, Oct 2012.
5 "SunPower Module 40-Year Useful Life" SunPower white paper, Feb 2013. Useful life is 99 out of 100 panels operating at more than 70% of rated power.
6 Higher than E Series which is highest of all 2600 panels listed in Photon Intl, Feb 2012.
7 1% more energy than E-Series panels, 8% more energy than the average of the top 10 panel companies tested in 2012 (151 panels, 102 companies). Photon Intl, Mar 2013.
8 Compared with the top 15 manufacturers. SunPower Warranty Review, Feb 2013.
9 Some exclusions apply. See warranty for details.
10 X-Series same as E-Series, 5 of top 8 panel manufacturers were tested by Fraunhofer ISE, "PV Module Durability Initiative Public Report," Feb 2013.
11 Compared with the non-stress-tested control panel. X-Series same as E-Series, tested in Atlas 25+ Durability test report, Feb 2013.
12 Standard Test Conditions (1000 W/m² irradiance, AM 1.5, 25° C).
13 Based on average of measured power values during production.

See http://www.sunpowercorp.com/facts for more reference information.
For further details, see extended datasheet: www.sunpowercorp.com/datasheets Read safety and installation instructions before using this product.

sunpowercorp.com

Document # 501866 Rev A /LTR_EN

Figure A-2: Solar panels